UNIVERZITA KARLOVA

PŘÍRODOVĚDECKÁ FAKULTA

Ústav hydrogeologie, inženýrské geologie a užité geofyziky

Studijní program: Geologie

Studijní obor: Užitá geofyzika

Bc. Martin Mazanec

STATISTICKÁ ANALÝZA KATALOGŮ PŘIROZENÉ A INDUKOVANÉ SEISMICITY

STATISTICAL ANALYSIS OF NATURAL AND INDUCED SEISMICITY CATALOGUES

DIPLOMOVÁ PRÁCE

Vedoucí závěrečné práce: Mgr. Leo Eisner, Ph.D.

Konzultant závěrečné práce: Prof. RNDr. Tomáš Fischer, PhD.

Černošice 2017

Prohlášení

Prohlašuji, že jsem závěrečnou práci zpracoval samostatně a že jsem uvedl všechny použité informační zdroje a literaturu. Tato práce ani její podstatná část nebyla předložena k získání jiného nebo stejného akademického titulu.

Souhlasím se zapůjčováním diplomové práce v knihovně UK, PřF.

V Černošicích, 20. 8. 2017

Martin Mazanec

Poděkování

Na tomto místě bych rád poděkoval zejména vedoucímu diplomové práce Mgr. Leo Eisnerovi, Ph.D. za odborné vedení, cenné rady a také za jeho ochotu a čas, který mi věnoval. Velký dík patří mým rodičům za to, že mi umožnili studovat a byli mi oporou během studií a mé přítelkyni za její podporu.

Za poskytnutá data bych rád poděkoval:
Firmě Seismik s.r.o., která poskytla seismické katalogy přírodní i indukované seismicity.

Panu Prof. RNDr. Tomášovi Fischerovi, PhD. za zprostředkování dat ze Západočeské seismické sítě WEBNET.

Za seismické katalogy v severní Kalifornii (USA) službě Northern California Earthquake Data Center (NCEDC).

Za Caltech dataset pro jižní Kalifornii (USA) instituci Southern California Earthquake Center (SCEDC).

Za seismický katalog v oblasti Sicílie (Itálie) děkuji Istituto Nazionale di Geofisica e Vulcanologia, Osservatorio Etneo (INGV).

U. S. Geological Survey Earthquake Hazards Programu za online seismickou databázi.

ABSTRAKT

Hlavním cílem této práce je analýza statistických vlastností přírodních a indukovaných seismických katalogů. Porovnáváme časové a magnitudové vlastnosti různých druhů zemětřesných katalogů a hledáme jejich podobnosti a odlišnosti. Na deset různých seismických katalogů přírodního a indukovaného zemětřesení aplikujeme šest vybraných seismostatistických kritérií, která se používají k charakterizování vlastností dvou základních zemětřesných typů - tzv. zemětřesných rojů a sekvencí zvaných mainshock-aftershock (hlavní otřes – dotřes neboli MS-AS).

Naše analýza neobjevila vhodný způsob, který by pouze na základně statistických časových a magnitudových vlastností obsažených v seismickém katalogu dokázal spolehlivě rozlišit přírodní a indukovanou seismicitu. Ukazujeme však, že katalogy indukované seismicity jsou svých chováním shodné s přírodními zemětřesnými roji.

Dále shrnujeme zhodnocení fungování studované skupiny šesti kritérií na odlišení sekvencí mainshock-aftershock a zemětřesných rojů. Poukazujeme na to, že žádné z testovaných kritérií nefunguje k odlišení jednotlivých druhů přirozené seismické aktivity zcela spolehlivě, pokud je použito samostatně.

ABSTRACT

The main goal of this thesis is to analyze the statistical properties of seismic catalogues of natural and induced seismicity, identify similarities and differences. We compare statistical temporal and magnitude information contained in different types of earthquake catalogues. Six seismostatistical criteria used for identification of natural swarms and mainshock-aftershock earthquake sequences are applied to 10 different catalogues of natural and induced seismicity.

We did not find a method to reliably distinguish between natural and induced seismicity based only on temporal and magnitude information contained in catalogues. We show that induced seismicity catalogues are similar to natural earthquake swarms.

We report how the set of 6 criteria presented here can be used for distinguishing between mainshock-aftershock sequences and swarm seismicity. We also show that none of the tested criteria can be used independently for distinguishing between different types of seismicity.

CONTENTS

LIST OF FIGURES

LIST OF TABLES

1 INTRODUCTION

Human activities such as operations related to natural resources extraction alter the stress field in the Earth's crust and may induce earthquakes (Cesca et al., 2012b). A growing number of confirmed cases of man-made seismicity (e.g. Ellsworth, 2013) and their socio-economic impact began receiving much more attention in recent years and have created a strong demand to characterize them and to find suitable methods to distinguish induced from natural seismicity (Schoenball et al., 2015). Reliable differentiation of the earthquake origin is crucial for the ability to mitigate and control the induced seismicity and safely carry out various underground operations. However, there is no standard method for the discrimination between natural and induced seismicity so far (Dahm et al., 2015). A probable reason is that usually very heterogeneous data are available, making it difficult to adopt one common approach.

In many cases all publically available information on earthquakes is limited to only earthquake catalogues. We set the main goal of this thesis to examine statistical properties of natural and induced seismicity based only on catalogue data. Furthermore some seismic catalogues do not even contain event locations or these locations are inaccurate, we limit our analysis to statistical temporal-magnitude features of various seismicity catalogues. We choose 6 criteria that are commonly used to characterize natural swarm or mainshock-aftershock earthquake sequence and apply them to 10 different earthquake catalogues representing natural swarms, tectonic mainshock-aftershock sequences as well as induced seismicity sequences to see if natural and induced earthquakes share the same behavior.

2 SEISMICITY

An Earthquake is a term used to describe physical process that leads to formation of seismic waves. Through the tectonic natural earthquakes accumulated stress is redistributed. Such process of stress redistribution is usually causing a sequence of earthquakes to develop in space and in time (Tosi et al., 2009).

A fault is defined as a displacement across a fracture, joint, or fracture zone. The size of an earthquake depends on the stress condition on the fault, how much slip occurs on the fault, how fast it fails, and over how large an area the slip occurs (Zoback, 2007). Earthquake size is usually measured by magnitude. There are several types of magnitude – for example local (M_L), surface waves (M_s), body waves (m_b), moment (M_w), etc. Each of these magnitudes is trying to measure released energy in the earthquake and ideally these types of magnitudes should be similar when measuring the same earthquake. Magnitude is measured in a common logarithm (logarithm with the base of 10) of the seismic moment estimated from amplitudes of seismic waves recorded by seismograph (Lowrie, 1997; Shearer, 2009).

A dataset of recorded seismic events is called seismic catalogue and contains information about spatio-temporal distribution of the seismic events in a certain area and other parameters of the earthquakes. One of the most important parameters of the seismic catalogue is the magnitude of completeness M_c - a threshold that depends mostly on the characteristics and geometry of the seismic monitoring network (Alparone et al., 2015; Vecchio et al., 2008). The magnitude of completeness for a catalogue and an area is magnitude for which all events greater than the magnitude of completeness are detected and reported in the catalogue of the area. Mignan and Woessner (2012) gives an overview of techniques to Evaluate M_c from statistical methods using earthquake catalogues. These methods are mostly based on the Gutenberg-Richter frequency-magnitude scaling law described below.

Earthquakes around the globe occur mostly in narrow seismic zones that are related to the plate tectonic boundaries (Figure 1). About 90% of all earthquakes result from tectonic events and 10% are related to volcanic activity, collapse of underground cavities, or man-made activities. The most active seismic zone is circum-Pacific zone, in which about 75–80% of the annual seismic energy is released. The Mediterranean-transasiatic zone is responsible for 15–20% of the energy release. The system of oceanic ridges and rises forms the third most seismic active zone, with 3–7% of the annually released seismic energy. All these seismic zones also include volcanic activity. The smallest active zone is the intraplate seismicity that occurs isolated from the main seismic zones (Lowrie, 1997). However, induced seismicity increased its importance in recent years. Events in Oklahoma are one of the reasons (Hall, 2015).

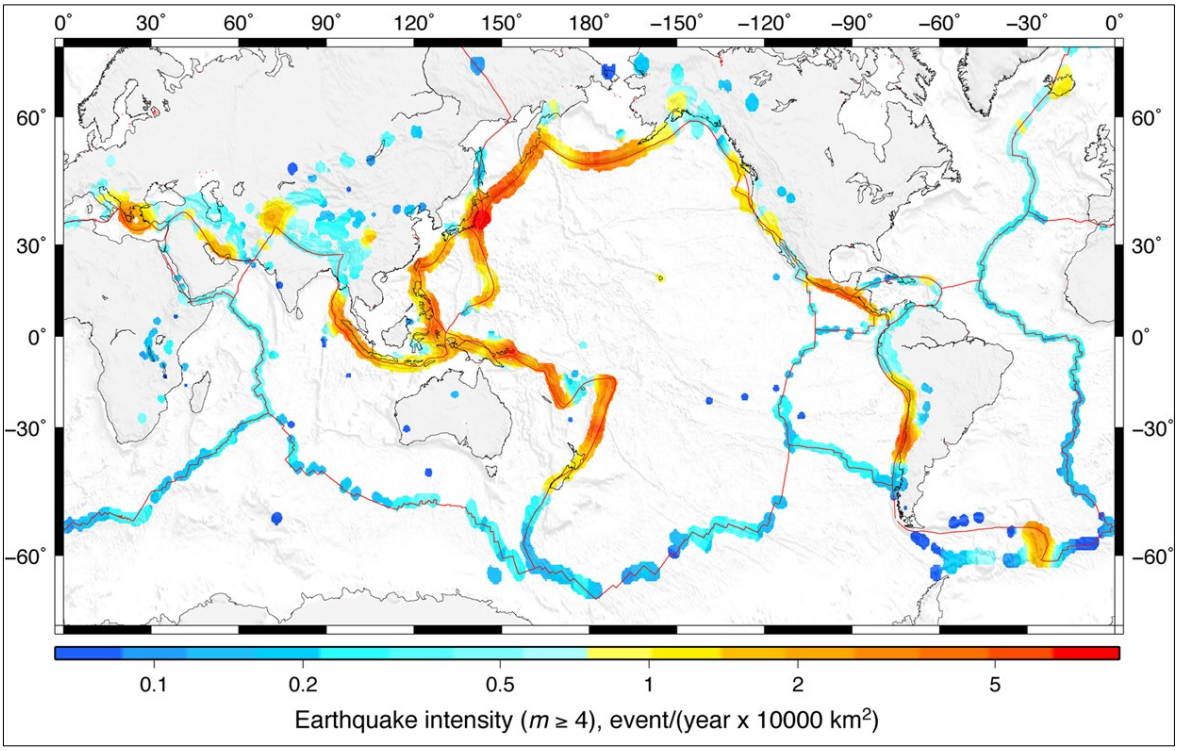

Figure 1. Global spatial distribution of earthquake intensity [in events per year per 10 000 km^2]: Events with magnitude greater or equal than 4 according to the NCEDC catalogue were considered during the period of 1975–2015. A point is plotted in this map if the circle of radius 100 km centered at the point contains at least 5 earthquakes of magnitude m ≥ 5. Red lines represent major tectonic faults (after Zaliapin and Ben-Zion, 2016).

Earthquake events usually occur in series (seismic sequences) related to each other in space and time. The largest earthquake in a sequence is called a mainshock M_{max}. By definition this earthquake releases the most of the energy in the sequence. Sometimes the mainshock is preceded by relatively smaller earthquakes called foreshocks, and almost always is followed by aftershocks (see Figure 2). Aftershock occurrence is usually attributed to the strain energy not released by the main shock or its foreshocks and usually last over a period of days to years. The larger the mainshock, the longer aftershocks will continue, and the larger and more numerous the aftershocks will be (Zaliapin and Ben-Zion, 2016).

The challenge of such characterization is a definition of a sequence. For example, how far (spatially or/and temporally) from the mainshock should an event to be considered as an aftershock or foreshock? There is no definition that would determine an earthquake event to be part of this or that sequence. In practice, an area around a largest event is usually selected (e.g. based on its magnitude size) and all events in the vicinity are defined as foreshock and aftershocks based on their relative timing. This is an approach used in the study and we discuss selection of earthquake sequences in Chapter 3.2.

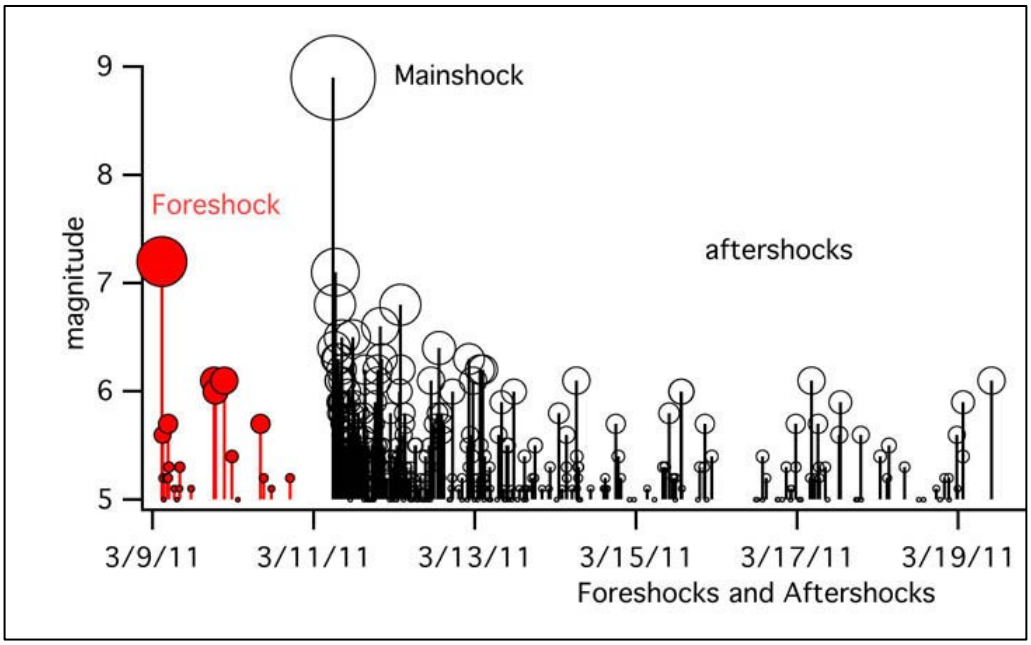

Figure 2. Illustration of temporal evolution of magnitudes in an earthquake sequence with foreshocks, mainshock and aftershocks (2011 M_w 9.0 Tohoku earthquake, from [1]).

Using the definition above we may follow Mogi who defined three basic types (displayed in Figure 3) of earthquake sequences (Mogi, 1963):

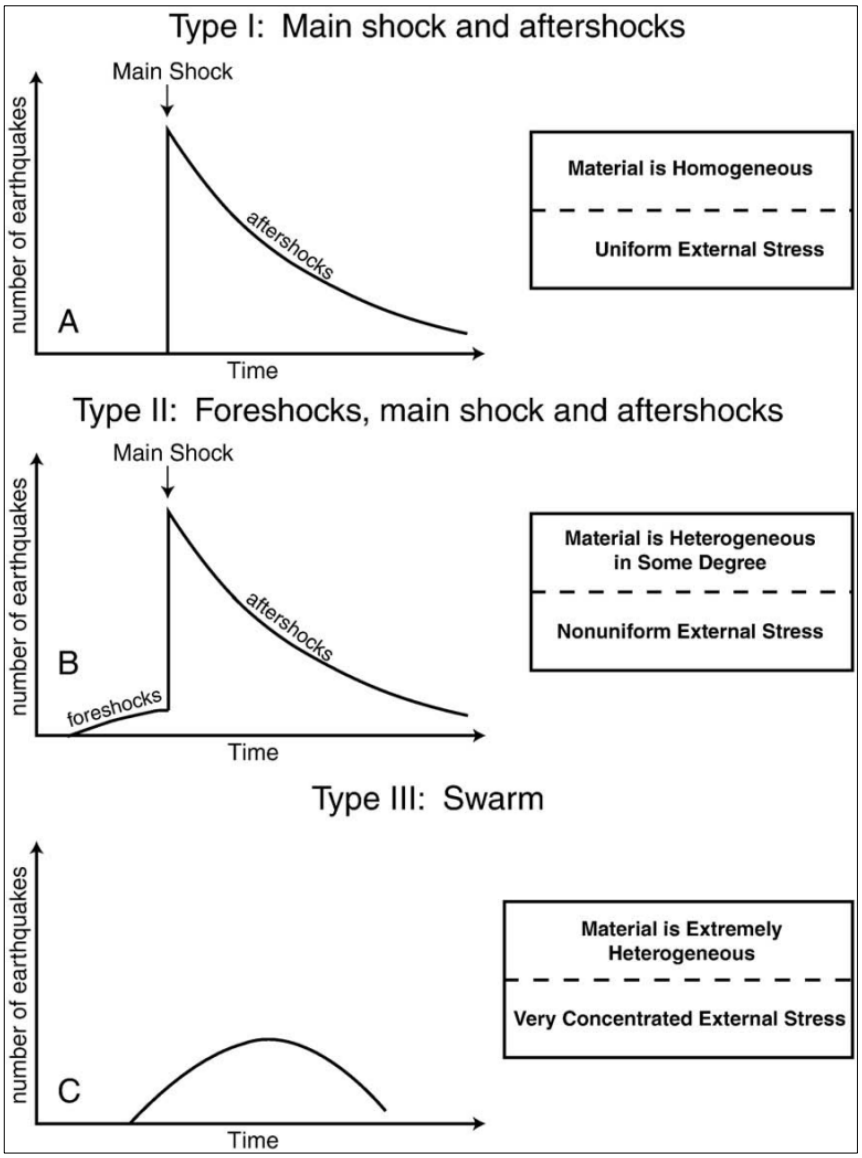

Figure 3. Generalized plots of number of earthquakes vs. time for the three types of earthquake sequences after Mogi (1963). Boxes on the right explain for each type occurrence conditions (Farrell et al, 2009).

Type I: Mainshock and aftershocks (MS-AS) sequence: a mainshock followed by a number of aftershocks of decreasing frequency and magnitude. Appears typically in homogeneous stress field and is caused by a uniformly applied external stress and single fault or fault structure (Figure 3A, Figure 4). Aftershocks occurrence is usually attributed to the strain energy not released by the main shock or its foreshocks (Mogi, 1963).

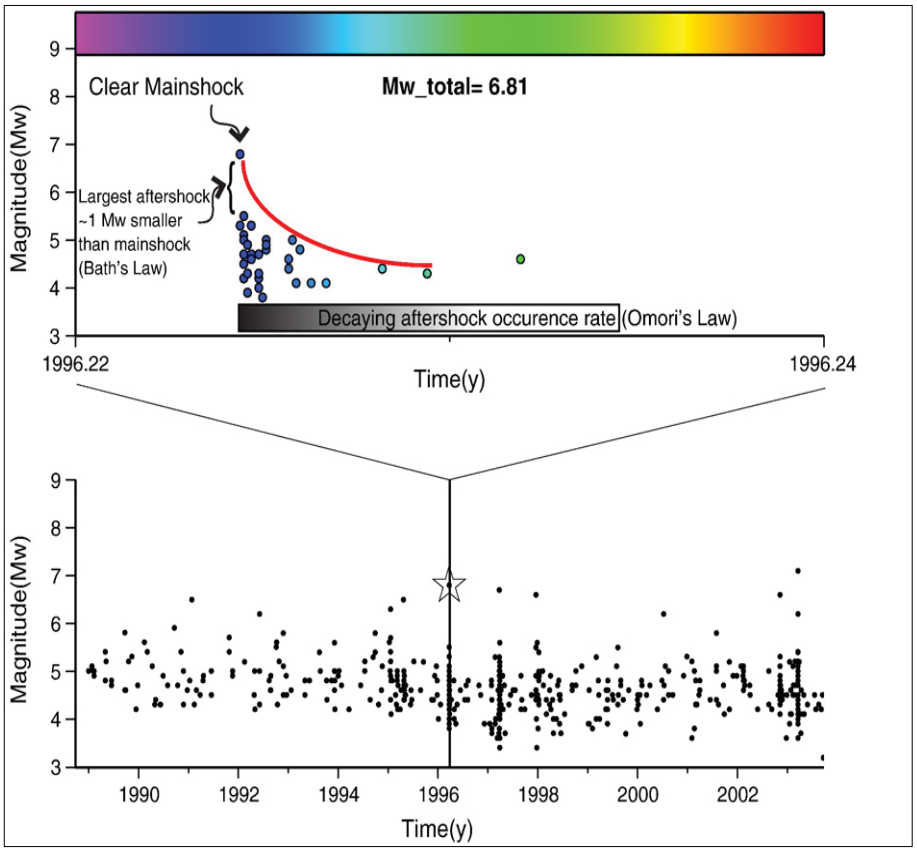

Figure 4. Example of a mainshock–aftershock (MS-AS) sequence. Top Panel: Red line represents Omoris Law . Bottom Panel: Star marks mainshocks of MS-AS sequences (Holtkamp and Brudzinski, 2011).

Type II: Foreshock, mainshock and aftershocks: Slow buildup of seismicity (*foreshocks*) MS-AS sequence (Figure 3B). This type tends to occur in an environment that is moderately heterogeneous, with a non-uniform external stress. Type II. is intermediate one between the Type I. and Type III (Mogi, 1963). However, in this thesis we do not distinguish between Type I and Type II and call them both as MS-AS sequences.

Foreshock sequences across the world have some characteristic features. Numerous observations show that foreshock activity increases approximately as the inverse of time before the mainshock. Also observations have shown that the *b-value* (described below) usually drops and is lower in foreshocks than in aftershocks seismicity (Avlonitis and Papadopoulos, 2014; Papazachos, 1975).

Type III. Swarm: A gradual increase and decay of seismic activity close in space and time without a significant mainshock (Figure 3C and Figure 5), see Sykes (1970). This type occurs in material that is extremely heterogeneous or having high fracture density, where a concentrated application of stress is. Fluids (such as intruding magma) are most likely involved in these sequences (Mogi, 1963).

Some of them are tectonic origin (Mogi, 1963) but most of them are volcanic origin, caused by stress perturbation associated with the migration of hydrothermal fluids or magma (e.g. Waite et al., 2002; Hill, 1977) or caused by aseismic slip and fluid pressure variations (Vidale and Shearer, 2006). CO_2 driven swarm activity is known in some regions, such as West Bohemia in the Czech Republic (Fischer and Horálek, 2003).

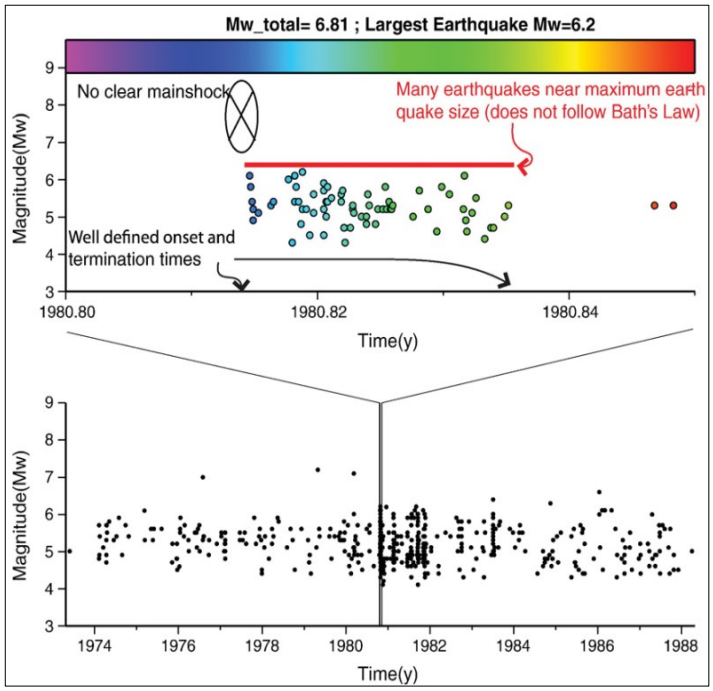

Figure 5. Example of temporal evolution of magnitudes in an earthquake swarm (the 1980 Vanuatu swarm). (Top Panel) Earthquake magnitude vs. time for ~3 weeks around the swarm. (Bottom Panel) Earthquakes over the Vanuatu region for 15 years surrounding the swarm. Vertical bars representing the time shown in the top two panels (after Holtkamp and Brudzinski, 2011).

It is observed that earthquake sequences follow statistical laws. All three earlier described types of natural seismicity follow this empirical scaling relation:

(1) Gutenberg-Richter (G-R) frequency-magnitude scaling, which refers to the relation between the magnitude size and number of seismic events in a sequence.

$$logN = a - bM \qquad (1)$$

where N is number of events greater or equal to magnitude M, a is parameter describing the overall number of events, b (*b-value*) is an important parameter and could be defined as ration of small and large events (Gutenberg and Richter, 1944). This parameter may vary with space and time and is strain sensitive. Typical observed value for tectonic mainshock-aftershock sequences is $b < 0.9$. For swarms (larger rate of small events) is value $b > 1$ (Mogi, 1963).

The statistical properties of aftershock sequences are associated with another two empirical scaling relations that swarm sequences do not follow:

(2) Omori (1894) observed that the frequency of aftershocks decays inversely with the time after the main shock. This empirical relation, known as the Omori law, was later modified by Utsu (1961):

$$n(t) = \frac{k}{(c+t)^p} \qquad (2)$$

where n is the number of aftershocks following the mainshock, k and c are constants that vary between earthquake sequences. The empirical constant k can be considered as a measure of aftershock productivity. Time t is measured from the mainshock and p is constant that modifies the decay rate (Lindman et al., 2006).

Båth's law quantifies the magnitude difference between the mainshock and the largest aftershock in a sequence as a statistical mean value of M_w 1.2 and is apparently independent of the mainshock magnitude (Båth, 1965; Purcaru, 1974).

2.1 INDUCED SEISMICITY

While most of the global seismic activity is caused by natural processes (such as volcanic activity or tectonic plates movement), human activities that alter the state of stress or the pore pressure within the Earth's crust may also produce earthquakes. These anthropogenic seismic events can occur in regions where natural seismicity rate would otherwise be lower (Grigoli et al., 2017; Huang and Beroza, 2015).

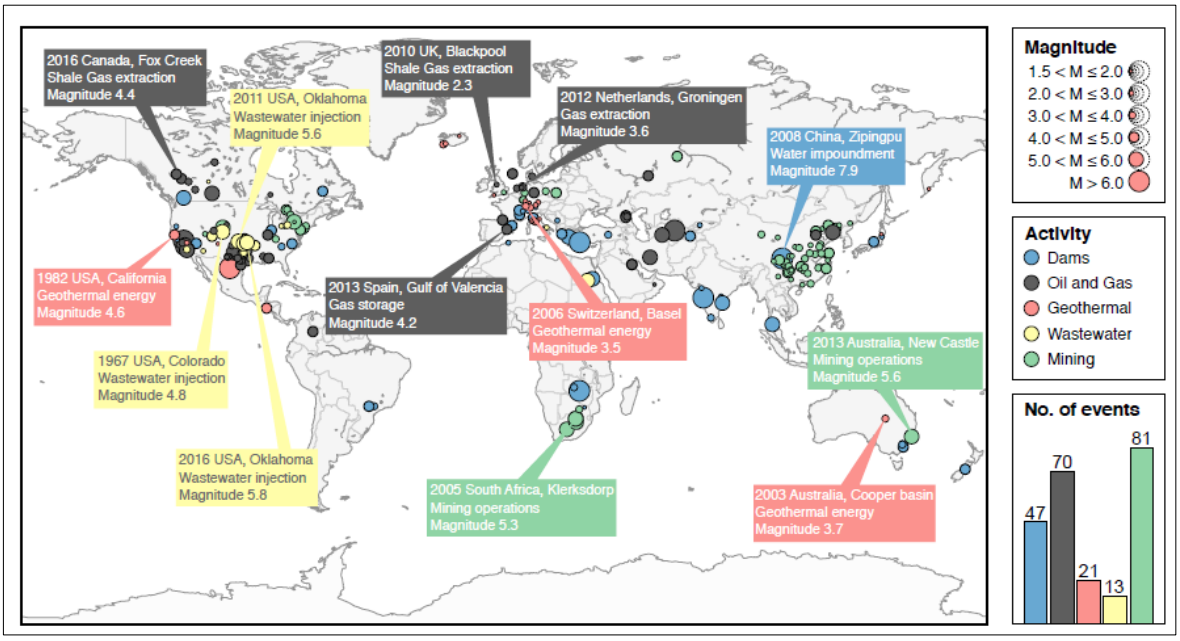

Figure 6. Overview of the global distribution of different types of anthropogenic seismicity, showing only the scientifically documented cases associated induced seismicity. Cases classified by magnitude size and industrial activity (Grigoli et al., 2017).

The most common operations causing induced seismicity (see Figure 7) are oil and gas non/conventional extraction (Suckale, 2009), mining (Gibowicz and Lasocki, 2001), water reservoirs or other large constructions (Mallika et al. 2012), geothermal energy exploitation (Barth and Langenbruch, 2012), underground fluid and gas storage operations and waste water disposal (Geobel et al., 2016). In this thesis we analyze seismic catalogues of induced seismicity associated with unconventional extraction, specifically seismicity induced by hydraulic fracturing. This type of oil and gas extraction is done by injecting fluid into the subsurface to create and connect hydraulic fractures resulting in an economical hydrocarbon production from tight formation (Ellsworth, 2013).

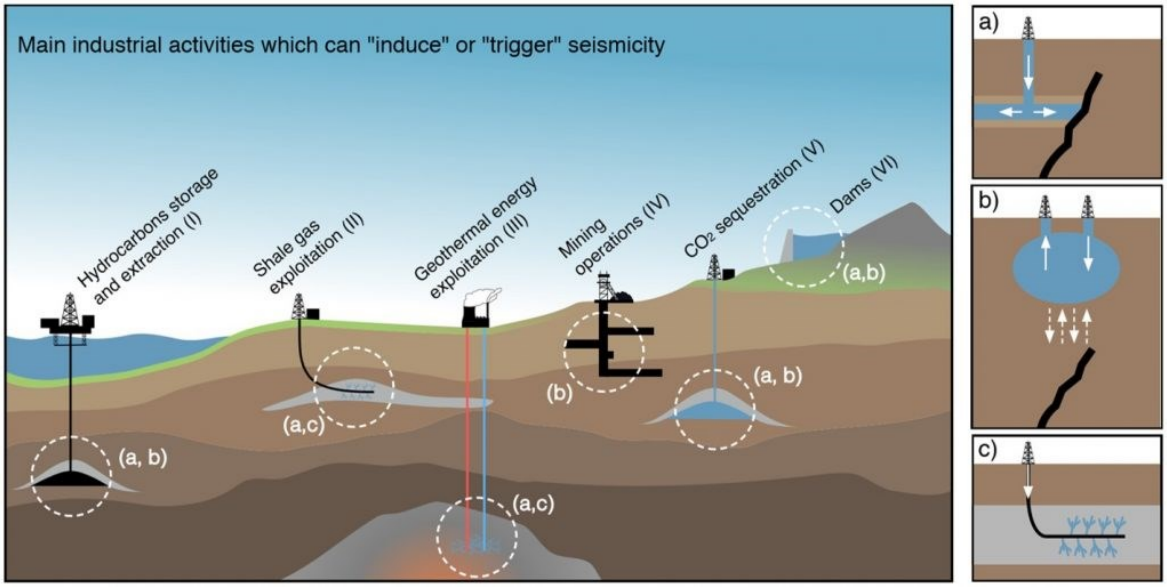

Figure 7. Diagram of main industrial activities responsible for induced seismicity. White characters (a, b, c) indicate three main mechanism of induced seismicity displayed in the three figures on the right side, described in Grigoli et al., 2017.

2.1.1 TRIGGERED VS. INDUCED SEISMICITY

Earthquakes caused by humans (anthropogenic) are either induced or triggered. The difference is described for example by Dahm et al. (2012) who characterizes induced seismicity as events entirely controlled by stress changes caused by human operations that would not occurred without them. The whole failure process is driven by the (human) induced stress. On the contrary nucleation of (human) triggered earthquake is triggered by (human) induced stress, but rupture propagation is driven by preexisting tectonic stress rates, so earthquake was just advanced by human action.

Additionally, induced (triggered) earthquakes usually occur in the upper 6 km of the crust and are often superficial while most natural earthquakes nucleate much deeper at 10-15 km. Due to shallow depth of induced seismicity, even weak events with $M < 3$ can be felt by the population and may pose a seismic hazard at the epicenter and are thus important for the subject (Dahm et al., 2010).

In this thesis we make no difference between human induced and triggered earthquakes. We do this because in practice it is often difficult to clearly distinguish between these two types (Davis et al., 1995) and is not essential.

Grigoli et al. (2017) lists several critical cases in Europe where seismicity close to industrial sites caused debate on induced seismicity (see global map of induced seismicity

in Figure 6). The most famous case is probably Basel (Switzerland), where seismicity was induced through hydraulic stimulation in geothermal energy exploitation project.

2.1.2 MECHANISM

There are a number of mechanisms that can produce induced seismicity. The pore pressure and state of stress situation play a crucial role in these processes. The pore pressure acts against the weight of the rock and the forces holding the rock together. Pore pressure alteration (e.g. due to fluid injection) may create new fractures or reduces the effective normal stress acting on the pre-existing fault causing its reactivation as displayed in Figure 8. (Grigoli et al., 2017; Zoback, 2007; [2]).

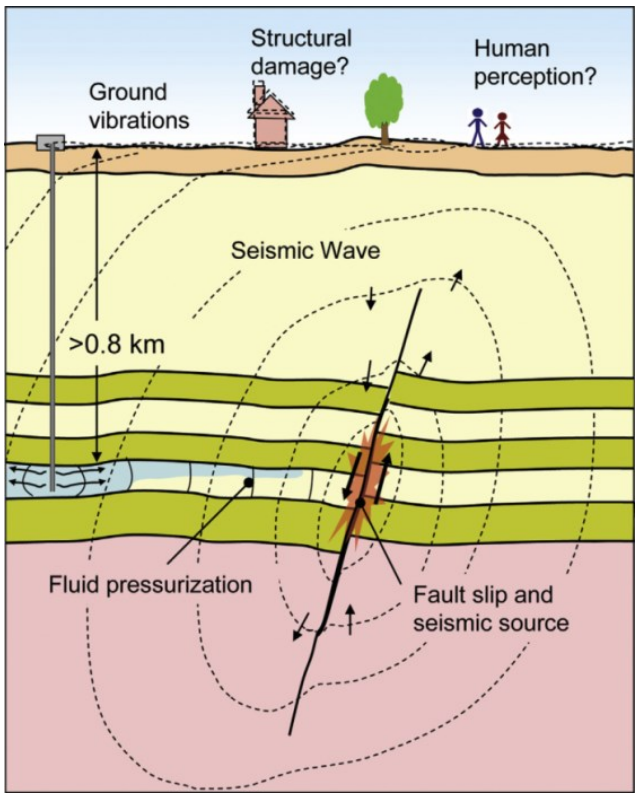

Figure 8. Schematic diagram of injection-induced fault reactivation, subsequent seismic wave propagation causing ground motions and potential impact on surface structures and human population (Rutqvist et al., 2014).

Other factors thought to be responsible may be thermal changes and/or chemical changes caused by fluid movement and injection. Induced stresses can range from a few tens of thousands to several millions of Pascals (Dahm et al., 2010; [2]).

3 DISTINGUISHING BETWEEN NATURAL AND INDUCED SEISMICITY

Seismicity induced by human (industrial) activity described in Chapter 2.1 is becoming intensively discussed. Earthquakes occurring in spatio-temporal proximity to anthropogenic operations are immediately under suspicion to be triggered or induced. Ability to differentiate between natural and induced seismicity is difficult task but essential if we wish to control and safely carry out (industry) underground operations (Opršal and Eisner, 2014). Understanding which seismicity originates from anthropogenic operations may reduce earthquake hazards. Although no reliable and clear rules have been established so far, number of studies discusses criteria to differentiate between these two types. Most of the current methods to distinguish potential sources of earthquakes are usually related to individual cases and are treated unequally (Dahm et al., 2010; Cesca et al., 2012a).

The spatial and temporal correlation between human activity and event rates is still the main tool to discriminate between natural and induced seismicity (Opršal and Eisner, 2014). However, many industrial fluid injection operations can transmit pore pressure changes several kilometers causing earthquake far from the industrial site (Grigoli et al., 2017). Therefore it is challenging to spatially select seismicity that should be correlated with anthropogenic activity.

One of the first attempts to deal with the discrimination issue has been made by Davis and Frohlich (1993) for fluid injection and modified for fluid withdrawal by Davis et al. (1995). This approach propose a list of three series of *yes-no* questions to indicate if the seismicity is induced. The main parameters of this methodology are (1) coincident timing, (2) coincident location and (3) fluid pressure changes. However, this method is only qualitative and is not applicable to define regions of potentially expected earthquakes (Dahm et al., 2010). The former methodology has been revisited by Frohlich et al. (2016) who proposes seismicity classification into four groups, based on the score in the five question test: (1) tectonic, (2) possibly induced, (3) probably induced and (4) almost certainly induced.

The discrimination problem is also discussed in different works. Following (Dahm et al., 2013), discrimination methods can be classified in three main groups: (1) physics based methods, (2) statistics based methods and (3) source parameters based methods.

1) Physics-based probabilistic model is based on Coulomb failure criterion, a seismicity model and seismicity comparison with the natural background or background tectonic stress rate. This approach requires detailed model stress loading and realistic modeling of stress changes caused by human operations.
2) Statistics-based seismicity model is based on empirical relations of natural seismicity, requires a set of seismic data to identify changes in the seismostatistics parameters (constant background activity rate and the behavior of aftershock sequences), that might be correlated with human operations.
3) Source parameter approach for collapse-type events is an assessment of non-double couple and isotropic components to assess the origin of an earthquake because non-double couple earthquakes rarely occur outside of volcanic areas naturally (e.g., Cesca et al. 2012b).

Combination of these approaches into common discrimination schemes – hybrid methods, were proposed by Passareli et al. (2012).

Most of these suggested methods require availability of data and parameters such as background data, site geology and tectonics, seismological source parameters or engineering parameters (see details in Dahm et al., 2012).

The contribution of Cesca et al. (2012a) summarizes several scientific and geophysical viewpoints, techniques and methods substantial in a process of induced and natural seismicity differentiation such as source location (e.g. Rudziński and Dębski, 2012), seismic source parameters estimation (e.g. Husen et al., 2012), waveform cross correlation (Plenkers et al., 2012), catalogue assessment and magnitude distribution (e.g. Barth and Langenbruch, 2012). Other indicator for induced seismicity might be moment sensor inversion and decomposition (Cesca et al., 2012b) or pore pressure changes laboratory studies (Turuntaev et al., 2012).

A more detailed investigation of recent earthquakes is needed to clearly characterize induced seismicity. Basic structural, geophysical, geological data and detailed information about man-made operations are often missing. Also our understanding of the earthquake triggering process is still incomplete (Dahm et al., 2010; Skoumal et al., 2015)

3.1 CRITERIA FOR DIFFERENTIATING OF EARTHQUAKE CATALOGUES

In the previous chapter three main methodological groups for natural and induced seismicity discrimination were discussed. All mentioned methods depend on number of accurate data or achieve high-quality results only in location for which they were formulated. Here we use the second methodological group - the statistics-based analysis of earthquake catalogues. The main advantage of the statistical approach is a lower requirement of input data since earthquake catalogs with times and magnitudes of events are usually available (Grigoli et al., 2017) while source mechanisms and sometimes even locations of all seismic events are poorly known and in addition, the anthropogenic activity is not public in many cases.

Here we choose 6 criteria that are commonly used to characterize natural swarm and mainshock aftershock earthquake sequence (MS-AS) and use them to analyze 10 selected earthquake catalogues (described in Chapter 3.2.) of different earthquake types (MS-AS, swarms and induced seismicity sequences) to see whether there is any statistical similarity in temporal-magnitude behavior among any type of the natural seismicity and anthropogenic induced seismicity. Numerous examples suggest that unusual swarm-like behavior of seismicity spatio-temporally correlated with the anthropogenic activity could be used to distinguish induced seismicity (e.g. Skoumal et al., 2015). Below we introduce selected criteria.

3.1.1 EVENTS DENSITY

One of the first criteria used to distinguish earthquake swarms was defined by Mogi (1963). Earthquake sequence is a swarm if the following criteria (based on empirical observations) are met:

a) The total number of earthquakes in a sequence is greater or equal 10.

b) The maximum daily number of earthquake events in the sequence $N_d\ max$ divided by the square root of the swarm duration T in days is greater than 2:

$$\frac{N_d\ max}{\sqrt{T}} > 2 \qquad (3)$$

3.1.2 MAINSHOCK POSITION WITHIN THE SEQUENCE

One of the characteristic features of seismic sequence is the position of the mainshock (M_{max}) within the earthquake sequence. For example Skoumal et al. (2015) describes situation in Ohio where swarms are distinguished from traditional MS-AS sequences because in swarms the largest earthquake occurs later in the sequence. Similar observation is described by Vidale and Shearer (2006) in southern California, Holtkamp and Brudzinski (2011) summarized the observations of the timing of the largest earthquake in the swarm sequence in circum-Pacific subduction zones is no different than the timing of any other earthquake in the sequence.

We analyze selected seismic catalogues to estimate the position of the mainshock by quantifying (1) the ordinal number of the mainshock within the sequence events and (2) the timing of the mainshock event relative to the rest of the seismicity in sequence. Here we simplify the method proposed by Mesimeri et al. (2013) and just compare the number of days before and after the mainshock within the sequence. Similar approach was chosen for the ordinal number of the largest event in the sequence.

3.1.3 MAINSHOCK – AFTERSHOCK MAGNITUDE COMPARISON

Zobin et al. (2005) observed that the difference in magnitude between the largest and the second largest event (also called here *magnitude gap)* in a swarm is usually smaller or equal to 0.5 magnitude unit. Swarms also typically have many earthquake events near the magnitude of the largest earthquake in a sequence (Holtkamp and Brudzinski, 2011) and they do not follow the Båth's law (described in Chapter 2).

Contrary to swarm sequences, the tectonic mainshock–aftershock sequences usually follow the Båth's law, so the difference of mainshock and largest aftershock should be around M_w 1.2. Other authors suggest that MS-AS earthquakes are typical of the occurrence of the largest event that exceeds the remaining events by 0.5 magnitude unit at minimum (e.g. Fischer et al., 2010).

These observations are supported by the work of Zaliapin and Ben-Zion (2016) who came up with global map of aftershock magnitude gap, shown in Figure 9. This map shows that large subduction zones have on average higher magnitude gap in contrary to ocean ridges and intraplate earthquakes where the seismicity is more swarm-like.

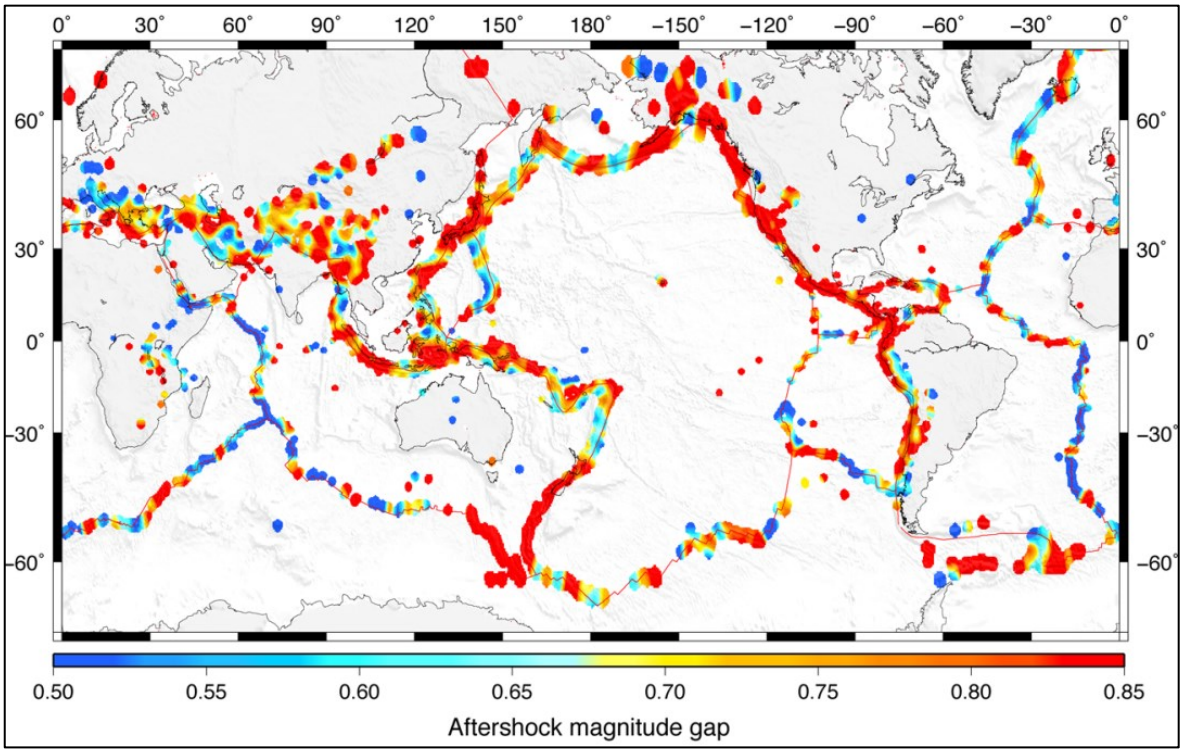

Figure 9. Worldwide map of the aftershock magnitude gap defined for families with aftershocks as the difference between the magnitudes of the main shock and the largest aftershock. This analysis is done for all families with main shock magnitude m ≥ 5 (Zaliapin et al., 2016).

We compare magnitude difference of two largest events in each of our selected seismic catalogues to see how the induced catalogues will be classified in comparison with the different types of natural seismicity and whether the magnitude difference observations mentioned above work in general.

3.1.4 COMPARISON OF THE NUMBER OF EVENTS AND MAGNITUDE OF THE MAINSHOCK

One way to simply quantify swarm-like behavior of a sequence is to compare the magnitude of the largest event (M_{max}) in a sequence to the overall number of events above the level of magnitude completeness M_c (Vidale and Shearer, 2006; Holtkamp and Brudzinski, 2011; Skoumal et al. , 2015). By plotting these two variables we may differentiate between swarms and tectonic earthquakes and see in which sector the induced seismicity occurs as shown in Figure 10.

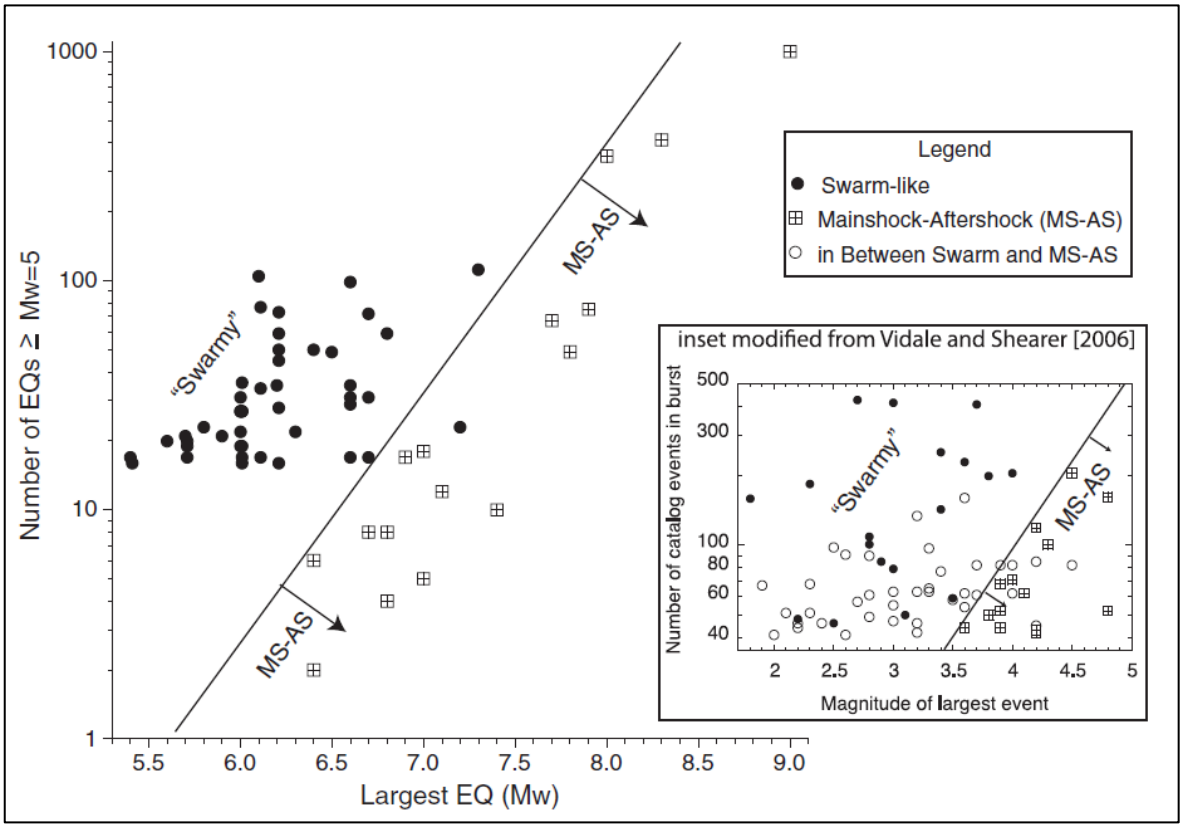

Figure 10. Number of earthquakes in a sequence (greater than M_w=5) relative to the magnitude of largest event for swarms and mainshock–aftershock sequences earthquakes in circum-Pacific subduction zones. Solid line marks the boundary between swarms and MS-AS sequences (Holtkamp and Brudzinski, 2011).

3.1.5 INTER-EVENT TIME

To further examine the earthquake sequences we investigate the temporal distribution of events within the sequence using the inter-event time (also known as *waiting time*). The interevent time (IET) distribution describes the time gap between two following events above the magnitude of completeness and is commonly used (e.g. Shcherbakov et al., 2005; Sicali et al., 2014). Farell et al. (2009) uses the combination of an inter-event time and a distance to identify swarms in the Yellowstone region. Here we estimate the IET for every event in the dataset and compare it with the sequence magnitude distribution with assumption that tectonic, induced and swarm sequences have each characteristic pattern that can be used to distinguished them. This approach is based on the study of Hristopulos and Mouslopoulou (2012) who assigned ordinal number to every event in the sequence and estimated sequence IET distribution. This criterion may also reveal differences between natural and induced seismicity. Inter-event times are driven by human operations in case of induced seismicity while natural seismicity is not controlled by human activity.

3.2 DATASETS

For further analyzes we choose ten different earthquake catalogues from all around the globe (Figure 11). These catalogues represent different types, swarms and MS-AS as well as natural and induced sequences. Each of the earthquake catalogues has its unique parameters such as size, location, duration and was detected by seismic network with specific resolution capability. Nine of the selected catalogues have verified (natural or induced) origin whereas the origin of the Azle, Texas catalogue is still a subject of discussion (as described in Chapter 3.2.2.3). Therefore we selected it to analyze if it shows any similarity of behavior with natural or induced earthquakes. Catalogues source is either public or private. Public catalogues contain information from various sources and we are not able to reliably verify and often even obtain some parameters like events location. Therefore, we limit our analysis to temporal-magnitude relationships. While origin times of events are determined with sufficient accuracy, magnitudes of events may not be very accurate, but at least the magnitudes were provided for all datasets.

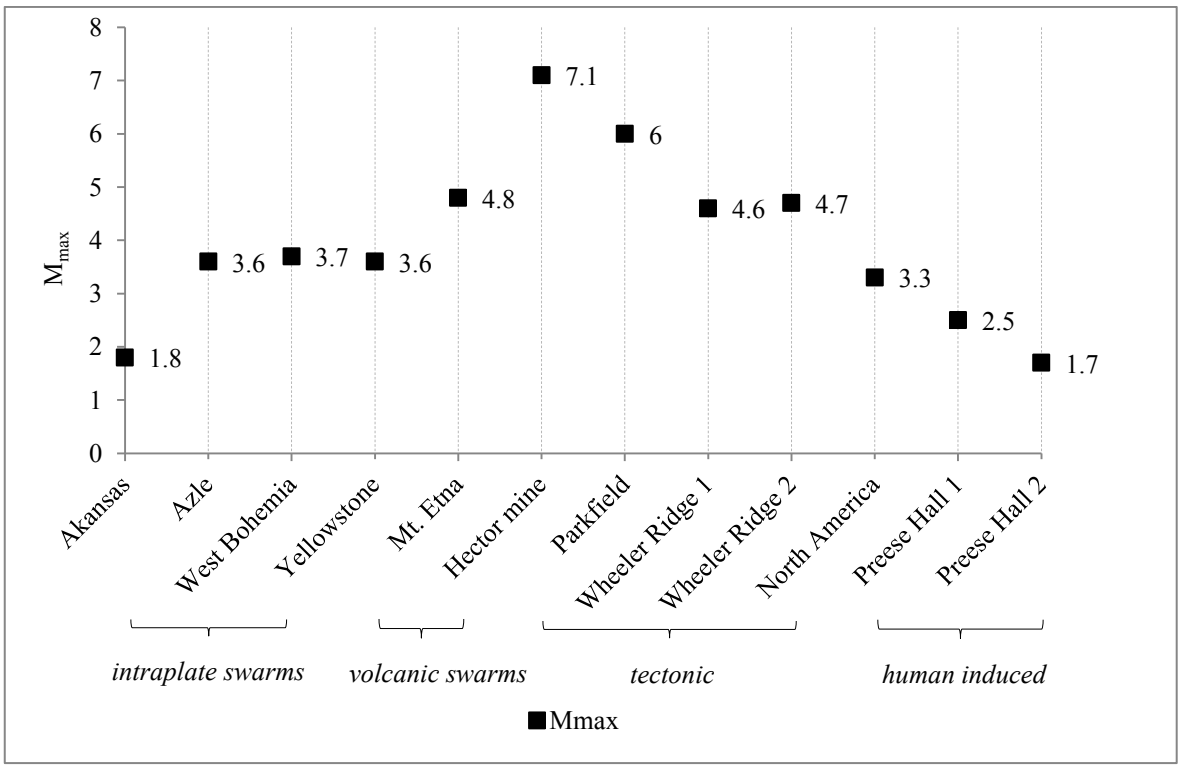

Figure 11. Four categories of twelve analyzed seismic sequences plotted with mainshock magnitudes (M_{max}).

In ideal case we would compare datasets with similar sizes of magnitudes to eliminate differences resulting from the scale. However, this is not available as induced seismicity is usually monitored with dedicated networks allowing detecting weak events (as shown in Figure 11) while natural seismicity is monitored from national networks with much larger spacing in the monitoring networks. The larger spacing in the seismic monitoring networks implies only larger events can be detected, i.e. magnitude of completeness is higher usually for the natural earthquake sequences. We believe that this does not influence this study as earthquakes are self-similar.

For the analysis we choose well-know, in literature described natural earthquakes that are statistically representative for each type of seismicity (MS-AS or swarm). The spatio-temporal dimension of the seismic catalogue is defined based on the mainshock magnitude size and available information about the earthquake parameters (e.g. area, duration) in the scientific literature. Next we define seismic sequence of the seismic catalogue as a time period in which the continual seismic activity with at least 10 events above the magnitude of completeness has an inter-event time (time gap) smaller than 10 days. If the seismic catalogue is split in to several sequences due to the time definition, we analyze only one or two chosen sequences of the catalogue. Therefore, we analyze 12 sequences from 10 seismic catalogues. The natural seismicity catalogs are obtained mostly from public sources (U.S. Geological Survey earthquake database [3] or local networks database, e.g. *WEBNET*, *NCEDC* as described below). Induced seismicity Preese Hall and North America catalogues described in following chapters were provided by Seimik s.r.o.

To determine the M_c we use a simple method known as the Maximum Curvature (MAXC) technique (Wyss et al. 1999; Wiemer and Wyss 2000), which is derived from the Guttenberg-Richter relationship. It is measured as the magnitude of the maximum curvature by computing the maximum value of the first derivative of the Gutenberg-Richter frequency-magnitude curve. This magnitude of completeness is the lower limit so we certainly know the magnitude of completeness is not lower (because it would not fit to G-R relationship). If possible we compare our computed M_c with the M_c determined for each region by different author to see if we have not underestimated the seismic catalogue completeness. Each seismic catalogue was cropped to its level of M_c and events with smaller magnitude than the magnitude of completeness were removed from the catalogue.

Following is categorized chosen catalogues description. Unless otherwise stated, seismic catalogue temporal evolution of magnitudes is plotted before the cut to M_c.

3.2.1 NATURAL VOLCANIC SWARM CATALOGS

3.2.1.1 Mt. Etna, Sicily, Italy

Mt. Etna, the highest active volcano in Europe, is located in eastern Sicily (Figure 12) in a complex geodynamic framework, along the main Eurasia–Africa convergent plate boundary (Dewey et al., 1989; Serpelloni et al., 2007). In this area, the major regional structural lineaments play a key role in the dynamic processes of the Mt. Etna volcano and are hypothesized to be the main seismogenic structures. These faults mostly follow two regional structural trends NE-SW and NNW-SSE (Bonaccorso et al. 1996; Gresta et al. 1998).

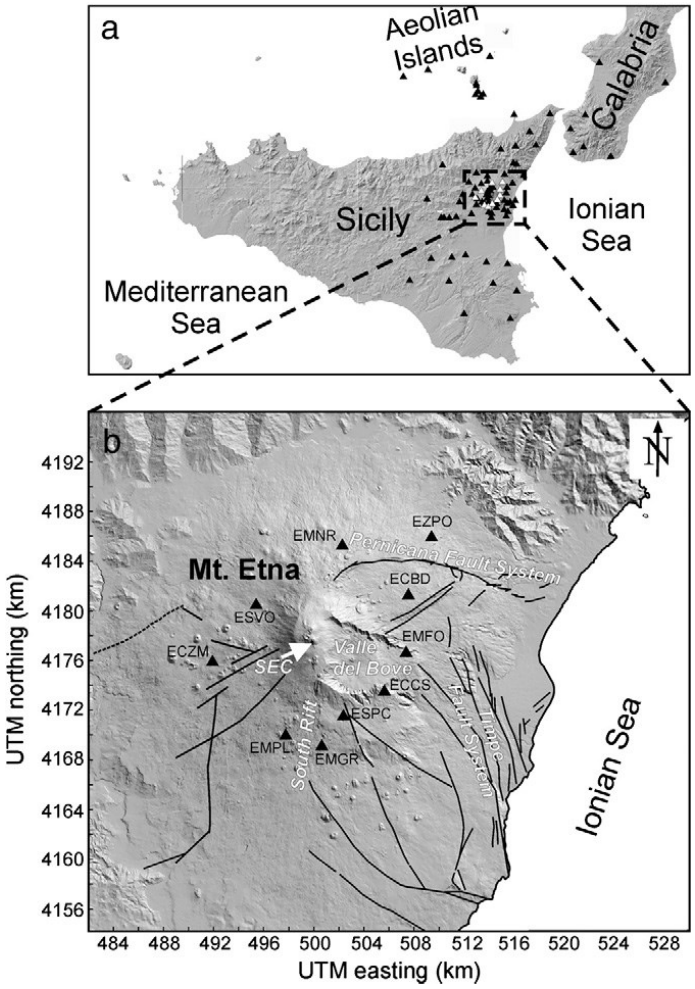

Figure 12. Map of the Mt. Etna earthquake region. (a) Map of Sicily and southern Calabria. The triangles indicate the stations of the seismic network, (b) Schematic structural map of Mt. Etna volcano. SEC indicates South East Crater (taken from Cannata et al., 2013).

Seismicity of the volcano area analyzed in Sicali et al. (2013) is characterized by a high rate of earthquakes of low and moderate energy and usually it occurs in form of swarms rather than with a MS-AS distribution (Alparone et al., 2010; Patanè et al. 2004). These seismic swarms occur both accompanied with eruptive phases (when the most energy is released) and during periods of ordinary background seismicity.

Table 1. Mt. Etna sequence statistical characteristics.

Mt. Etna						
Nr. of events	**start date**	**end date**	**M_{max}**	**M_{max} date**	**M_c**	**earthquake type**
107	*4.12.2009*	*31.12.2009*	*4.8*	*19.12.2009*	*2.0*	*volcanic swarm*

In this study a significant eruption – released seismic sequence, which occurred in the northwestern side of the volcano in 2009, is analyzed (for details see e.g. Alparone et al., 2010). This catalogue displayed in Figure 13 of Mt. Etna seismicity is resulting from the monitoring activities of the Istituto Nazionale di Geofisica e Vulcanologia, Osservatorio Etneo (Gruppo Analisi Dati Sismici, 2012). The local seismic network displayed in Figure 12 is made up of more or less 100 stations, located in an area of eastern Sicily, the Aeolian Islands and southern Calabria (Cannata et al., 2013). Seismic sequence characterized in Table 1 with magnitude completeness 2.0 is representative of volcanic swarm seismicity.

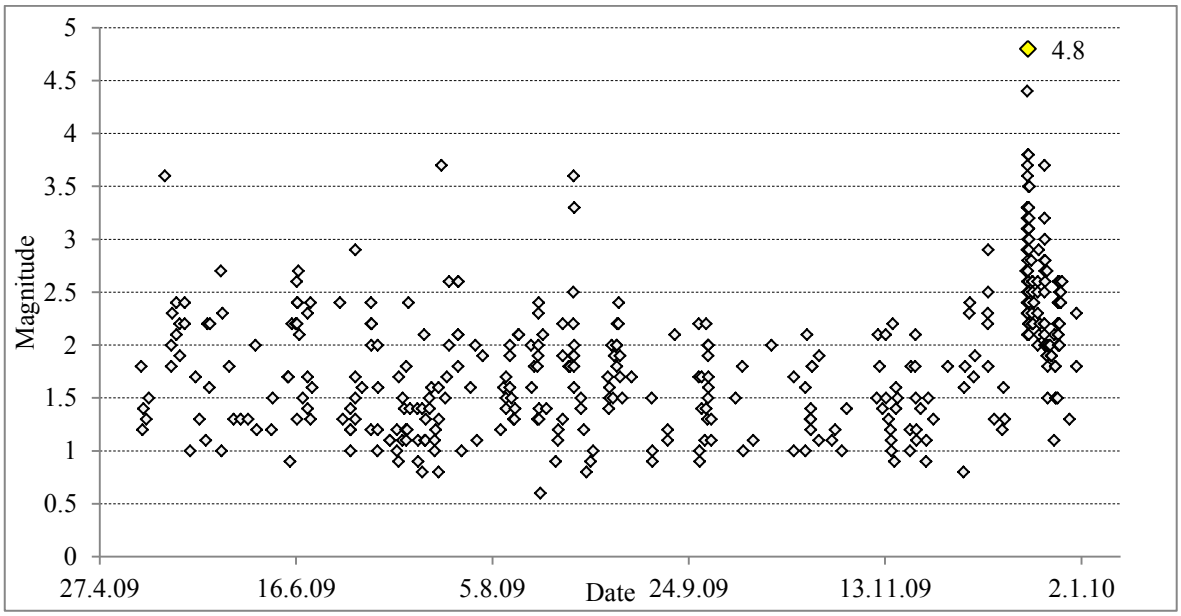

Figure 13. Mt. Etna seismic sequence 2009 temporal evolution of magnitudes. Mainshock is highlighted with the yellow square.

3.2.1.2 Yellowstone, United States of America

The Yellowstone volcanic field (Figure 14) of is one of the largest active caldera system in the world, with the highest concentration of hydrothermal features, reflecting its unique high convective ground water circulation related to magma crystallization (Christiansen, 2001; Fournier et al., 1989). Its volcanic history is marked by three caldera-forming eruptions. Last of these eruptions (0.64 Ma) shaped a 45 km by 70 km collapse caldera that subsided up to 500 m along caldera rim normal faults (Christiansen, 2001) (Waite and Smith, 2004). The Yellowstone Plateau belongs to the Intermountain seismic belt and is one of the most seismically active areas of the western U.S. (Smith and Arabasz, 1991).

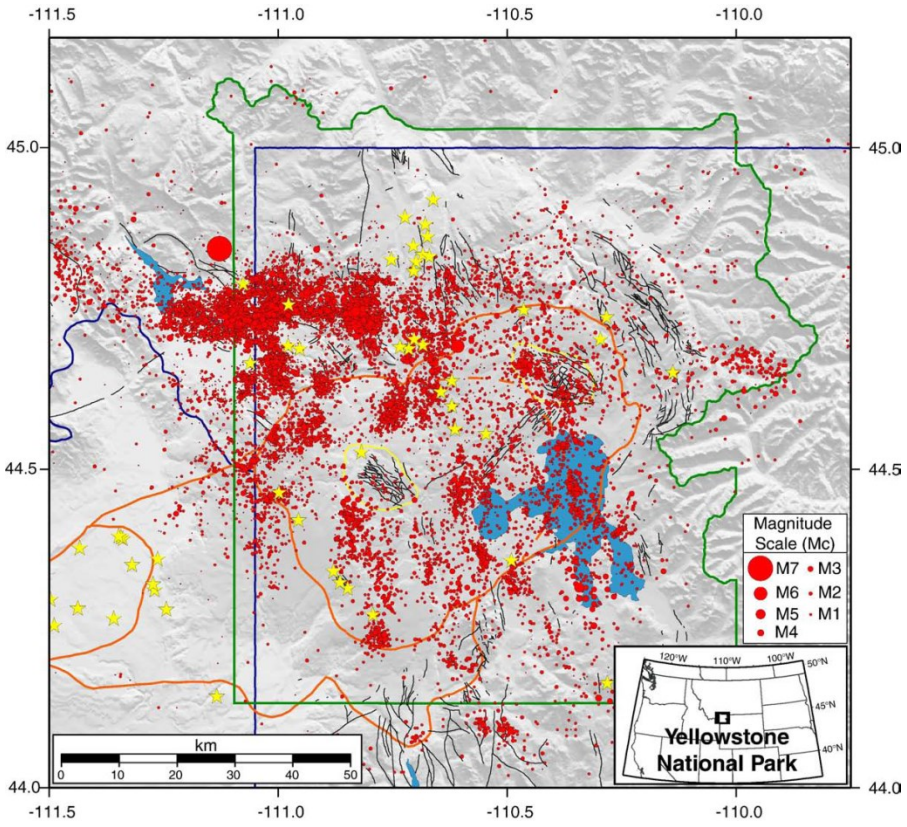

Figure 14. Illustration topographic map with earthquakes (red dots) of the Yellowstone region from 1973 to 1981 and 1984 to 2006. Late Quaternary faults are shown as black lines, caldera vents displayed as yellow stars. Detail description in Farraell et al. (2009).

Seismicity in Yellowstone is characterized by spatio-temporally clustered small, shallow swarm earthquakes (Farrell et al., 2009), that are probably attributed to the migration of magmatic or hydrothermal fluids (Waite and Smith, 2002).

Regional earthquakes have been continuously monitored since 1973 by permanent and temporary seismic stations operated by the U.S. Geological Survey (USGS), and the University of Utah Seismic Stations (UUSS). The seismic network characteristics and locations are summarized e.g. in Husen and Smith (2004). This deployment of local monitoring array has provided data for the earthquake catalogue that is analyzed in this study. Because of the time gap over 10 days defining here an earthquake sequence a single sequence (displayed in Figure 16) with the biggest number of events was selected from the long-term seismic catalogue (Figure 15). Table 1 shows statistical characteristics of this sequence.

Table 2. Yellowstone 2013 sequence Nr. 1 statistical characteristics.

YELLOWSTONE						
Nr. of events	**start date**	**end date**	**M_{max}**	**M_{max} date**	**M_c**	**earthquake type**
132	*1.9.2013*	*14.10.2013*	*3.6*	*15.9.2013*	*1.5*	*volcanic swarm*

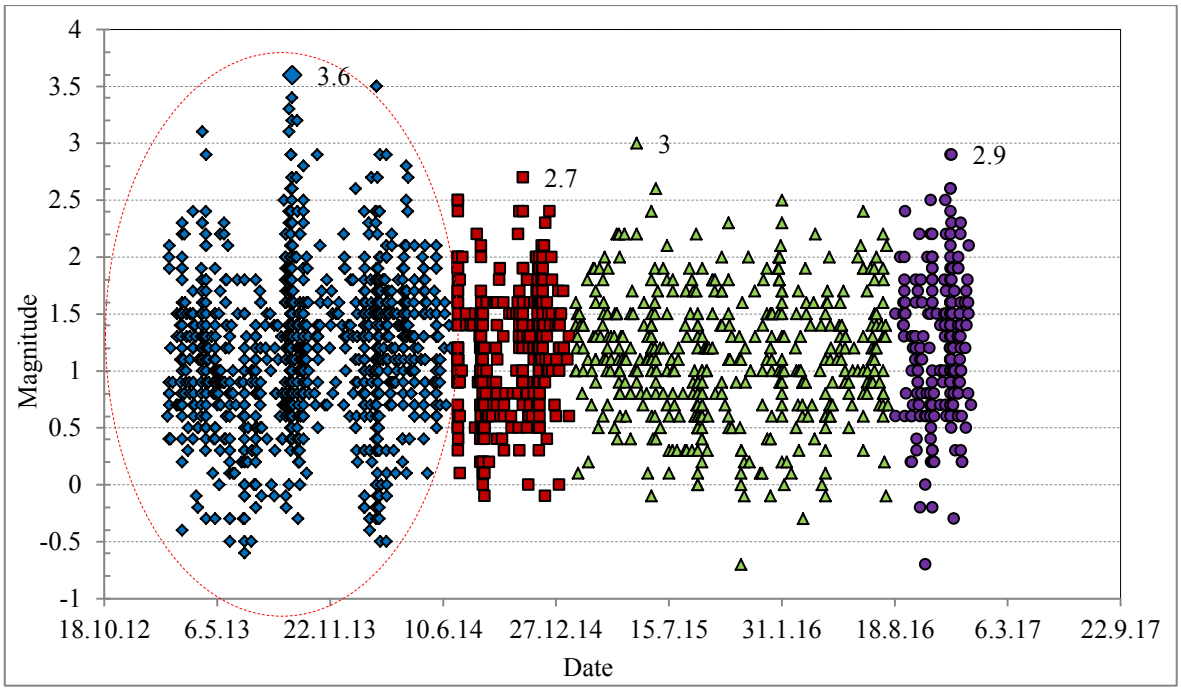

Figure 15. Yellowstone 2013 – 2015 seismic catalogue temporal evolution of magnitudes. From four temporally separated sequences (each plotted with different symbol and color) the first one (in dashed ellipse) was selected for further analyzes.

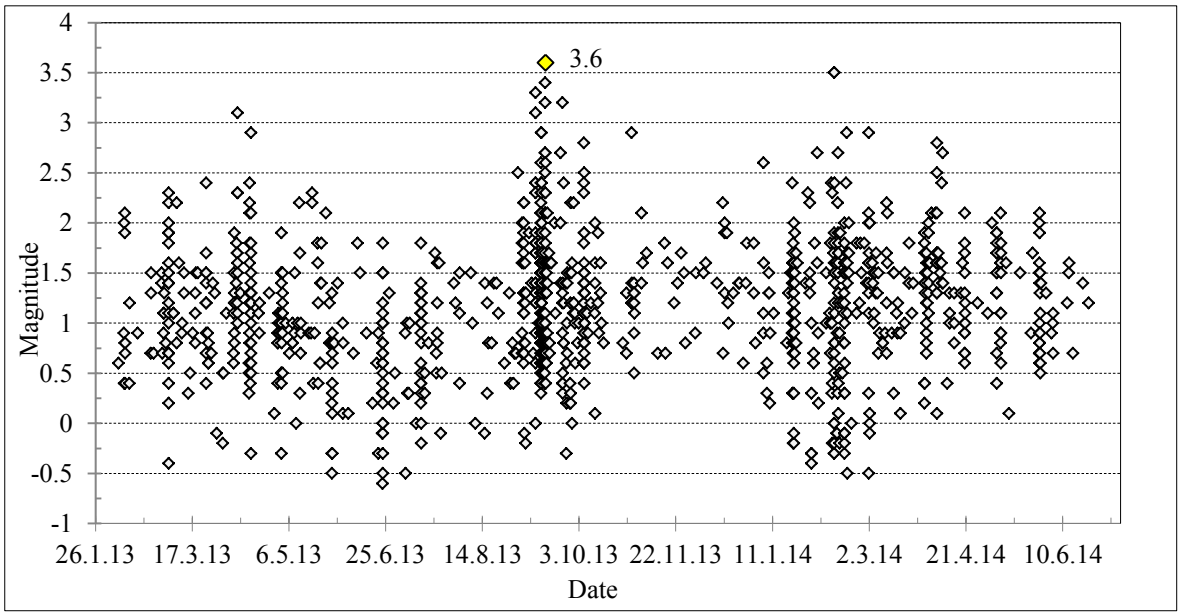

Figure 16. Yellowstone sequence Nr. 1 temporal evolution of magnitudes. Mainshock is highlighted with the yellow square.

3.2.2 NATURAL INTRAPLATE SWARM CATALOGUES

3.2.2.1 Arkansas, United States of America

The Arkansas seismicity is well-known for swarm-like character driven by fluid migration (e.g. Rabak et al., 2010). We use private dataset acquired with 5 monitoring stations in an area approximately 40 km from the well-known Enola swarm area (Jechumtalova, 2017).

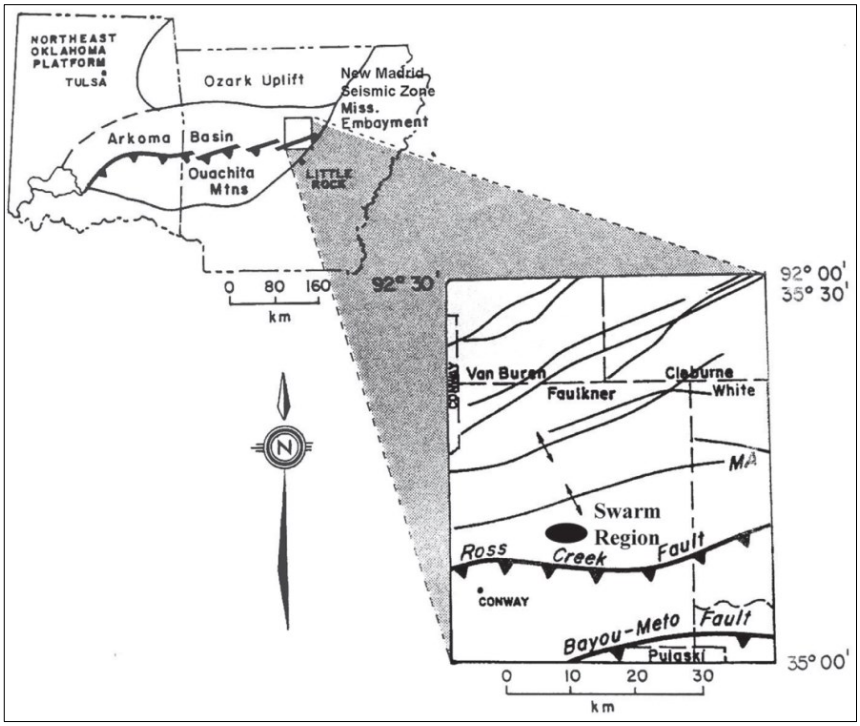

Figure 17. The Enola swarm region (in inset map highlighted by black ellipse) in the Arkoma Basin. Unlabeled curves in the inset map are normal faults Thrust faults have symbols on the hanging wall. MA = Morrilton anticline. Figure from Rabak et al. (2010).

The Enola swarm region is located in the Arkoma Basin, an intraplate setting north of the frontal Ouachita transition zone (Figure 17) and dominant part of the area is dominated by E-W trending folds and faults caused by Paleozoic N-S compression (VanArsdale and Schweig, 1990). Within the area of interest the Paleozoic sandstones and carbonates occur to a depth of 5 km, where the Precambrian basement starts (Schweig et al. 1991).

Earthquake swarm activity has been observed since January 1982 near the town of Enola and was potentially triggered by magma intrusion or natural fluid migration (e.g. Johnston, 1982).

Table 3. Arkansas swarm sequence Nr. 5 characteristics.

ARKANSAS						
Nr. of events	**start date**	**end date**	**M_{max}**	**M_{max} date**	**M_c**	**earthquake type**
990	*1.10.2015*	*11.10.2015*	*1.8*	*1.10.2015*	*-0.8*	*intraplate swarm*

Temporal evolution of magnitudes of seismic events detected with the local network is shown in Figure 18. The catalogue contains approximately 7 main high activity periods. From 7 sequences (clusters) in time period 2014 – 2015 one (Nr. 5) was chosen for further analyzes. This sequence is shown in detail in Figure 19 and its statistical parameters are described in Table 3. Catalogue is characterized with M_c -0.8 which is due to local seismic stations in the vicinity of swarm area. Arkansas intraplate swarms sequences in our catalogue are distinctly temporally separated with the maximum magnitudes not exceeding M 3.

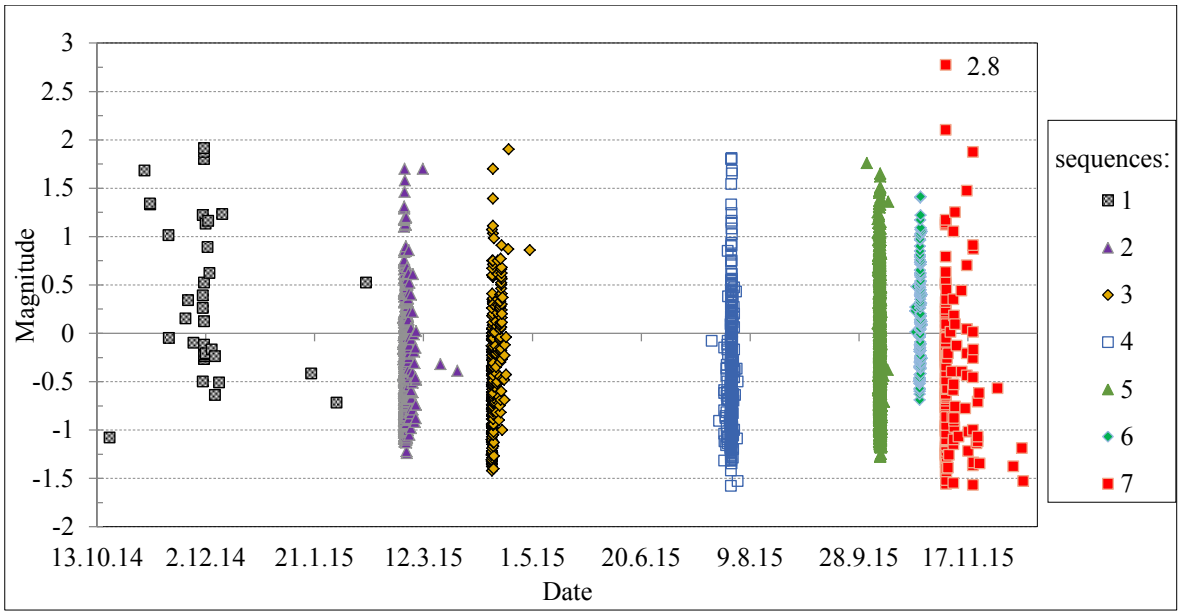

Figure 18. Temporal evolution of magnitudes of Arkansas seismic catalogue which contains 7 sequences (each plotted with different symbols and color) in time period 10/2014 - 12/2015. Sequence Nr. 5 (green tringles) was selected for further analyses.

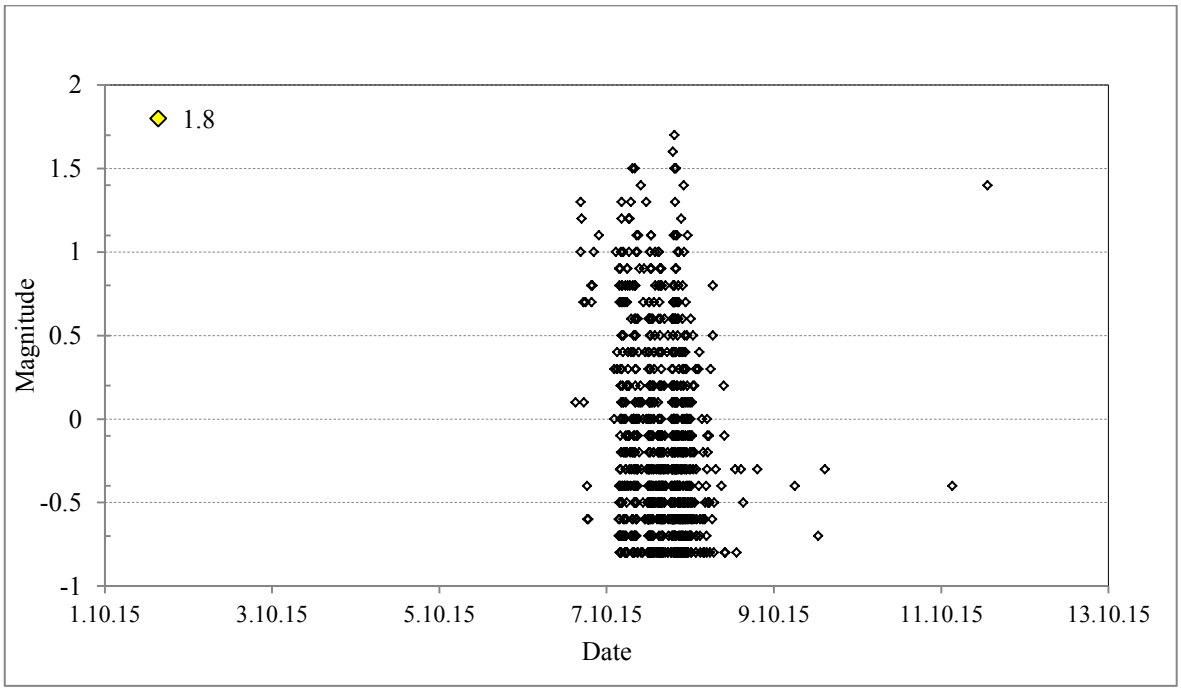

Figure 19. Temporal evolution of magnitudes for events M≥-0.8 in the Arkansas sequence Nr. 5 with highlighted mainshock (yellow square).

3.2.2.2 West Bohemia, Czech Republic

The West Bohemia natural earthquake swarm region is unique European intraplate area that displays present activity of geodynamic processes, such as degassing of CO_2 and persistent seismic activity (Fischer et al., 2013). This region belongs to the western part of the Bohemian Massif and is situated in the transition zone among three different Variscan structural units (see Figure 20): (I) the Saxothuringian, (II) the Teplá-Barrandian and (III) the Moldanubian (Babuška and Plomerová 2008). The most seismic active area is located at the intersection of two tectonic structures: the ENE–WSW trending Eger Rift with the Eger Graben in the center and the N–S striking Regensburg–Leipzig–Rostock Zone (Bankwitz et al., 2003).

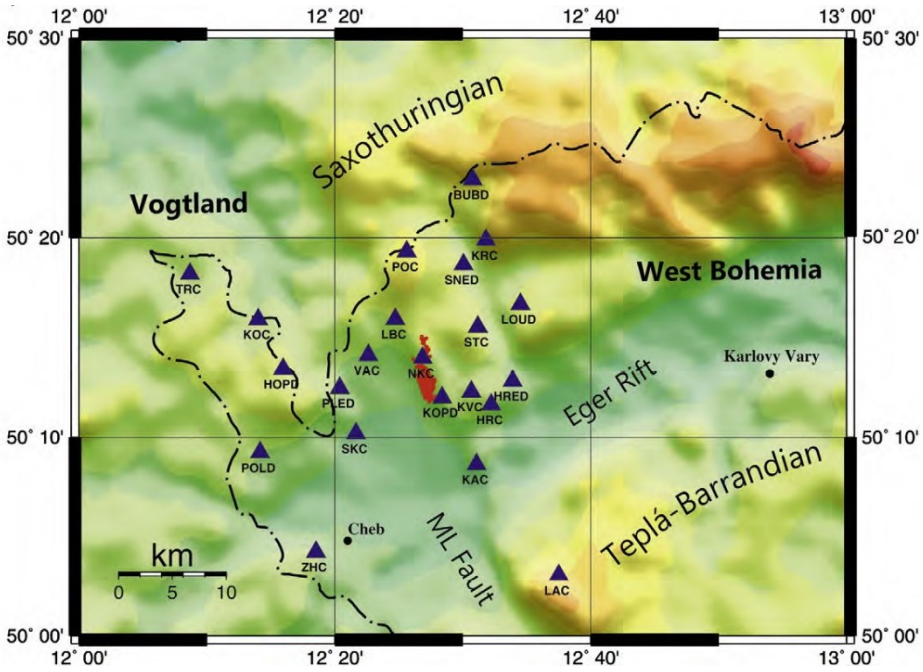

Figure 20. Topographic map of West Bohemia swarm region with marked seismic stations of the WEBNET network (blue triangles), hypocenters location of the 2008 swarm (red dots) and tectonic units of the Bohemian Massif. ML Fault - Mariánské Lázně Fault (modified after Fischer et al. (2013)).

Seismic activity has been reported since the 16th century (Grünthal et al., 1989) and is dominated by periodically repeating earthquake swarms with magnitudes not exceeding M_L 5 (Fischer et al., 2013). These intraplate swarms origin is discussed is the connection to the recent Quaternary volcanism (Ibs-von Seht et al., 2008).

Table 4. West Bohemia swarm sequence statistical characteristics.

WEST BOHEMIA						
Nr. of events	**start date**	**end date**	**M_{max}**	**M_{max} date**	**M_c**	**earthquake type**
1921	*6.10.2008*	*10.12.2008*	*3.7*	*12.10.2008*	*0.7*	*intraplate swarm*

For further analyzes significant swarm in fall 2008 (for details see e.g. Fischer et al., 2010) was chosen (Figure 21). This catalogue contains events in the magnitude range $-0.5 < M_L < 3.7$ with a magnitude of completeness M_c of 0.7 and was recorded by 13 to 23 permanent stations of the regional WEBNET (West Bohemia seismic network). This intraplate swarm is strongly clustered in space and time, is relatively short in duration and rapidly releasing seismic moment compared to previous swarm activity in the region. The magnitude–frequency distribution of the 2008 swarm shows a b-value close to 1 (Fischer et al., 2010). Characteristics of the 2008 swarm are displayed in Table 4.

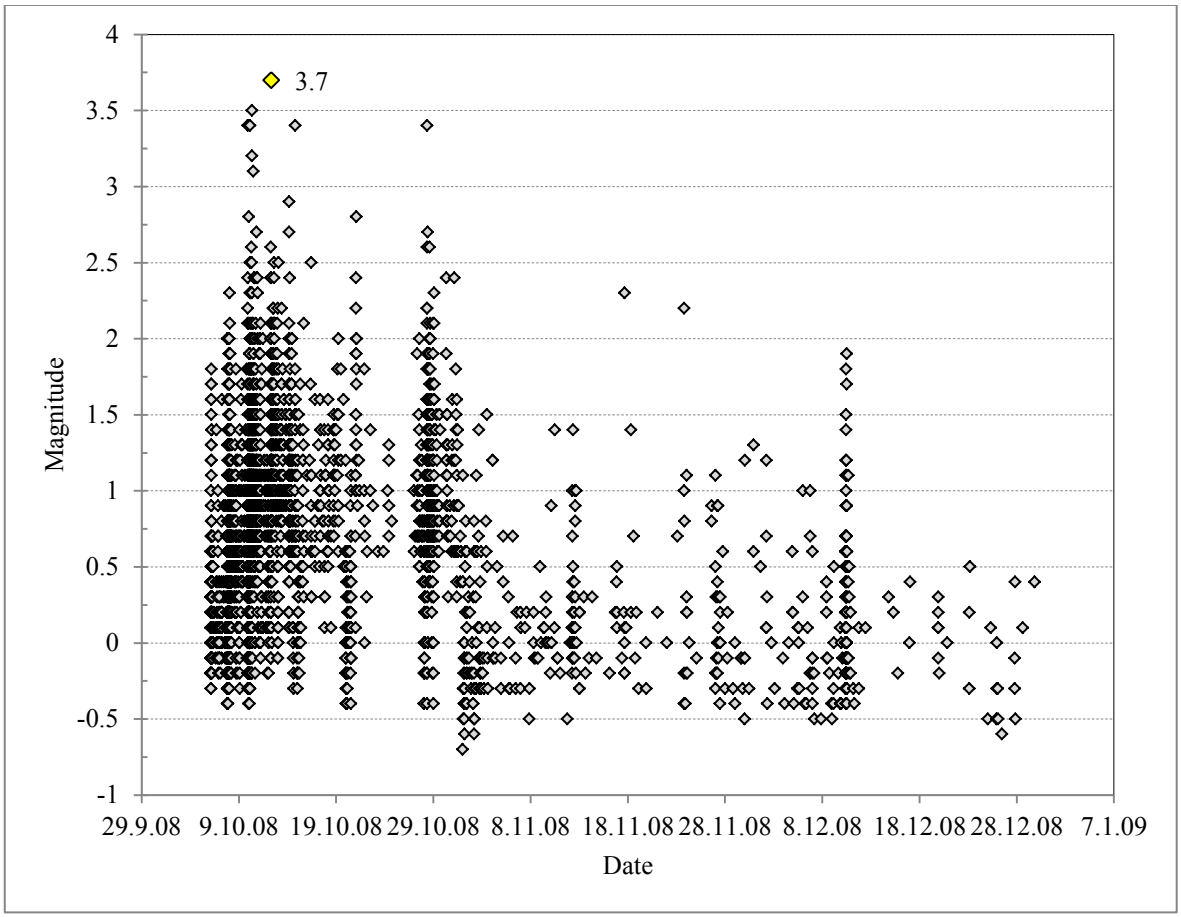

Figure 21. West Bohemia 2008 swarm sequence temporal evolution of magnitudes with the highlighted mainshock (yellow square).

3.2.2.3 Azle, Texas, United States of America

From November 2013 through February 2014, a series of earthquakes has been registered and felt in the area of the Newark East Gas Field (NEGF) near the cities of Azle and Reno in Texas (see map in Figure 23). Seismicity occurs on two steeply dipping, conjugate faults a primary normal fault and a shallower antithetic normal fault both consistent with the general strike of the Newark East fault zone (Pollastro et al., 2007; Hornbach et al., 2015). Figure 23 displays also NEGF cross-section with earthquake locations and basic Fort Worth Basin geology formations.

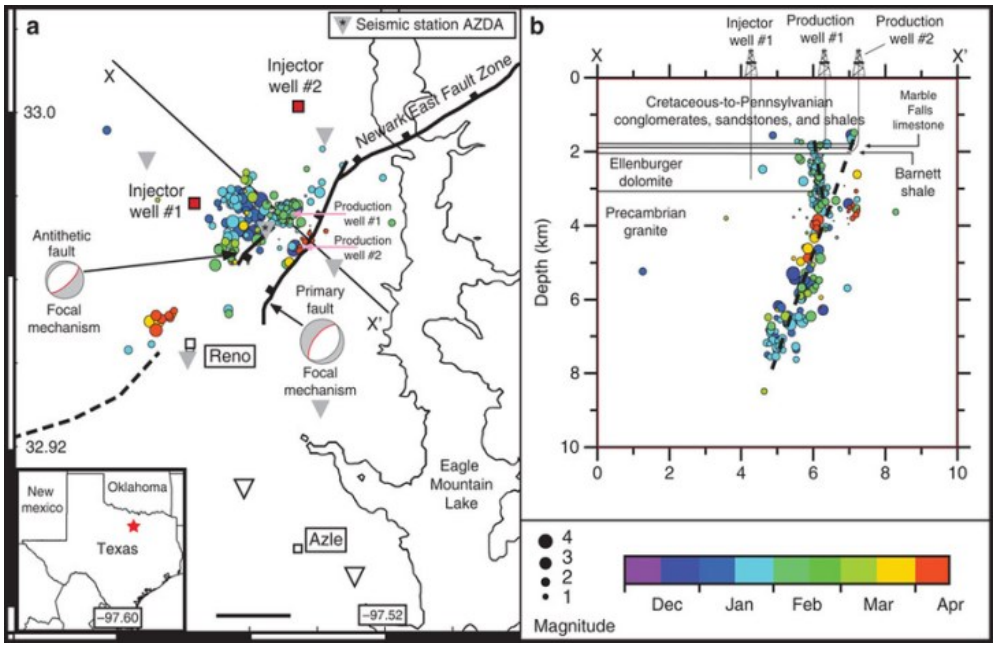

Figure 22. Azle earthquake region map. a) Map showing the situation in NEFZ with injection wells (red squares), production wells (pink arrows) and earthquake epicenters (colored circles) recorded by the temporary seismic network (grey/white triangles – active/inactive station). Line X–X' shows the location of the cross-section shown in (b) where earthquake locations, interpreted faults (dashed) and geology structures (Hornbach et al., 2015).

In NEGF hydraulic fracturing is applied to produce gas from the low permeability Mississippian Barnett Shale and brine and fracturing fluid produced from production wells are reinjected through disposal wells completed in the Ellenburger formation (Hornbach et al., 2015). Historically, there has been no evidence for seismicity in this region or along this fault. The natural or anthropogenic origin of the recent seismicity is still questioned. In Hornbach et al. (2015) brine production combined with wastewater disposal is discussed as the most likely cause of recent seismicity. We analyze this seismic sequence to see if we can find any similar statistical behavior with any of the natural or induced catalogues.

Earthquake activity of selected catalogue was registered by seismic network which consist of the U.S. Geological Survey stations and temporary seismic stations additionally deployed in December 2013 and January 2014. Events detection was obtained by cross-correlation. Figure 22 displays seismic stations positions. For the network settings details see Hornbach et al. (2015) and references therein.

Table 5. Azle sequence statistical characteristics.

AZLE						
Nr. of events	**start date**	**end date**	**M_{max}**	**M_{max} date**	**M_c**	**earthquake type**
418	*4.11.2013*	*15.2.2014*	*3.6*	*8.12.2013*	*1.2*	*intraplate swarm*

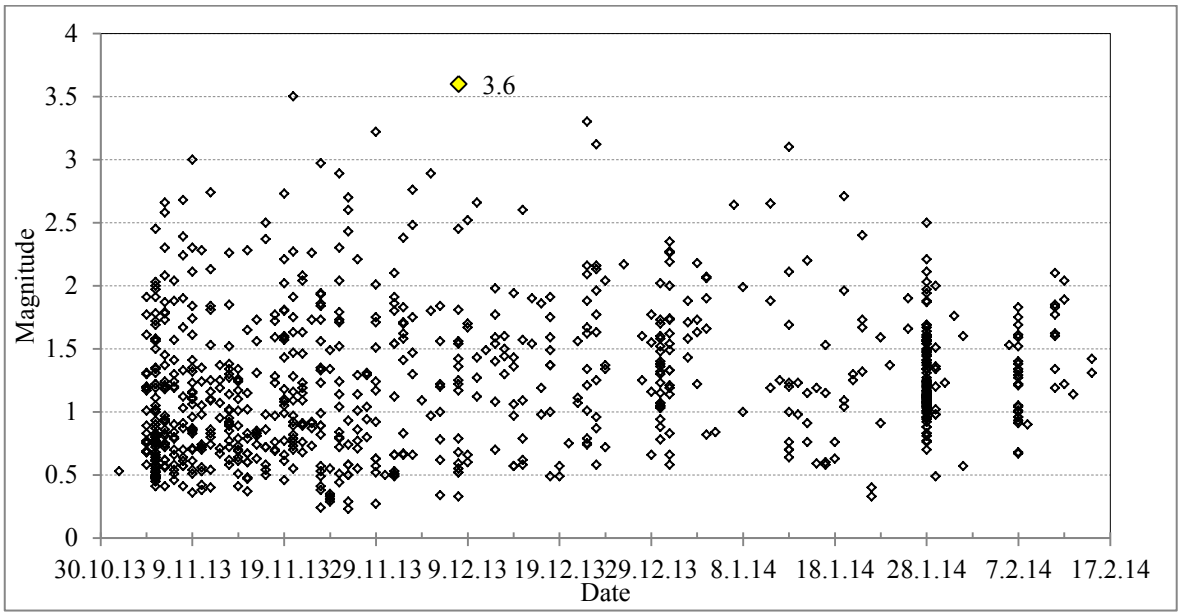

Figure 23. Texas Azle sequence temporal evolution of magnitudes. Mainshock is highlighted with the yellow square. Sequence contains two mainshocks with the same magnitude.

3.2.3 TECTONIC CATALOGUES

3.2.3.1 Hector Mine, California, United States of America

On 16 October 1999, the M_w 7.1 Hector Mine earthquake occurred in the Mojave Desert, California, approximately 200 km east-northeast of Los Angeles (Rymer et al., 2002). The earthquake ruptured the surface along the Lavic Lake fault, the Bullion fault, and segments of several other faults within the Eastern California Shear Zone (ECSZ) (Scientist from the USGS et al., 2000). The ECSZ is characterized by high seismicity, a high tectonic strain rate, and a broad, distributed zone of NNW trending faults (Dokka and Travis, 1990). Parsons and Dreger (2000) speculate that the 1992 nearby Landers earthquake M 7.3 triggered the Hector Mine earthquake through elastic stress transfer (see the regional map showing both earthquakes in Figure 24). For the purpose of this study we shall neglect this discussion and assume this earthquake as an example of MS-AS.

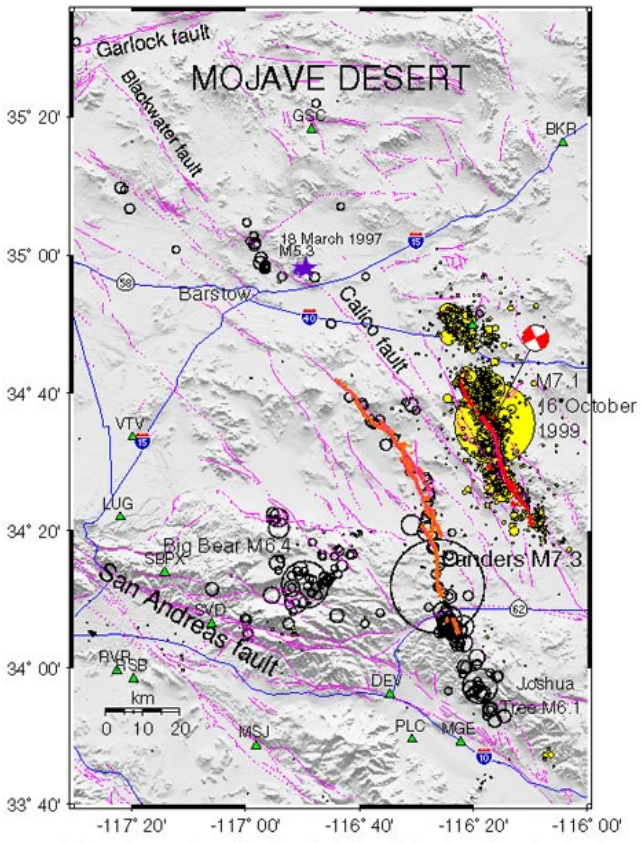

Figure 24. Map of the Mojave Desert region showing regional faults (light pink lines) and topography (gray-scale). Black circles indicate seismicity related to the 1992 Joshua Tree-Landers-Big Bear sequence. Filled yellow circles represent 1999 Hector Mine earthquake. Red lines show surface rupture associated with the Landers and Hector Mine earthquakes. TriNet seismic stations displayed as green triangles (Scientist from the USGS et al., 2000).

Table 6. Hector Mine tectonic sequence statistical characteristics.

HECTOR MINE						
Nr. of events	**start date**	**end date**	**M_{max}**	**M_{max} date**	**M_c**	**earthquake type**
3107	*15.10.1999*	*28.11.2000*	*7.1*	*16.10.1999*	*2.1*	*tectonic MS-AS*

In our selection the Hector Mine earthquake with the significant mainshock-driven seismicity represents typical tectonic MS-AS sequence, displayed in Figure 25. The mainshock Mw 7.1 was preceded within 20 hours by 18 recorded foreshocks of $1.5 \leq M \leq 3.8$ and followed by a massive long-lasting aftershock activity with a gradual decay. Seismic catalogue contains data from the Southern California Seismic Network (SCSN), operated by the U.S. Geological Survey and the California Institute of Technology (TriNet), see Figure 24 (Hauksson et al., 2002).

For this seismic catalogue $M_c = 1.5$ with the MCAX technique was calculated. However, after comparison of our M_c value with suggested values in Felzer et al. (2002) and Wiemer et al. (2002) we decided to use $M_c = 2.1$. This helped us to decrease the large number of events and temporally shorten the sequence. We analyzed the catalogue with our discrimination criteria for both M_c values (2.1 and 1.5) and the overall conclusions were identical. Here we present results for Mc 2.1. For Hector Mine MS-AS statistical characteristics see Table 6.

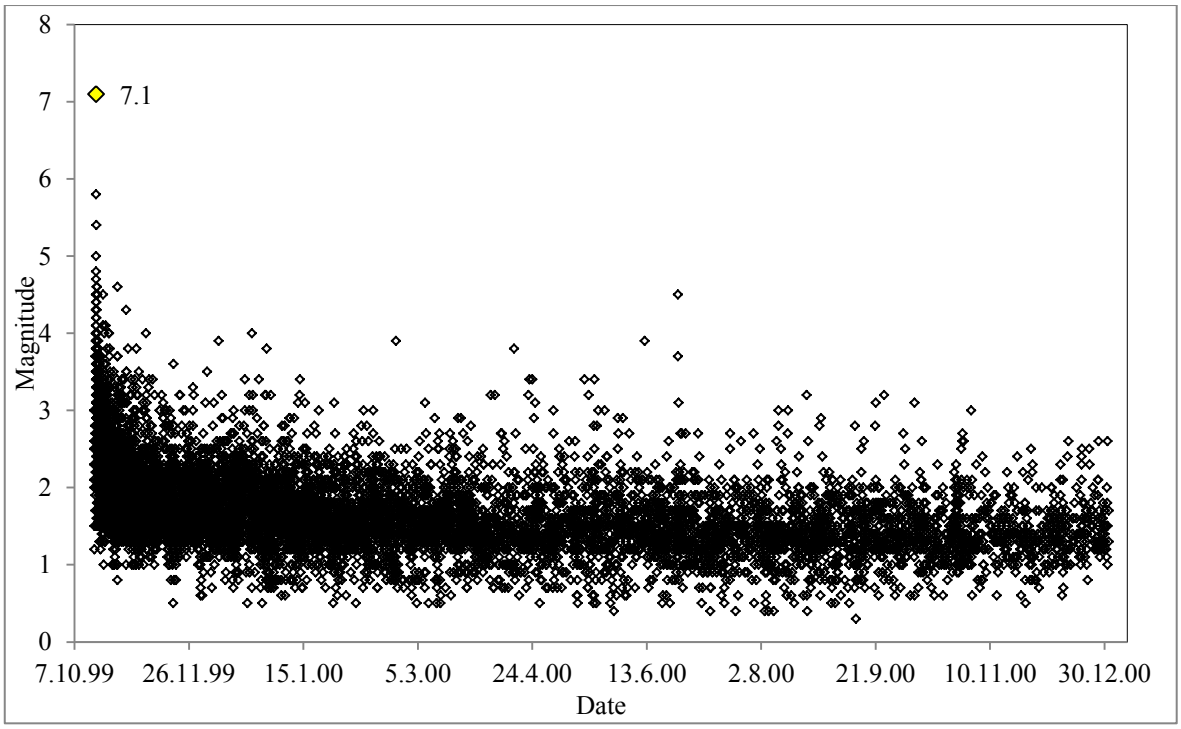

Figure 25. Hector Mine tectonic sequence 1999-2000 temporal evolution of magnitudes. Mainshock Mw 7.1.is highlighted with the yellow square.

3.2.3.2 Parkfield, California, United States of America

The 2004 M_w 6.0 Parkfield earthquake occurred on 28 September on the San Andreas Fault with the epicenter located 11 km southeast of the town Parkfield in central California (see Figure 26). Parkfield is the transitional section of the San Andreas Fault between the creeping section to the northwest and the locked section to the southeast. The geologic structure is very complex to the east of the fault, where mostly Mesozoic sedimentary and metamorphic rocks are exposed. To the west, the geologic structure is less complex, with sedimentary deposits of late Cenozoic age over more complex Mesozoic bedrock of the Salinian block (Langbein et al., 2005; Shakal et al., 2005).

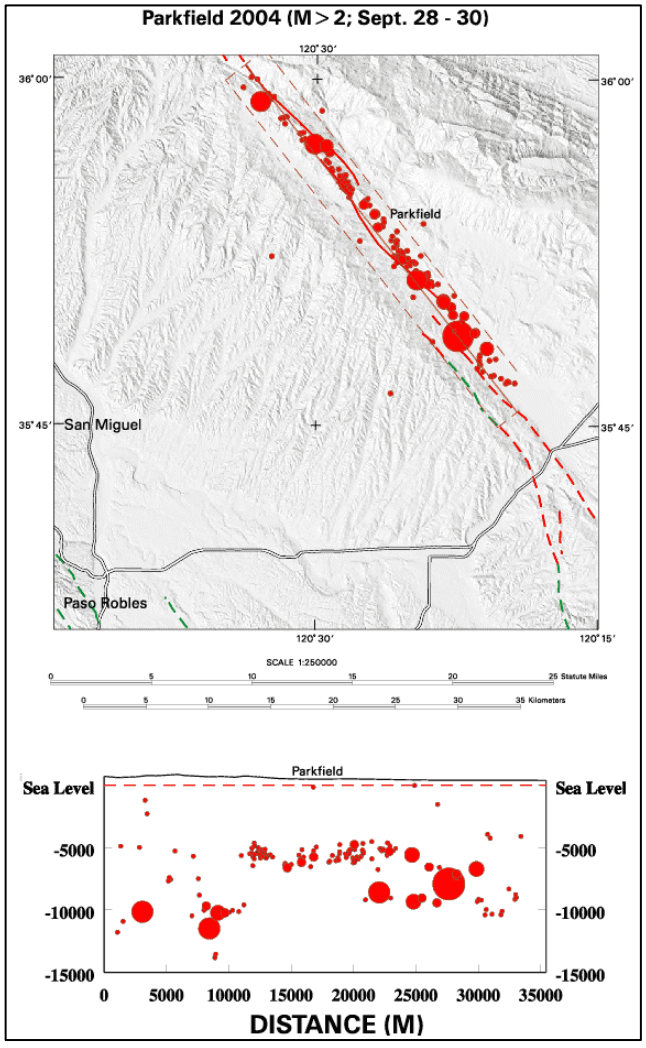

Figure 26. Parkfield 2004 earthquake schematic map. Map is showing M>2 aftershocks following the 2004 M_w 6.0 earthquake in Parkfield. Below the map is a cross-section showing events size and depth along the fault within the dashed red box [4].

Here we analyze seismic catalogue obtained from the Northern California Earthquake Data Center (NCEDC, 2014) acquired by the Parkfield strong-motion array, which acquired in the time of 2004 earthquake 56 three-component recordings of acceleration were within 20 km of the fault, with 48 of these being within 10 km of the fault. This array includes instruments installed and maintained by the California Geological Survey (CGS) and the U.S. Geological Survey (USGS) (see Mcjunkin and Shakal, 1983).

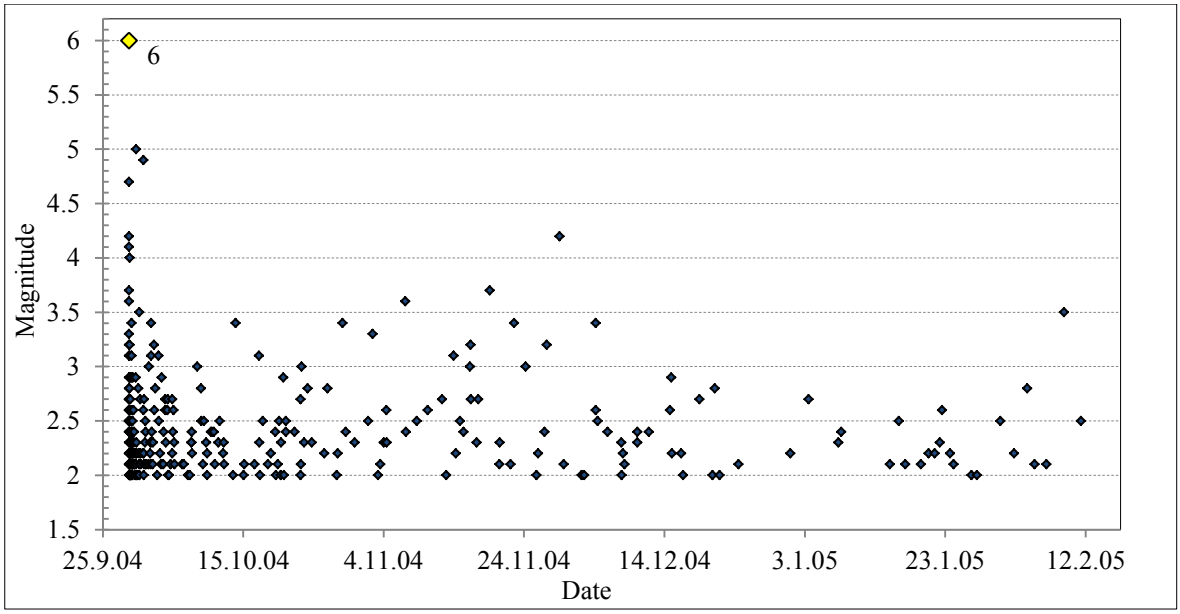

Figure 27. Parkfield 2004 tectonic sequence temporal evolution of magnitudes plotted events with M≥2. Mainshock is highlighted with the yellow square.

Parkfield tectonic catalogue (Figure 27) analyzed in this study consists of 331 events above the M_c = 2 (for more statistical details see Table 7.). This earthquake was selected for its characteristic tectonic MS-AS behavior with the large mainshock in the beginning of the sequence.

Table 7. Parkfield tectonic sequence statistical characteristics.

PARKFIELD						
Nr. of events	**start date**	**end date**	**M_{max}**	**M_{max} date**	**M_c**	**earthquake type**
331	*28.9.2004*	*11.2.2005*	*6.0*	*28.9.2004*	*2.0*	*tectonic MS-AS*

3.2.3.3 Wheeler Ridge, California, United States of America

California settlement Wheeler Ridge located in the southwestern San Joaquin Valley felt in 2005 two moderate magnitude tectonic earthquakes. First earthquake M 4.6, called here as Wheeler Ridge 1 (WR 1) occurred on April 16 with mainshock located 21 km west of Wheeler Ridge with 6 km depth and the second M 4.7, called here Wheeler Ridge 2 (WR 2) occurred on September 22 [5].

Wheeler Ridge is located in the *Big Bend* region of the San Andreas Fault, where the generally NW-SE trending fault strikes more E-W (see the map in Figure 28). This region is an E-W trending anticline that is actively deforming on the upper plate of the Pleito–Wheeler Ridge thrust fault system (Keller et al., 1998).

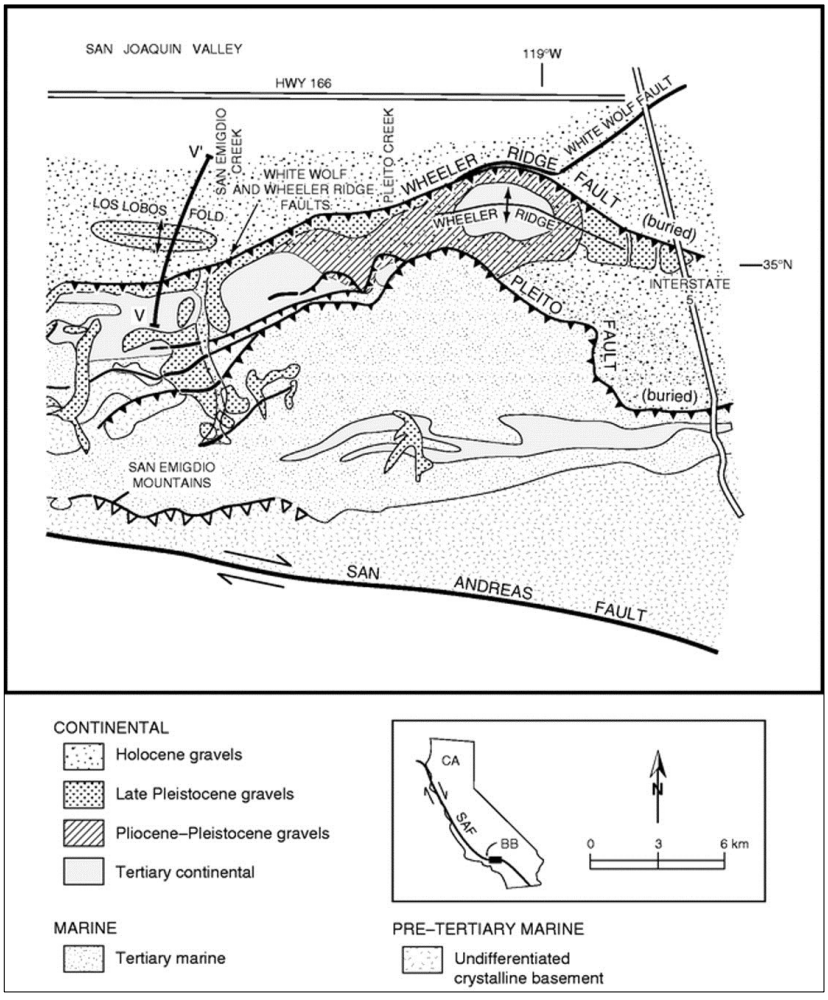

Figure 28. Generalized geologic setting at Wheeler Ridge location (top map). Small frame shows San Andreas fault (SAF) position along the California, location of the Wheeler Ridge earthquakes - Big Bend is marked as BB (Keller et al., 1998).

Data for the catalogue used in this study were provided by Southern California Earthquake Center (SCEDC, 2013) and acquired by the USGS National Strong-Motion Network (NSMN). Catalogue displayed in Figure 29 consists of two sequences WR 1 and WR2 temporally separated by time gap of 11 days. Discrimination analysis was carried for this tectonic MS-AS out on both sequences separately. See statistical characteristics of WR 1 and WR 2 in Table 8 respectively in Table 9.

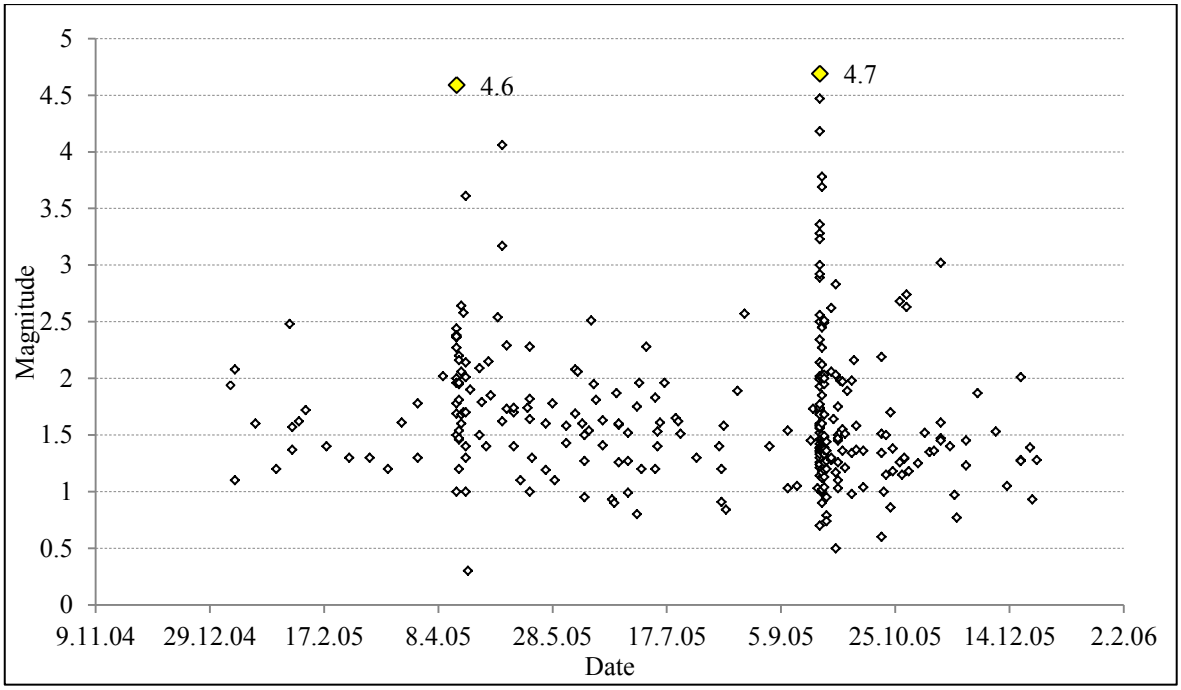

Figure 29. Wheeler Ridge 2005 seismic catalogue temporal evolution of magnitudes with two clusters separated with eleven day time gap. Mainshocks are highlighted with the yellow square.

Table 8. Wheeler Ridge 1 tectonic sequence statistical characteristics.

WHEELER RIDGE 1						
Nr. of events	**start date**	**end date**	**M_{max}**	**M_{max} date**	**M_c**	**earthquake type**
65	*10.4.2005*	*22.7.2005*	*4.6*	*16.4.2005*	*1.6*	*tectonic*

Table 9. Wheeler Ridge 2 tectonic sequence statistical characteristics.

WHEELER RIDGE 2						
Nr. of events	**start date**	**end date**	**M_{max}**	**M_{max} date**	**M_c**	**earthquake type**
114	*18.9.2005*	*8.12.2005*	*4.7*	*22.9.2005*	*1.4*	*tectonic*

3.2.4 INDUCED SEISMICITY CATALOGUES

3.2.4.1 North America

Private catalogue of seismicity induced by hydraulic fracturing operations is located in North America continent. We do not specify exact location or other related details here. Hydraulic fracturing was applied in the depth of ~ 2.5 km. Seismicity was monitored by local broad band seismic network consisting of 7 stations with approximate 5 km spacing. Hydraulic fracturing operations were carried out below the array and the volumes and pressures were controlled and modified when large seismic events occurred to reduce magnitudes of the largest events. Magnitudes are determined as moment magnitudes.

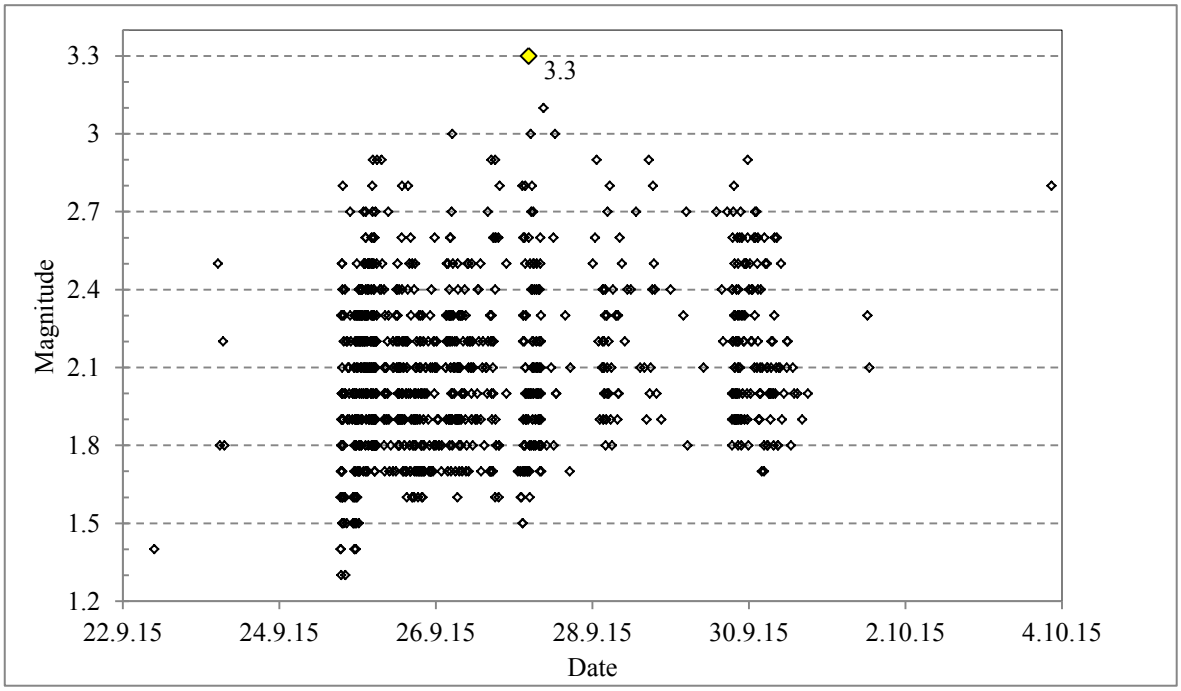

Figure 30. North America catalogue temporal evolution of magnitudes. Mainshock is highlighted with the yellow square.

Characteristic feature of the North America catalogue displayed in Figure 30 is seismicity clustered in time without any outstanding mainshock. The magnitude range is from 1.3 to 3.3 with two maximum magnitudes reaching 3.3 with time difference 40 minutes. Dataset characteristic are summarized in Table 10.

Table 10. North America sequence statistical characteristics.

NORTH AMERICA						
Nr. of events	**start date**	**end date**	**M_{max}**	**M_{max} date**	**M_c**	**earthquake type**
503	*23.9.2015*	*4.10.2015*	*3.3*	*27.9.2015*	*2.1*	*human induced*

3.2.4.2 Preese Hall, United Kingdom of Great Britain and Northern Ireland

This dataset represents an example of induced seismicity caused by hydraulic fracturing at the first shale gas well in Preese Hall well (Clarke et al., 2014).

Seismic activity was triggered as the nearby preexisting fault was reactivated by the hydraulic fracturing in a strike-slip mode (mostly horizontal movement of blocks) because of its steep dip (angle of the fault with respect to the surface), optimal orientation relative to the current stress field, elevated pore pressure and other parameters (for details see Clarke et al., 2014), all of which resulted in a high slip tendency.

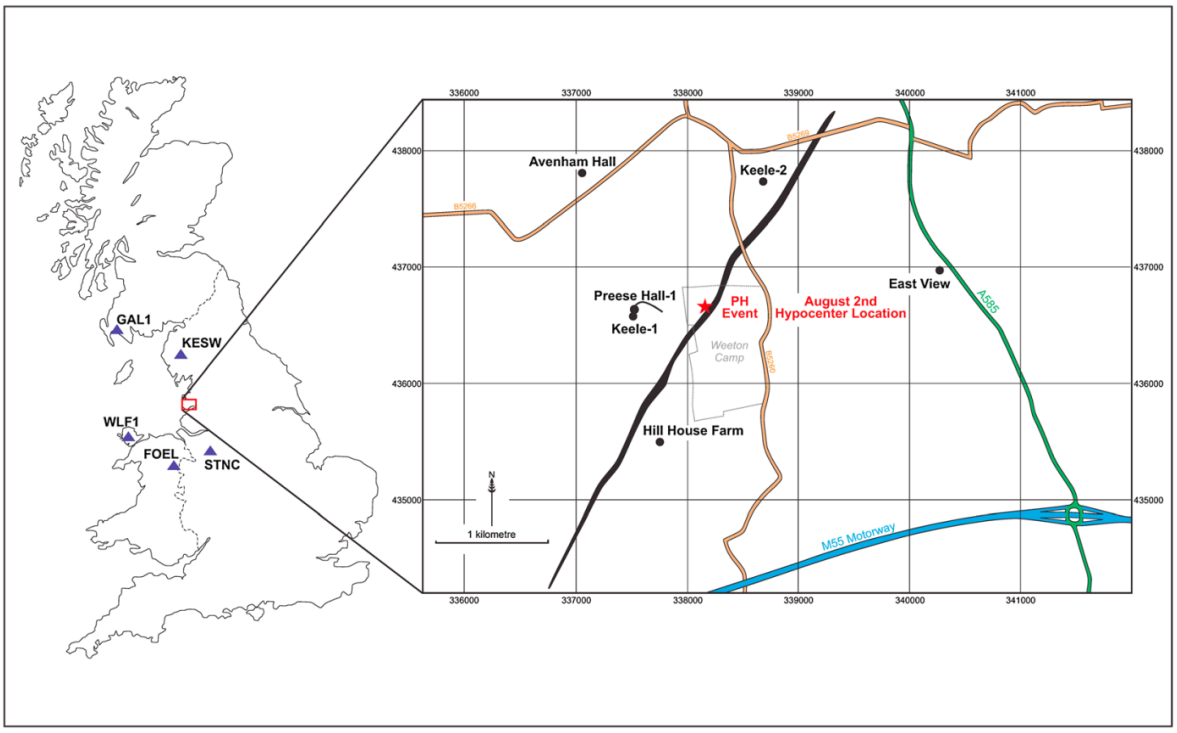

Figure 31. Situation map of Preese Hall area. Local stations are displayed as black dots and the national array stations as triangles. Short black curve indicates subvertical projection of the well trajectory and the black bold line shows a projection of the fault (Clarke et al., 2014).

Figure 31 shows location of the national seismic array stations and local temporary seismometer stations used to obtain the dataset. Figure 32 displays a timeline of deployment as well as the injection and seismic activity. Waveform cross correlation method is used by Clarke et al. (2014) to detect the events in the sequence. The events were not located (because the stations were too far) and only magnitudes and origin times were determined.

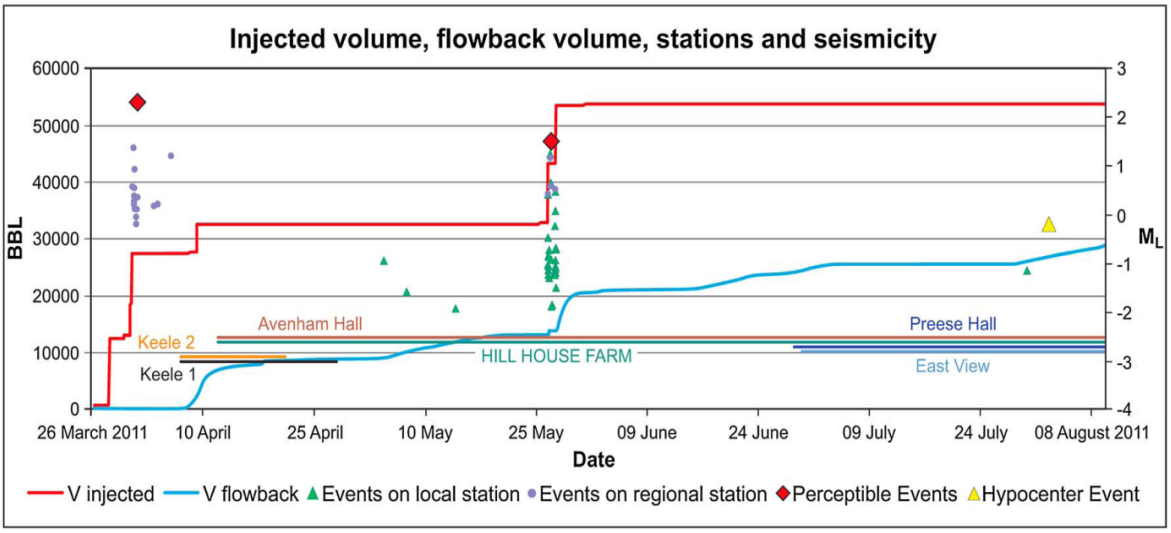

Figure 32. Injection and seismicity in the vicinity of the Preese Hall. The red curve represents injected volume, blue curve represents flow back volume from the well head (BBL - barrels). Violet dots symbolize seismic events detected on regional seismic stations, green triangles represent events detected on two local stations (Clarke et al., 2014).

Table 11. Preese Hall 1 sequences statistical characteristics.

PREESE HALL 1						
Nr. of events	**start date**	**end date**	**M_{max}**	**M_{max} date**	**M_c**	**earthquake type**
12	*31.3.2011*	*5.4.2011*	*2.5*	*1.4.2011*	*0.0*	*human induced*

Due to time gap exceeding 10 days the catalogue was split into two sequences: Preese Hall 1 (PH 1) and Preese Hall 2 (PH 2). This split also corresponds with 2 stages of hydraulic fracturing separated by more than 45 days. As shown in Figure 32 sequence Preese Hall 1 (Table 11) was obtained by regional seismic stations therefore its completeness is much lower than the sequence Preese Hall 2 (Table 12) which was detected by local stations.

Table 12. Preese Hall 2 sequences statistical characteristics.

PREESE HALL 2						
Nr. of events	**start date**	**end date**	**M_{max}**	**M_{max} date**	**M_c**	**earthquake type**
27	*26.5.2011*	*27.5.2011*	*1.7*	*27.5.2011*	*-1.0*	*human induced*

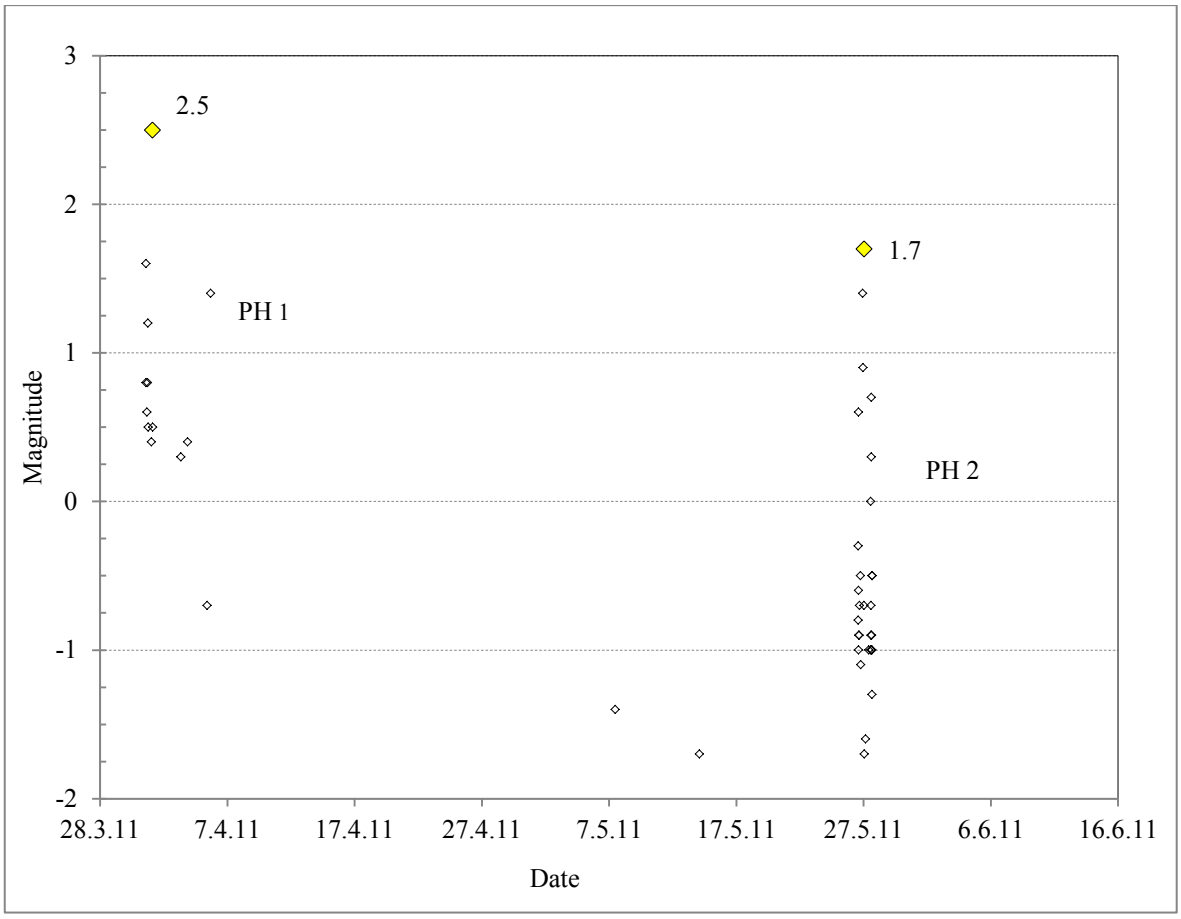

Figure 33. Temporal evolution of magnitudes of two sequences in Preese Hall (PH 1 and PH2) related to fluid injection volume. Mainshock is highlighted with the yellow square.

3.3 APPLICATION OF DIFFERENTIATION CRITERIA TO SEISMIC DATASETS

In this chapter we present results and discussion of analysis in which six criteria were applied on ten seismic catalogs. For each criterion we discuss statistical behavior assumption based on which tested seismic sequences are classified as a swarm or MS-AS.

3.3.1 EVENTS DENSITY

All tested catalogues contain more than 10 events and therefore the criteria can be applied to them. However, there is a large variation in the number of events in each dataset. Sequences with tectonic earthquakes with large mainshock usually have a very large amount of events in contrast with fluid injection induced earthquakes (e.g. Preese Hall) where only weak events were induced and no local monitoring network was available.

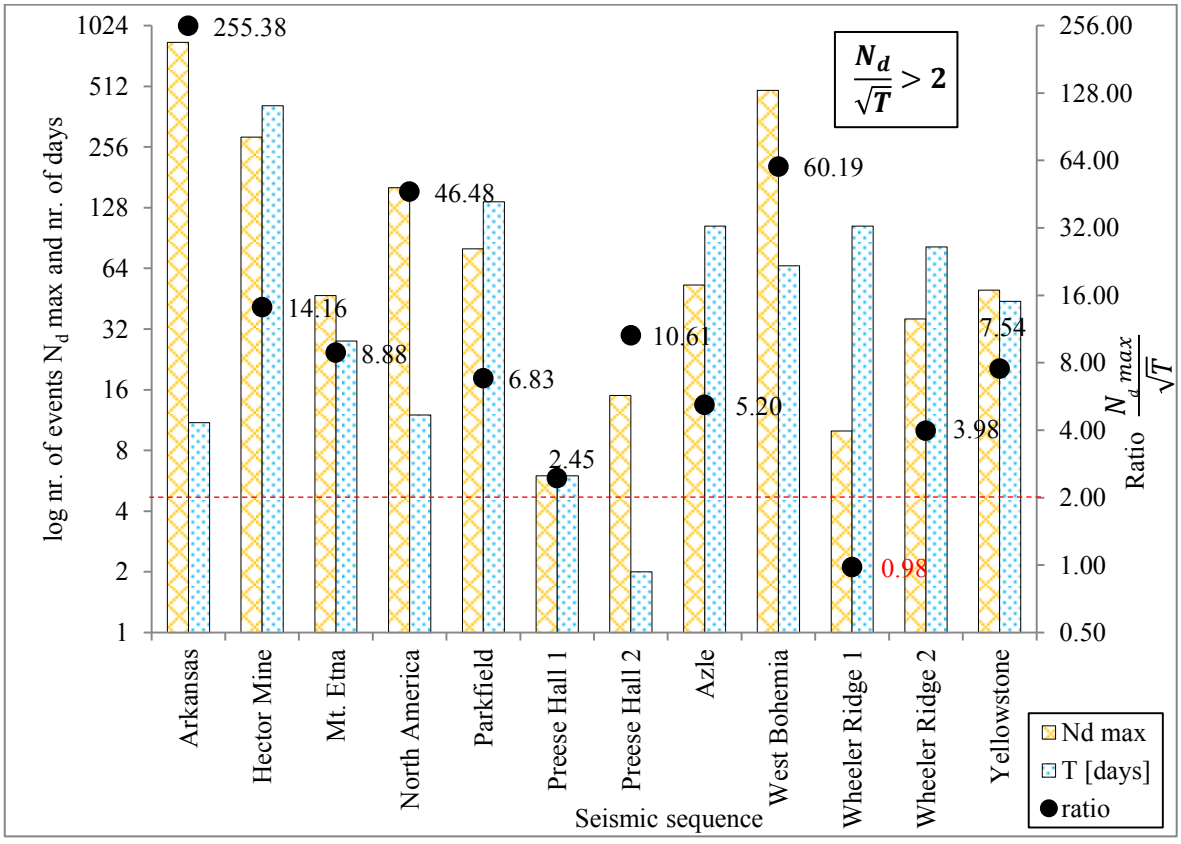

Figure 34. Plotted results for events density criterion. Comparison of seismic sequence duration T (blue dotted bars in days) and the maximum daily number of earthquake events in a sequence N_d max (yellow bars). Note that vertical axis is logarithmic with base 2. Black dots represent the ratio of $\frac{N_d\ max}{\sqrt{T}}$ *and red dashed line shows the ratio's lower limit for identification of swarms by Mogi (1963).*

The main criterion for differentiation between MS-AS and swarms is defined by empirical equation (Nr. 3): $\frac{N_d\ max}{\sqrt{T}} > 2$, described above (in Chapter 3.1.1).

All except one sequence are identified as swarms by this equation. Typical examples of earthquake swarms are West Bohemia and Arkansas datasets that reach the highest value for the equation Nr. 3. (high ratio due to abundant seismic activity in a short time). Also other swarms such as Mt. Etna sequence seems reach high value of 8.88. The Yellowstone volcanic swarm dataset has the ratio 7.54. However Azle sequence has smaller value of 5.20 bring it closer to classical tectonic and induced earthquake sequences.

The North America dataset has the highest ratio value (46.48) of all the tested induced seismicity catalogues. The Preese Hall 1 sequence is the only one of the tested sequences to have the equal number of T and $N_d\ max$ and with the equation Nr. 3 criterion reaching value 2.45 exceeds the defined limit for swarm just by 0.45. This induced dataset contains only 12 events in a 6 days long seismic sequence. In the second sequence of the Preese Hall catalogue dominates the $N_d\ max$ because the sequence last only two days and so the ratio is 10.61.

The Wheeler Ridge 1 sequence representing tectonic earthquakes is the only one of the tested datasets to have the ratio lower than the limit (see Figure 34), which is due to the long duration of seismic activity (107 days) and maximum daily activity of just 10 events. Although Wheeler Ridge 1 is tectonic MS-AS, ratio value 3.98 ranks its second sequence as swarm. Also large tectonic earthquakes like M_w 6.0 Parkfield or M_W 7.1 Hector Mine with the ratio 6.83 and 14.16, respectively, are identified as swarms.

It appears that the original threshold for a swarm definition is not suitable for datasets with very low magnitude of completeness as the number of events per day exponentially increases with lower magnitude of completeness. All natural swarm sequences were correctly identified as swarms by high values for the ratio of equation Nr. 3. However, we expected large tectonic MS-AS to show values below 2. But results of Hector Mine, Parkfield or Wheeler Ridge 2 show that this criterion is not able to differentiate between swarm and MS-AS and probably the original threshold of swarm identification should be higher (maybe 5?). This threshold does not show anything significant for the datasets representing induced seismicity, since their ratio vary from 2.45 to 46.48.

Perhaps such criterion is more suitable for catalogues spanning longer duration, but this criterion might be also very sensitive to definition of the duration of the sequence and magnitude of completeness as suggested above. In our study we define sequence as period between the first event to the last event before at last 10 day gap without seismicity. We tested other definitions of seismic sequence but none of them showed significantly better results. Obviously the definition of duration also depends on the quality of the catalogue characterized by magnitude of completeness and perhaps only comparing catalogues with the same magnitude of completeness would provide more meaningful results.

3.3.2 MAINSHOCK POSITION WITHIN THE SEQUENCE

Possible characterization among swarm, induced and MS-AS is the position of the mainshock within the sequence. We analyzed the time position of the mainshock and the number of foreshocks and aftershocks.

Table 13 shows number of events before and after the mainshock for and the time position of the mainshock for each dataset. We assumed swarm sequences to have the ratio of foreshocks and aftershocks close to 1 or dominance of foreshocks. The position of the mainshock could be random as it is not the control element of the sequence. In contrary we expected MS-AS datasets to be dominated by aftershocks (i.e. number of aftershock events and also days after the mainshock) because the sequence should be driven by the significant mainshock event. For example, the Hector Mine sequence is consistent with this expectation with 3096 aftershocks (10 foreshocks) and 409 days of activity after the mainshock and one day before the mainshock.

Table 133. Summary of results for mainshock position criterion. Number (Nr.) of foreshocks and aftershocks in studied datasets and their ratio is displayed in left 4 columns. Time position of the mainshock within the seismic sequence (in days) and its ratio is displayed in the right 4 columns.

Seismic sequence	Nr. of foreshocks (F)	Nr. of aftershocks (A)	ratio F/A	Nr. of days before the M_{max} (F_{days})	Nr. of days after the M_{max} (A_{days})	ratio A_{days}/F_{days}
Arkansas	*0*	*949*	*0*	*0*	*10*	-
Azle	*192*	*225*	*1.17*	*34*	*69*	*2.03*
Hector mine	*10*	*3096*	*0.003*	*1*	*409*	*409*
Mt. Etna	*29*	*77*	*0.38*	*15*	*12*	*0.80*
North America	*324*	*178*	*1.82*	*4*	*7*	*1.75*
Parkfield	*0*	*330*	*0*	*0*	*136*	-
Preese Hall 1	*7*	*4*	*1.75*	*1*	*4*	*4.00*
Preese Hall 2	*11*	*14*	*0.78*	*1*	*0*	*0*
West Bohemia	*1022*	*898*	*1.14*	*6*	*59*	*9.83*
Wheeler Ridge 1	*1*	*63*	*0.02*	*6*	*97*	*16.17*
Wheeler Ridge 2	*3*	*110*	*0.03*	*4*	*77*	*19.25*
Yellowstone	*91*	*40*	*2.28*	*14*	*29*	*2.07*

The other tectonic datasets – Parkfield and Wheeler Ridge show similar pattern of behavior with very little foreshocks and mainshock position in the first day of the sequence for Parkfield (330 aftershocks and 136 days after the M_{max}) and 1 and 3 foreshocks for WR1

and WR2, respectively (63 and 110 aftershocks, respectively). Also the time position of the M_{max} shows dominance of the aftershock days.

We observe two types of seismic temporal position of the mainshock in swarm datasets. The first type represents Arkansas intraplate swarm seismicity where each earthquake cluster is distinctly temporally separated (see Figure 19). In this case, the mainshock is the very first event of each sequence. The second type represents West Bohemia swarm region, where constant low magnitude background seismic activity accompanies the distinct clusters (see Figure 21). This means no dominance of either foreshocks or aftershocks and sequence have long durations. Analogous situation as in West Bohemia is in Azle dataset where number of foreshocks and aftershocks is nearly the same and the duration of aftershock is nearly twice as long as foreshocks. The Yellowstone swarm region has very similar ratio of days of foreshocks to days of aftershocks as Azle but twice more foreshocks than aftershocks. Results of Mt. Etna show twice more aftershocks than foreshocks but equal number of days before and after the mainshock which classifies Mt. Etna sequence as swarm according to our assumption.

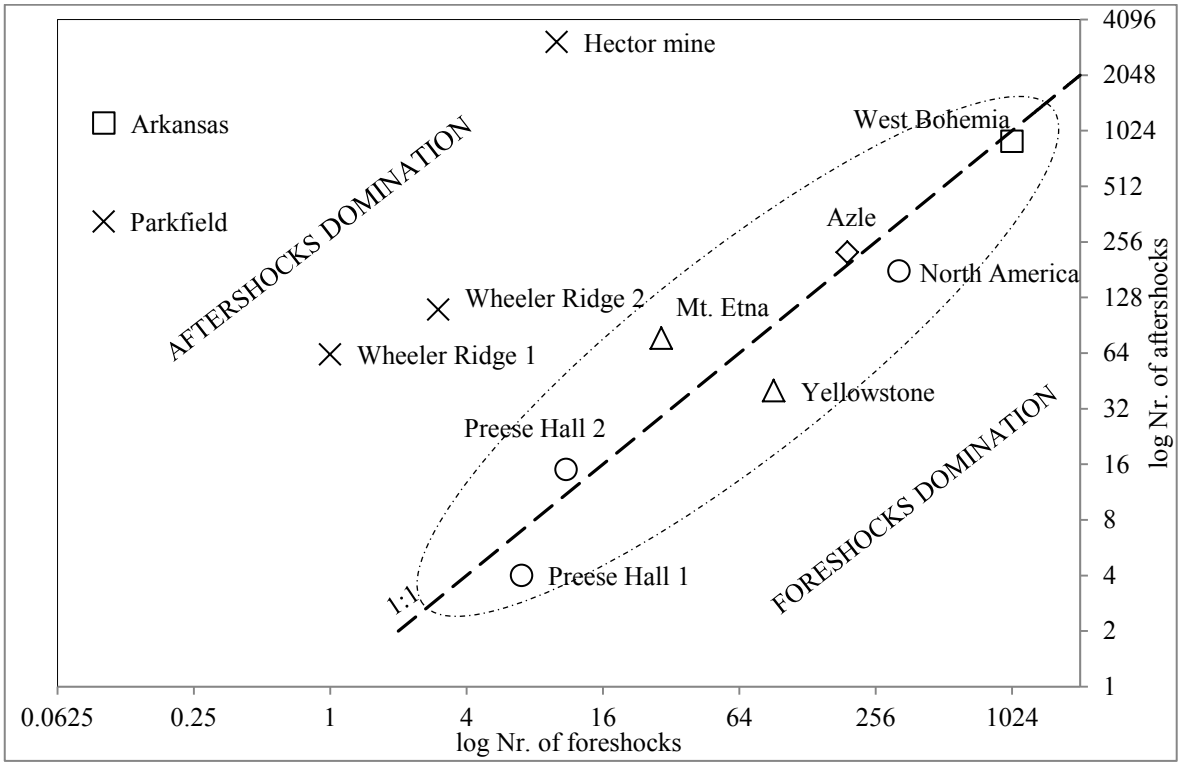

Figure 35. Plotted results for mainshock position criterion. Comparison of the number of events before (foreshock) and after (aftershock) the main event. Crosses represent tectonic sequences, triangles represent volcanic sequences, circles represent induced seismicity and squares represent intraplate swarms. Swarm-like behavior is interpreted with dashed ellipse.

Preese Hall 1 seismic sequence shows mainshocks in the beginning of with just one day activity before the mainshock. Preese Hall 2 lasts only 2 days with the mainshock in the last day. Here we need to consider that the injection of stage 2 lasted only one day (as mentioned Clarke et al., 2014). PH 1 has more foreshocks with ratio 7 to 4, PH 2 has more aftershock but we need to consider that much smaller magnitudes were detected during PH 2. North America induced seismicity dataset shows twice more foreshocks but the sequence last longer after the main shock with 4:7 ratio of days before to after the mainshock.

Figure 35 shows the comparison of numbers of foreshocks and aftershocks and the swarms are close to the dashed line representing the same number of foreshock as aftershocks. All the induced seismicity sequences are close to swarms in this plot.

Criterion analyzing the time position of the mainshock reveals eleven out of twelve tested datasets to have mainshock in the forepart of the sequence. This indicates that the criterion by itself cannot distinguish swarms and MS-AS or natural and induced seismicity.

Comparison of the number of foreshocks and aftershocks shows that the MS-AS usually have significant dominance of the aftershocks, while mainshock position in the swarm is later in the sequence or without evident dominance of any of the event types. The Arkansas dataset with the position of the mainshock in the very beginning of the sequence is the exception.

As observed, combination of these two criteria could be useful tool for distinguishing MS-AS from swarm sequences.

3.3.3 MAINSHOCK – AFTERSHOCK MAGNITUDE COMPARISON

Table 14 displays the comparison of magnitude difference of two largest events in each of our selected catalogue.

Tectonic MS-AS earthquakes like M_W 7.1 Hector Mine or M_w 6.0 Parkfield show the magnitude difference of the mainshock and the largest aftershock 1 or more. During the large tectonic event large fault plane suddenly moves which results in a release of great amount of energy that causes big magnitude difference. However, other tectonic earthquake - Wheeler Ridge achieves much smaller values (0.5 for WR 1 and 0.2 for WR 2), which might be result from slower intraplate loading and more creep-like behavior.

All natural swarm sequences have low differences in magnitude between the mainshock and the second largest event. The differences are approximately 0.1 – 0.2 except the Mt. Etna dataset with 0.4 which is consistent with the observation of Holtkamp and Brudzinski (2011), that swarms typically have many earthquakes near the magnitude of the mainshock.

Induced catalogs have large variation in this criterion. The North America sequence has two largest events with the same magnitude, which indicates swarm behavior. Preese Hall 2 sequence has also swarm-like value of the magnitude difference. However, Preese Hall 1shows high value which classifies this sequence rather to the MS-AS category. This high magnitude difference is probably result of triggering highly stressed fault and perhaps this criteria has potential to differentiate between triggered and induced seismicity.

Table 14. Results of the mainshock - aftershock magnitude comparison for tested catalogues. $M_{max\ II}$ represents second largest event in the sequence.

Seismic sequence	M_{max}	$M_{max\ II}$	M_{max} - $M_{max\ II}$
Arkansas	*1.8*	*1.7*	*0.1*
Azle	*3.6*	*3.5*	*0.1*
Hector mine	*7.1*	*5.8*	*1.3*
Mt. Etna	*4.8*	*4.4*	*0.4*
North America	*3.3*	*3.3*	*0.0*
Parkfield	*6*	*5.0*	*1.0*
Preese Hall 1	*2.5*	*1.6*	*0.9*
Preese Hall 2	*1.7*	*1.4*	*0.3*
West Bohemia	*3.7*	*3.5*	*0.2*
Wheeler Ridge 1	*4.6*	*4.1*	*0.5*
Wheeler Ridge 2	*4.7*	*4.5*	*0.2*
Yellowstone	*3.6*	*3.4*	*0.2*

This criterion properly distinguished all the tested natural swarm sequences (for the magnitude difference upper limit 0.5 for swarms). It was also successful in distinguishing the large tectonic MS-AS with magnitude difference of the two largest events exceeding 1. However, if we consider Båth's law limit for aftershock sequences M_w 1.2 most of the tectonics tectonic earthquakes would not be classified as MS-AS.

This difference between swarms and MS-AS probably results from the different driving mechanisms as discussed above. Swarms are likely due to pore pressure increase while MS-AS result from shear stress loading. Hence in MS-AS shear stress is very high and most of slip occurs during the mainshock, while many comparable segments of fault are activated due to injections but these segments do not slip at the same time unless the sequence is triggered.

3.3.4 COMPARISON OF THE NUMBER OF EVENTS AND MAGNITUDE OF THE MAINSHOCK

Figure 36 shows total number of events above the M_c as a function of the mainshock magnitude in each of the studied sequence. This figure splits up MS-AS and swarms in two clear, separated parts in the plot. As proposed by Holtkamp and Brudzinski (2011) we interpreted the borderline separating the swarm and MS-AS sections with a dashed line.

In the left *swarms* section in the Figure 36 all the natural swarms are located except the volcanic Mt. Etna sequence, which is situated in the close vicinity of the Wheeler Ridge 2 tectonic dataset. Both of these sequences have magnitude of the mainshock just below the 5 and almost the same number of events. Induced seismicity datasets shows as swarms. All the MS-AS are located in the right *MS-AS* section.

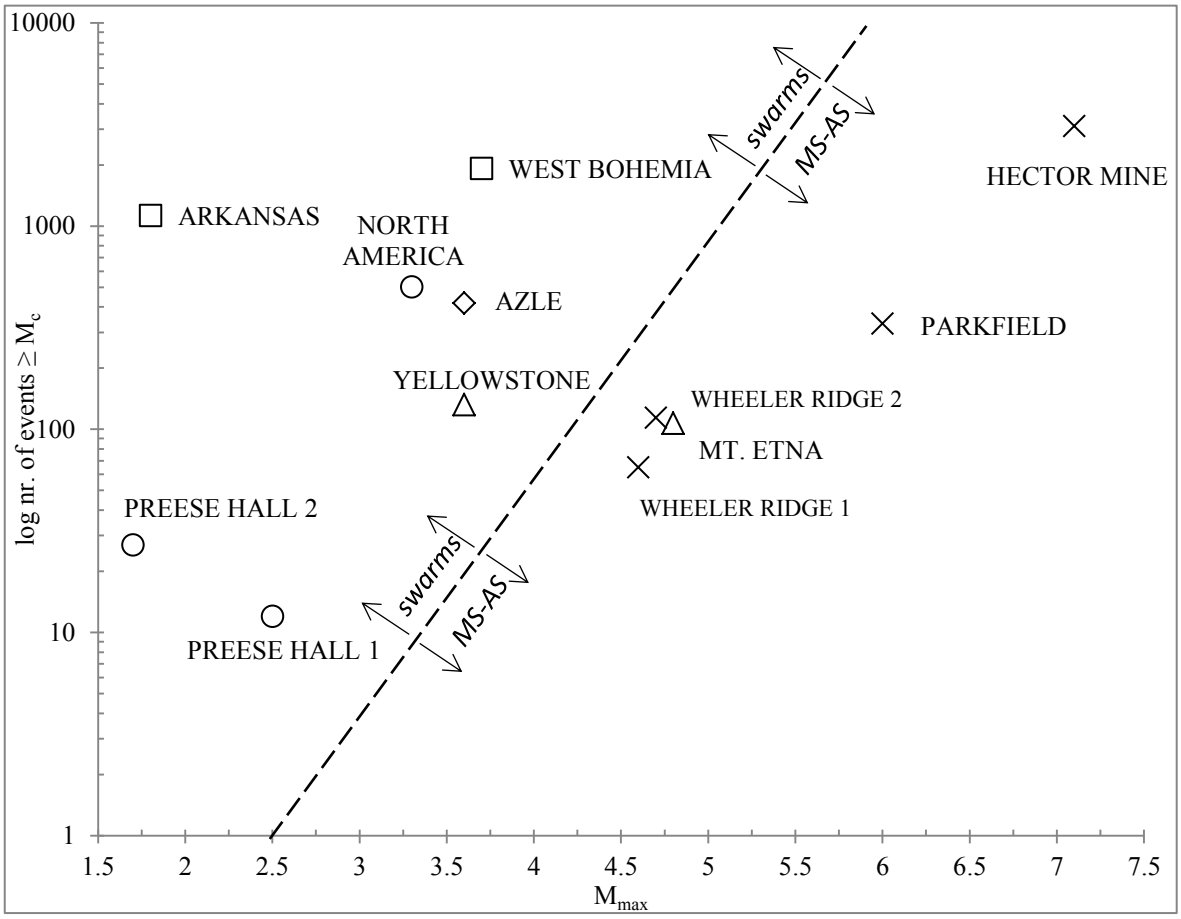

Figure 36. Plotted comparsion of the number of events above the magnitude of completeness M_c and the mainshock magnitude M_{max}. Crosses represent tectonic earthquakes, triangles represent volcanic earthquakes, circles represent induced seismicity and squares represent intraplate swarms. Dashed line shows interpretation of the separating borderline defining the swarm and MS-AS sections.

This tested criterion shows that the number of events in swarms is not a function of the mainshock magnitude in the sequence. In contrast, the number of events in MS-AS is controlled by the size of the mainshock, as the bigger mainshock gives rise to more aftershocks.

Similar results were presented by Vidale et al. (2006) or Holtkamp and Brudzinski (2011).

This method probably correlates with the higher b-value or higher number of small events relative to the largest events in the swarms and this plot is just different type of representation of this fact.

3.3.5 INTER-EVENT TIME

For each dataset inter-event time distribution is shown in the same plot with the magnitude distribution (Figure 37 – Figure 48). The left vertical axis shows logarithmic scale of the IET in seconds and right vertical axis displays magnitude size. Note that the IET and magnitudes are plotted by the ordinal number of the events (horizontal axis). The position of the mainshock within the sequence is shown with the yellow square because its position is discussed in the IET evolution. The first event in the sequence has the IET = 0.

NATURAL SWARM CATALOGUES

We expected IET of swarm sequences to not depend on the mainshock.

Arkansas dataset IET is plotted in the Figure 37 with the mainshock position in the very beginning of the sequence. The longest IET was found right after the mainshock and in the end of the sequence. This implies that the sequence started slowly and then it slowly ended with high activity in between without significant temporal gaps.

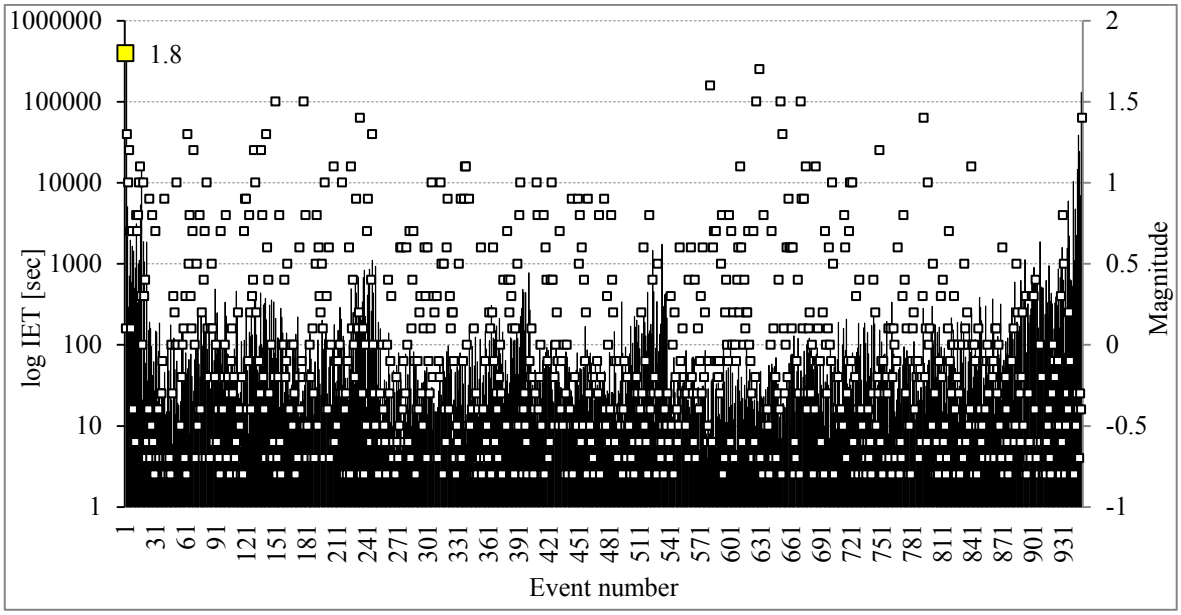

Figure 37. Arkansas IET distribution (black bars) plotted with the magnitude distribution (white squares). Mainshock is shown with the yellow square and described with the magnitude value.

The Azle dataset shown in the Figure 38 can be characterized by large variations of the IET with no changes associated with the mainshock in the IET distribution. There are few periods of high seismic activity increase associated with short IET.

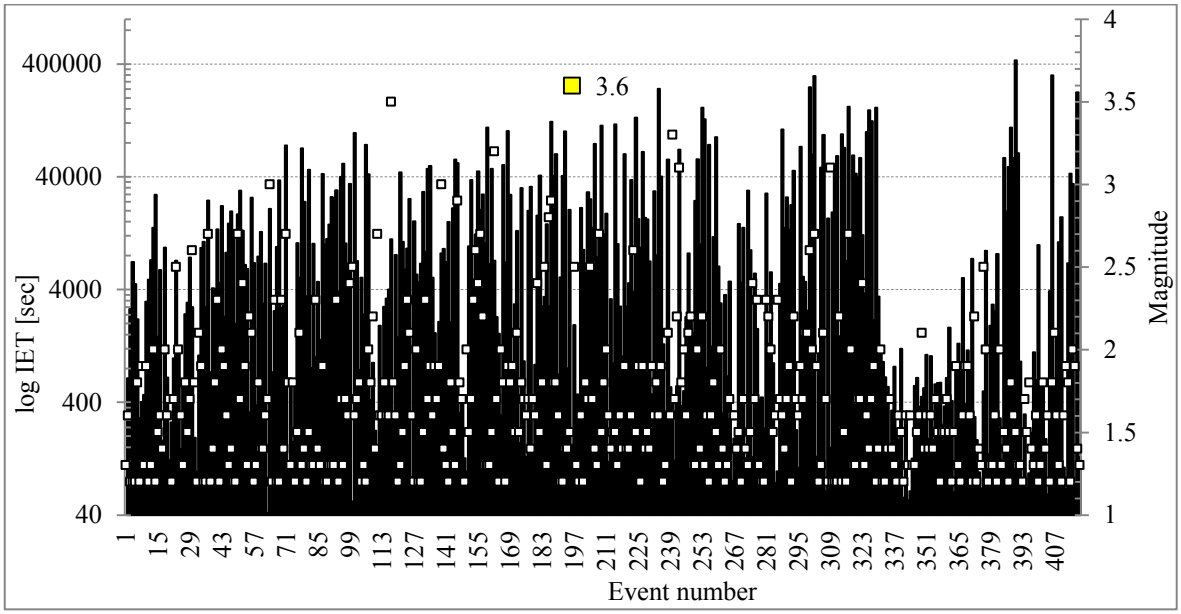

Figure 38. Azle IET distribution (black bars) plotted with the magnitude distribution (white squares). Mainshock is shown with the yellow square and described with the magnitude value.

In the West Bohemia 2008 swarm IET seems to periodically achieve very short IET followed by slow increase in the IET as in an aftershock sequence (see Figure 39). Such behavior seems to indicate combination of MS-AS sequences and swarm activity. This is also consistent with the fact that some (but not all) events with M_L>3 are followed by short IET resulting from large number of weak aftershocks.

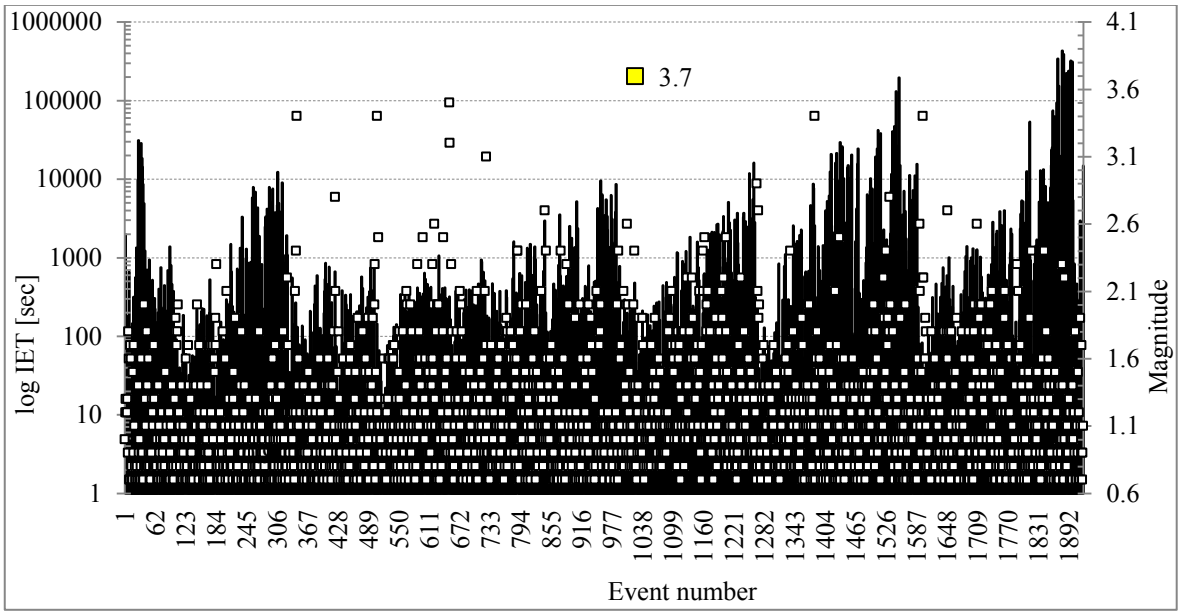

Figure 39. The West Bohemia 2008 swarm IET distribution (black bars) plotted with the magnitude distribution (white squares). Mainshock is highlighted with the yellow square and described with the magnitude value.

The Yellowstone volcanic earthquake sequence plotted in the Figure 40 shows *swarm-like* pattern with random IET without any significant influence of MS-AF sequences. Note that the mainshock of 3.6 is not followed by short IET indicating no significant aftershocks sequence.

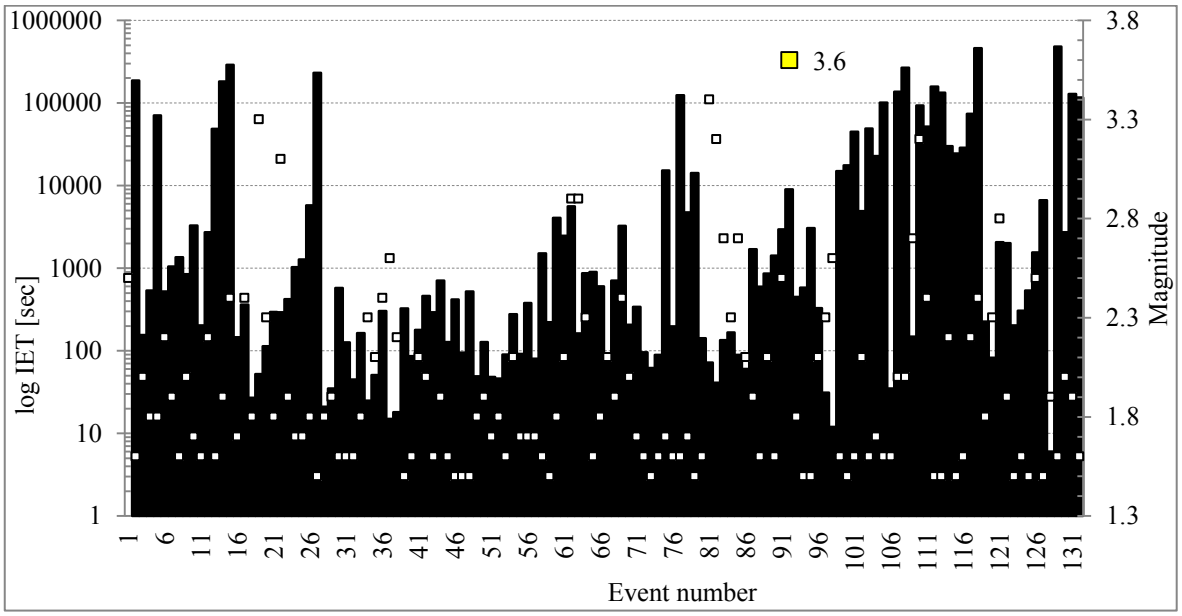

Figure 40. The Yellowstone volcanic swarm IET distribution (black bars) plotted with the magnitude distribution (white squares). Mainshock is showed with the yellow square and described with the magnitude value.

Mt. Etna catalogue (Figure 41) shows temporal oscillation with the longest IET in the beginning and in the end of the sequence similar to the Arkansas sequence but the largest event in this case is not at the beginning of the sequence.

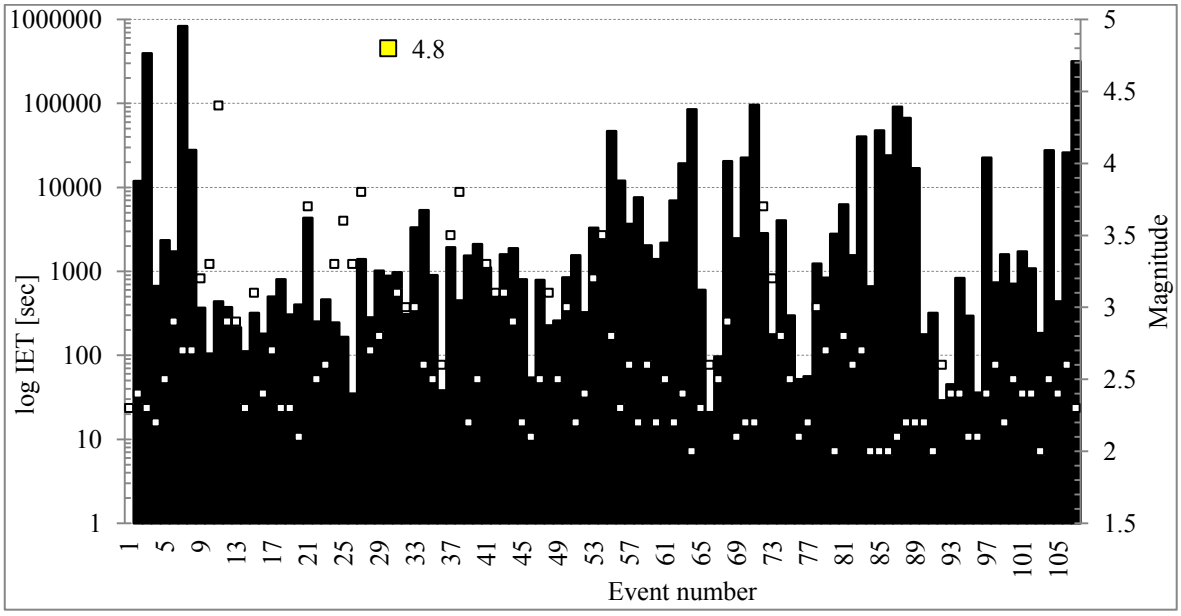

Figure 41. Mt. Etna 2009 sequence IET distribution (black bars) plotted with the magnitude distribution (white squares). Mainshock is showed with the yellow square and described with the magnitude value.

TECTONIC MS-AS CATALOGS

Hector Mine tectonic earthquake IET in the Figure 42 is an example of seismicity MS-AS sequence. The minimum IET is right after the mainshock followed by gradual increase of inter-event time and decrease of the magnitudes. The M_w 7.1 mainshock is preceded by 10 foreshocks with diverse IET.

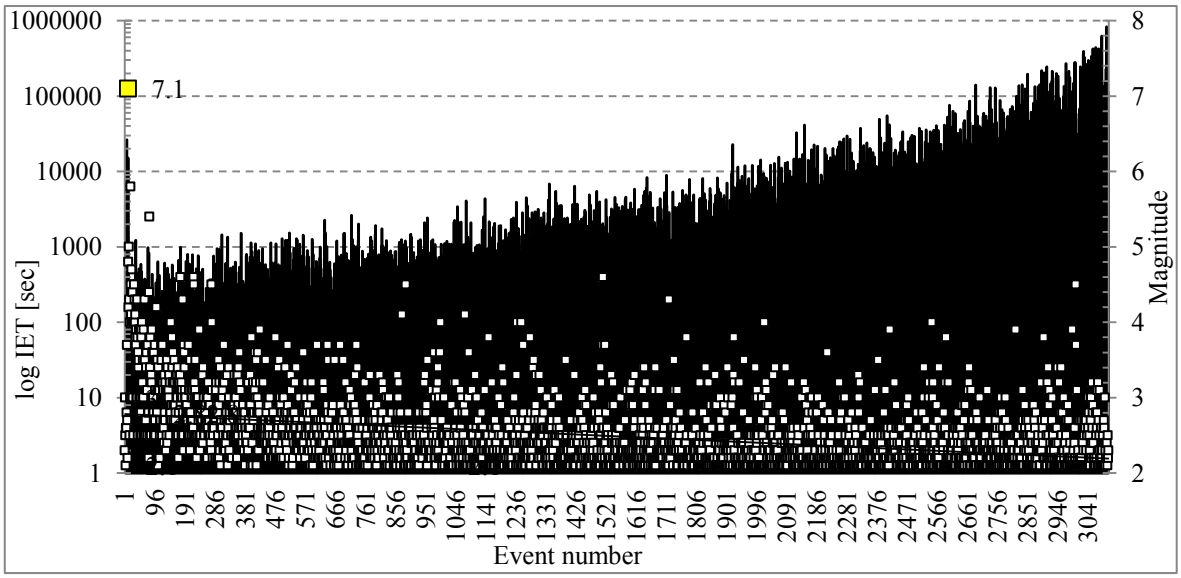

Figure 42. The Hector Mine IET distribution (black bars) plotted with the magnitude distribution (white squares). Mainshock is showed with the yellow square and described with the magnitude value.

Tectonic Parkfield sequence shows a similar pattern of IET as Hector Mine (Figure 43).

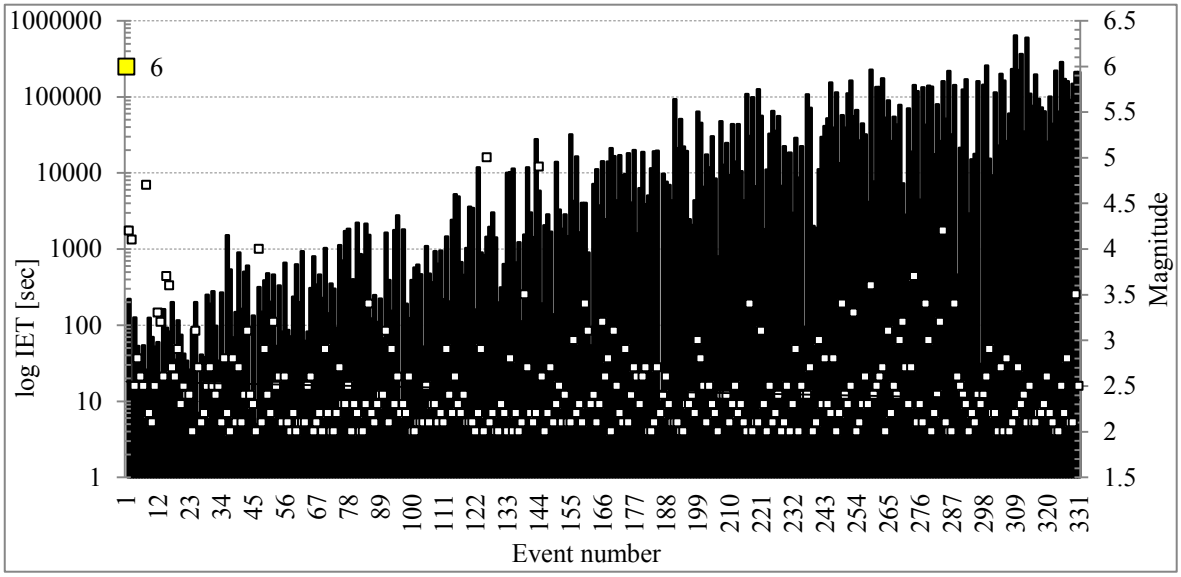

Figure 43. Parkfield 2004 IET distribution (black bars) plotted with the magnitude distribution (white squares). Mainshock is shown with the yellow square.

Wheeler Ridge catalogue shows in both sequences short IET associated with the mainshock in the beginning of the sequence and gradual increase of IET typical for the tectonic MS-AS (see Figure 44 and Figure 45). In both sequences the large IET are also associated with the foreshocks indicating nearly random timing of the foreshocks.

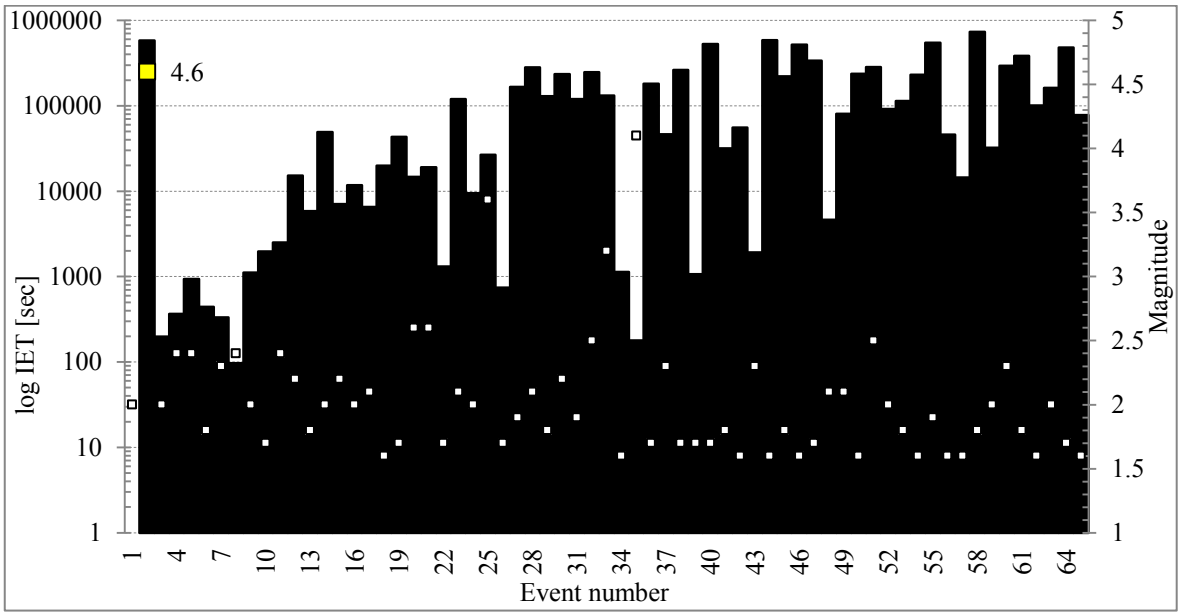

Figure 44. Wheeler Ridge sequence 1 IET distribution (black bars) plotted with the magnitude distribution (white squares). Mainshock is highlighted with the yellow square and described with the magnitude value.

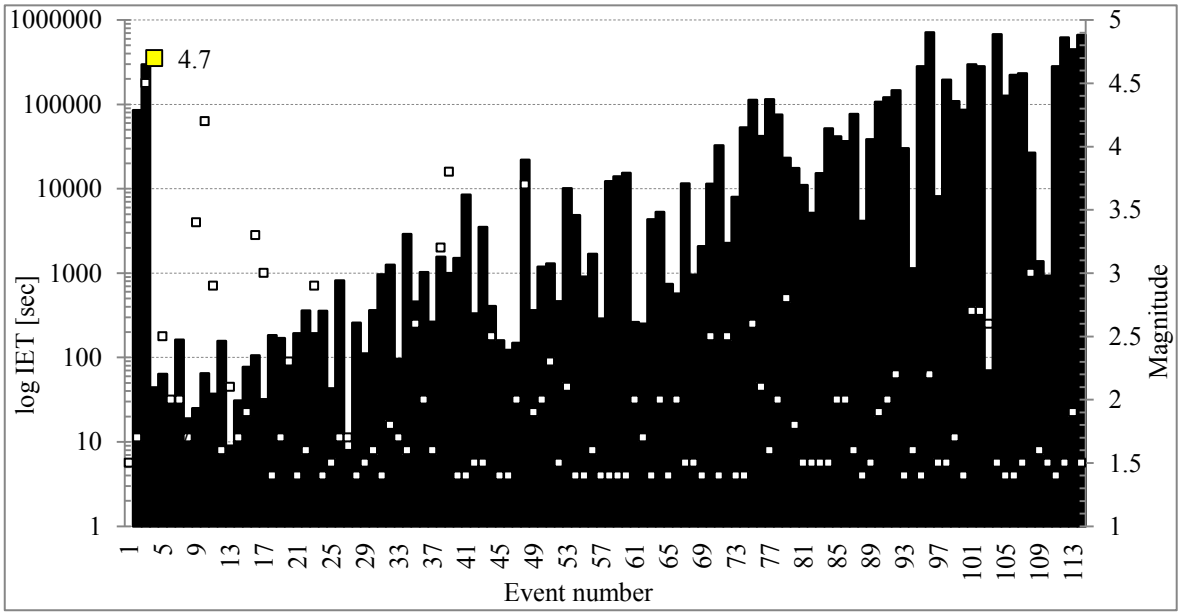

Figure 45. Wheeler Ridge sequence 2 IET distribution (black bars) plotted with the magnitude distribution (white squares). Mainshock is highlighted with the yellow square and described with the magnitude value.

INDUCED SEISMICITY CATALOGUES

The sequences of induced seismicity show nearly random IET similar to the pattern as natural swarms but with influence of artificial fluid injection.

Figure 46 shows IET distribution in the North America induced seismicity catalogue. IET has nearly random-like value with the longest IET at the beginning and in the end of the sequence. The mainshock is not associated with any anomalous IETs.

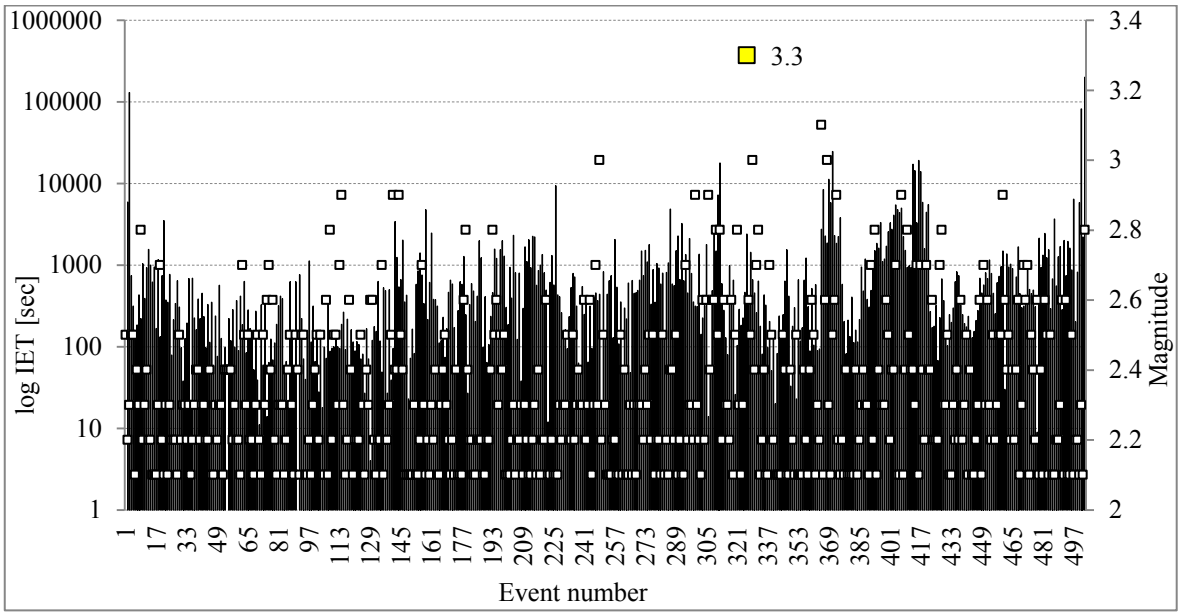

Figure 46. The North America IET distribution (black bars) plotted with the magnitude distribution (white squares). Mainshock is highlighted with the yellow square and described with the magnitude value.

The Preese Hall 1 induced sequence contains only 12 events and it is hard to statistically to characterize it. However, we can observe that the mainshock is not associated with any anomalous the sequence (see Figure 47).

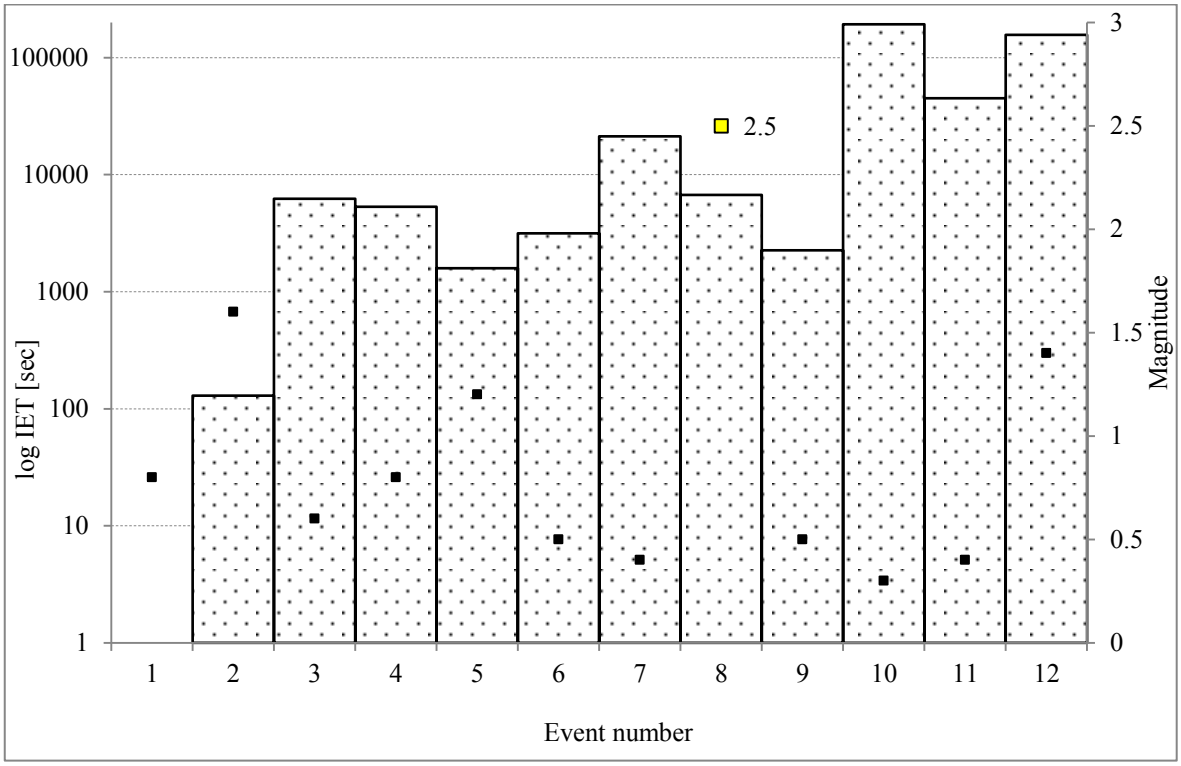

Figure 47. Preese Hall 1 IET distribution (white bars) plotted with the magnitude distribution (black squares). Mainshock is highlighted with the yellow square and described with the magnitude value.

The Preese Hall 2 inter-event time distribution with the gradually increase of IET before the mainshock and decrease after the mainshock is somewhat surprising as a decrease of IET is usually associated with the large events (see Figure 48).

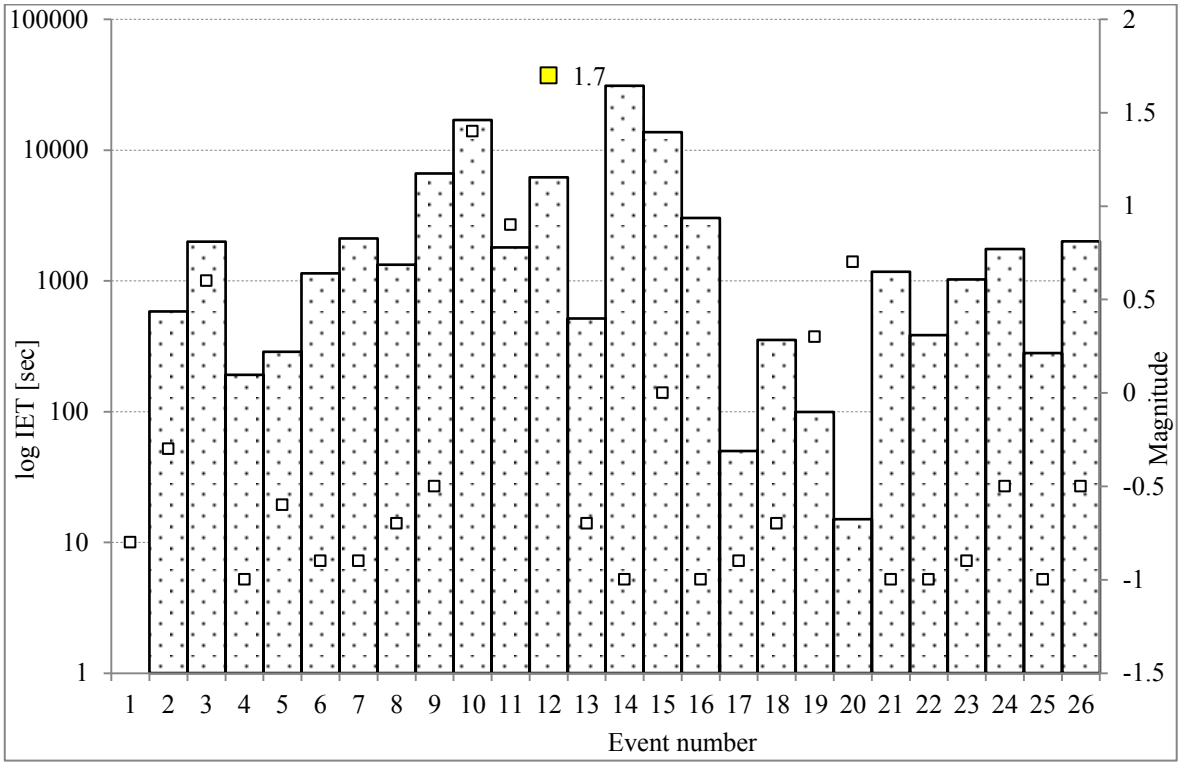

Figure 48. Preese Hall 2 IET distribution (white bars) plotted with the magnitude distribution (black squares). Mainshock is highlighted with the yellow square and described with the magnitude value.

The inter-event time distribution shows three main important characteristics:

1) There is no evidence in the natural swarms of the IET to be driven by the mainshock.
2) Large tectonic MS-AS datasets all show seismicity controlled by the mainshock with exponential increasing of the IET after the mainshock.
3) Foreshocks of the large MS-AS sequences are associated with large IET.
4) Induced seismicity datasets are similar to natural *swarms* but the largest events influence the IET.

This criterion is able to reveal differences between natural swarms and MS-AS as described above. Induced seismicity inter-event times are driven by human activity so without the correlation with the injection volume it is difficult to distinguish natural and induced *swarm-like* seismicity.

4 DISCUSSION

We analyzed ten seismic catalogues (divided in to twelve sequences) representing different types of seismicity: natural swarms and natural MS-AS as well as induced earthquakes. We applied six criteria for distinguishing MS-AS and swarm to all these datasets.

For each criterion, certain assumptions were discussed for which the dataset was interpreted either as a swarm or MS-AS. Note that results presented in Table 15 is subjective interpretation based on discussed assumptions and mentioned published observations. If the assumption was not fully met, a question mark was attributed to the predominant result (e.g. *swarm?*). The overall result (last column of the table) comes from the *swarm* and *MS-AS* ratio (penultimate column of the table), which is proportion of summed individual results for each criterion. Although there is no defined ratio value for the overall result which determines the sequence to be swarm or MS-AS we interpret the predominant character of each sequence (the last column of the Table 15).

Six criteria clearly identified three datasets as swarms (Azle, North America and West Bohemia). All three catalogs have the similar pattern of temporary-magnitude distribution with clustered low magnitude seismicity without any distinct mainshock. Azle, Texas seismic catalogue with questionable origin was classified as a swarm which excludes its tectonic origin. But its natural or induced origin is still a question of discussion and further analysis. Wheeler Ridge 2, Parkfield and Hector Mine tectonic datasets were determined as MS-AS by five criteria and one incorrectly identified as swarm. The same scores identified the Preese Hall 2 and natural volcanic Mt. Etna datasets as swarms. Four out of six criteria identified Preese Hall 1 and Arkansas to be swarms and Wheeler Ridge 1 as MS-AS.

In conclusion, the analysis revealed that all three induced seismicity catalogues were identified as swarms. However, none of these criteria is able to clearly distinguish between induced and natural swarms. None of the criteria alone is always correctly identifying the type of the dataset probably due to the fact that the dataset themselves may contain errors and are only statistical realizations or random processes. For more accurate identification of the type of datasets we suggest using set of criteria as we used here.

When comparing the types of datasets with the result of each criteria (see Table 15), we observe that these criteria were not always successful in the earthquake type determination. In the following paragraphs we discuss possible reasons of these inaccuracies.

Table 15. Overall results of 6 criteria analyzes for distinguishing swarms and MS-AS. Individual results are added and the overall RESULT RATIO shows the ratio of swarm/MS-AS number. Last column shows the overall result based on our interpretation.

Seismic sequence	1. Events density	2. Time position of the mainshock		3. Mainshock – aftershock magnitude comparison	4. Comparison of the number of events and magnitude of mainshock	5. Inter-event time	RESULT RATIO swarm vs. MS-AS	RESULT
		Nr. of foreshocks and aftershocks	Time position of the mainshock					
Arkansas	*swarm*	*MS-AS*	*MS-AS*	*swarm*	*swarm*	*swarm*	*4/2*	*swarm?*
Azle	*swarm*	*swarm*	*swarm*	*swarm*	*swarm*	*swarm*	*6/0*	*swarm*
Hector mine	*swarm*	*MS-AS*	*MS-AS*	*MS-AS*	*MS-AS*	*MS-AS*	*1/5*	*MS-AS*
Mt. Etna	*swarm*	*swarm*	*swarm*	*swarm*	*MS-AS*	*swarm*	*5/1*	*swarm*
North America	*swarm*	*swarm*	*swarm*	*swarm*	*swarm*	*swarm*	*6/0*	*swarm*
Parkfield	*swarm*	*MS-AS*	*MS-AS*	*MS-AS*	*MS-AS*	*MS-AS*	*1/5*	*MS-AS*
Preese Hall 1	*swarm*	*swarm*	*MS-AS?*	*MS-AS?*	*swarm*	*swarm?*	*4/2*	*swarm?*
Preese Hall 2	*swarm*	*swarm*	*MS-AS?*	*swarm*	*swarm*	*swarm?*	*5/1*	*swarm*
West Bohemia	*swarm*	*swarm*	*swarm?*	*swarm*	*swarm*	*swarm?*	*6/0*	*swarm*
Wheeler Ridge 1	*MS-AS*	*MS-AS*	*MS-AS*	*swarm?*	*MS-AS*	*MS-AS*	*1/5*	*MS-AS*
Wheeler Ridge 2	*swarm*	*MS-AS*	*MS-AS*	*swarm*	*MS-AS*	*MS-AS*	*2/4*	*MS-AS*
Yellowstone	*swarm*	*swarm*	*swarm*	*swarm*	*swarm*	*swarm*	*6/0*	*swarm*

The least successful seems to be the event density criterion based on Mogi (1963) which identified 11 out of 12 datasets as swarms of which at least three were tectonic MS-AS. As discussed above, this criterion is very sensitive to definition of the duration of the sequence and also depends on the catalogue quality. Catalogue quality (given by the seismic network resolution, processing, size of the earthquake, etc.) can be characterized by the magnitude of completeness for the purpose of this study. The magnitude of completeness varies from -0.8 to 2.1 in the studied datasets which might be reason why this criterion failed as number of events exponentially increases with magnitude of completeness. While duration of an earthquake sequence may slightly increase with lower M_c it is obvious that with the

lower M_c number of events registered per day dramatically increases for lower M_c. Probably for this reason the threshold for differentiation between swarms and natural MS-AS needs to be higher for the dense networks with lower M_c.

The criterion of comparing the number of foreshocks and aftershocks is less dependent on the catalogue quality but more sensitive to definition of foreshock and aftershocks. The only failure of this swarm is observed for the Arkansas dataset which represents unusual swarms (see Chapter 3.3.2).

Time position of the mainshock does not show as a reliable criterion. It can only clearly identify large tectonic catalogues driven by the mainshock in the beginning of the sequence. Although mainshock does not control the seismicity in swarms, its position can also be in the beginning of the sequence (as e.g. Arkansas or West Bohemia swarm dataset).

Criterion comparing the magnitude difference of the two largest events has the advantage of being insensitive to the quality of the dataset as duration and magnitude of completeness play very minor role. However, this criterion does not properly identify induced seismicity if it occurs in highly stressed enlivenment. Therefore Preese Hall 1 of the induced seismicity sequences was classified as MS-AS with this criterion.

Comparison of the number of events and magnitude of mainshock is reasonably reliable. As mentioned earlier it is probably just a different type of *b-value* representation. However, because of the graphical representation, the interpretation borderline may be sensitive on the type of plotted data. For example, the Mt. Etna volcanic swarm dataset is classified as MS-AS by this criterion because of the higher mainshock (Figure 36).

Inter-event time distribution can be useful tool in distinguishing MS-AS from swarms. It shows clearly increase of IET for large MS-AS and shows large variability of IET for swarms and induced events. It also indicates lower IET after the large events in tectonically driven data while no anomalies for the fluid driven datasets. A more objective characterization may need to be developed (such as linear fit to IET with time).

5 CONCLUSIONS

Ten earthquake catalogues were used to analyze and compare statistical properties of natural and induced seismicity. These seismic catalogues (divided into twelve sequences) represent different types of natural earthquakes such as swarms and MS-AS. Six criteria for distinguishing MS-AS and swarms were applied on these data.

All three tested induced seismicity sequences are identified as swarms and can be distinguished from the MS-AS. This observation is in consistence with our assumption that human induced seismicity behaves similar to natural swarm. As mentioned above natural swarms are mostly associated with the migration of hydrothermal fluids or magma (e. g. Hill, 1977), and therefore the natural swarms and induced seismicity are similar.

However, none of the used statistical criteria is able to clearly distinguish induce swarms from natural swarms. Perhaps with additional information on human activity it is possible (e. g. correlation with fluid injection parameters).

Combination of these criteria may be a useful tool for distinguishing induced seismicity from natural tectonic MS-AS in region with lack of the natural swarm seismicity.

Based on our analysis Azle, Texas seismic catalogue with questionable origin was classified as a swarm but its natural or induced origin cannot be reliably distinguished.

We also observe that none of the used criteria is always reliable for distinguishing different types of earthquake sequences. Each of them failed for at least one dataset and gives good result for specific type of seismic sequences. The most successful criterion is comparing the number of foreshocks and aftershocks and criterion of IET distribution which are both observed to be less sensitive to the quality of the seismic catalogue. However, a reliable discrimination of earthquake sequences requires using criteria such as ones we use here. Combination of all six criteria reliably distinguished four out of five natural swarms and three out of four natural MS-AS.

6 REFERENCES

Alparone S., Maiolino, V., Mostaccio A., Scaltrito A., Ursino A., Barberi G., D'Amico S., DiGrazia G., Giampiccolo E., Musumeci C., Scarfì L., Zuccarello L., 2015. Instrumental seismic catalogue of Mt Etna earthquakes (Sicily,Italy):ten years(2000–2010) of instrumental recordings. Annals of Geophysics 58 (4), S0435

Avlonitis M., Papadopoulos G. A., 2014. Foreshocks and b value: bridging macroscopic observations to source mechanical considerations. Pure and Applied Geophysics, 171, 10, p. 2569–2580

Babuška V., Plomerová J., 2008. Control of paths of quaternary volcanic products in western Bohemian Massif by rejuvenated Variscan triple junction of ancient microplates. Stud Geophys Geod 52:607– 630

Bankwitz P., Schneider G., Kämpf H., Bankwitz E., 2003. Structural characteristics of epicentral areas in Central Europe: study case Cheb Basin (Czech Republic). J Geodyn 35/1–2:5–32

Barth A., Wenzel F, Langenbruch C., 2012. Probability of earthquake occurrence and magnitude estimation in the post shut-in phase of geothermal projects. J Seismol. doi:10.1007/s10950-011-9260-9

Båth M., 1965. Lateral inhomogeneities in the upper mantle. Tectonophysics 2:483–514

Bonaccorso A., Ferrucci F., Patanè D., L. Villari, 1996. Fast deformation processes and eruptive activity at Mount Etna (Italy). J. Geophys. Res., 101, 17467-17480

Cannata A., Alparone S., Ursino A., 2013. Repeating volcano-tectonic earthquakes at Mt. Etna volcano (Sicily, Italy) during 1999-2009. Gondwana Research, 24, 1223-1236

Cesca S., Dost B., Oth, A., 2012a. Preface to the special issue "Triggered and induced seismicity: probabilities and discrimination". J. Seismol., 17

Cesca S., Rohr A., Dahm T., 2012b. Full moment tensor inversion and decomposition to discriminate induced seismicity. J Seismol., 147

Clarke H., Eisner L., Styles P., Turner P., 2014. Felt seismicity associated with shale gas hydraulic fracturing: The first documented example in Europe. Geophys. Res. Lett. 41, 8308–8314

Christiansen R. L., 2001. The Quaternary and Pliocene Yellowstone Plateau volcanic field of Wyoming, Idaho, and Montana. U.S. Geol. Surv. Prof. Pap., 729-G

Corfield, S. M., Gawthorpe R. L., Gage M., Fraser A. J., Besly B. M., (1996), Inversion tectonics of the Variscan foreland of the British Isles, J. Geol. Soc., 153, 17–32

Dahm T., Becker D., Bischoff M., Cesca S., Dost B., Fritschen R., Hainzl S., Klose C. D., Kühn D., Lasocki S., Meier T., Ohrnberger M., Rivalta E., Wegler U., Husen S., 2012. Recommendations on the discrimination between human-related and natural seismicity. J Seismol. 17, 1, p. 197

Dahm T., Hainzl S., Becker D., Bischoff M., Cesca S., Dost R., Fritschen R., Kühn D., Lasocki S., Klose Chr., Meier Th., Ohrnberger M., Rivalta E., Shapiro S., Wegler U., 2010. How to discriminate induced, triggered and natural seismicity. In Proceedings of the workshop "Induced Seismicity", Nov 15–17, 2010, Luxembourg. Eds.: J. Ritter and A. Oth. Cahier du Centre Europeen de Geodynamique et de Seismologie, Vol. 30, pp 69–76

Dahm, T., Becker, D., Bishoff, M., Cesca, S., Dost, B., Fritschen, R., Hainzl, S., Klose, C. D., Kühn, D., Lasocki, S., Meier, T., Ohrnberger, M., Rivalta, E., Wegler, U., Husen, S., 2013. Recommendation for the discrimination of human-related and natural seismicity. Journal of Seismology, 17, 1, p. 197-202

Dahm, T., Cesca S., Hainzl S., Braun T., Krüger F., 2015. Discrimination between induced, triggered, and natural earthquakes close to hydrocarbon reservoirs: A probabilistic approach based on the modeling of depletion-induced stress changes and seismological source parameters, J. Geophys. Res. Solid Earth, 120

Davis S. D. and Frohlich C., 1993. Did (or will) fluid injection cause earthquakes? ~ criteria for a rational assessment, Seism. Res. Lett. 64, 207-224

Davis S., Nyffenegger P., Frohlich C., 1995. The 9 April 1993 earthquake in south-central Texas: was it induced by fluid withdrawal? Bull. seism. Soc. Am., 85, 1888–1896

Dewey J.F., Helman M. L., Turco E., Hutton D. H. W., Knott S. D., 1989. Kinematics of the western Mediterranean. Alp. Tectonics Geol. Soc. Spec. Publ. 45, 265–283

Dokka R. K., Travis C. J., 1990. Role of eastern California shear zone in accommodating Pacific-North America plate motion, Geophys. Res. Lett., 17(9), 1323-1326

Ellsworth W. L., 2013. Injection-Induced earthquakes, Science, 341, 142-149

Farrell J., Husen S., Smith R. B., 2009. Earthquake swarm and b-value characterization of the Yellowstone volcano–tectonic system. J. Volcanol. Geotherm. Res. 188, 260–276

Felzer K. R., Becker T. W., Abercrombie R. E., Ekström G., Rice J. R., 2002. Triggering of the 1999 MW 7.1 Hector Mine earthquake by aftershocks of the 1992 MW 7.3 Landers earthquake, J. Geophys. Res., 107(B9), 2190

Fischer T., Horálek J., Michálek J., Boušková A., 2010. The 2008 West Bohemia earthquake swarm in the light of the WEBNET network, J. Seismol.14, 4,665-682

Fischer T., Horálek J., Hrubcová P., Vavryčuk V., Bräuer K., Kämpf H., 2013. Intra-continental earthquake swarms in West-Bohemia and Vogtland: A review. Tectonophysics 611, 1-27

Fournier R. O., 1989. Geochemistry and dynamics of the Yellowstone National Park hydrothermal system. Annu. Rev. Earth Planet. Sci., 17, 13– 53

Frohlich C., DeShon H., Stump B., Hayward C., Hornbach M., Walter J. I., 2016. A historical review of induced earthquakes in Texas. Seismol. Res. Lett.,87(4), 1022–1038

Gresta S., Peruzza L., Slejko D., Distefano G., 1998. Inferences on the main volcanotectonic structures at Mt. Etna (Sicily) from a probabilistic seismological approach. J. Seismol., 2, 105-116

Grigoli F., Cesca S., Priolo E., Rinaldi A. P., Clinton J. F., Stabile T. A., Dost B., Fernandez M. G., Wiemer S., Dahm T., 2017. Current challenges in monitoring, discrimination, and management of induced seismicity related to underground industrial activities: A European perspective, Rev. Geophys., 55

Gruppo Analisi Dati Sismici, 2012. Catalogo dei terremoti della Sicilia Orientale - Calabria Meridionale (1999–2012). INGV, Catania (http://www.ct.ingv.it/ufs/analisti/catalogolist.php)

Grünthal G., 1989. About the history of earthquake activity in the focal region Vogtland/Western Bohemia. In: Bormann, P. (Ed.), Monitoring and Analysis of the Earthquake Swarm 1985/86 in the Region Vogtland/Western Bohemia. Akad. der Wissensch. der DDR, Potsdam, p. 30–34

Gutenberg B., Richter C.F., 1944. Frequency of earthquakes in California. Bull. Seismol. Soc. Am. 34, 185–188

Hauksson E., Jones L. M., Hutton K., 2002. The 1999 Mw 7.1 Hector Mine, California, earthquake sequence: complex conjugate strike-slip faulting. Bull. Seismol. Soc. Am. 92, 1154–1170

Hill D.P., 1977. A model for earthquake swarms, J. geophys. Res. 82, 1347– 1352 Holtkamp S. G., Brudzinski M. R., 2011. Earthquake swarms in circum-Pacific subduction zones. Earth Planet. Sci. Lett., 305(1-2), 215–225

Hristopulos D.T., Mouslopoulou V., 2012. Strength statistics and the distribution of earthquake intereventtimes. Physica A2013,392, 485–496

Huang Y., Beroza G. C., 2015. Temporal variation in the magnitudefrequency distribution during the Guy-Greenbrier earthquake sequence. Geophys. Res. Lett., 42, 6639–6646

Husen S., Kissling E., von Deschwanden A., 2012. Induced seismicity during the construction of the Gotthard Base Tunnel, Switzerland: hypocenter locations and source dimensions. J Seismol.

Husen S., Smith R. B., 2004. Probabilistic earthquake relocation in three-dimensional velocity models for the Yellowstone National Park region. Wyoming. Bull. Seismol. Soc. Am. 94, 880–896

Ibs-von Seht M., Plenefisch T., Klinge K., 2008. Earthquake swarms in continental rifts—a comparison of selected cases in America, Africa, and Europe. Tectonophysics 452:66–77

Jechumtalova Z., 2017. Verification of Network Design for Induced Seismicity, (79th EAGE Conference & Exhibition 2017 – Workshop Programme Paris, France, 12-15 June 2017), abstract

Johnston A. C., 1982. Arkansas' earthquake laboratory. Eos, Transactions, American Geophysical Union 63, 1,209–1,210

Keller E.A., Zepeda R.L., Rockwell T.K., Ku T.L., Dinklage W.S., 1998. Active tectonics at Wheeler Ridge, southern San Joaquin Valley, California. Geol. Soc. Am. Bull. 110, 298–310.

Langbein J., Dreger D., Fletcher J., Harde-beck,J.L., Hellweg, M., Ji, C., Johnston, M., Murray,J.R., Nadeau, R.M. and Rymer, M. (2005)Preliminary report on the 28 September 2004, 6.0Parkfield, California earthquake. Seismol. Res.Lett.76,10–26.

Lindman M., Lund B., Roberts R., Jonsdottir K., 2006.Physics of the Omori law: inferences from interevent time distributions and pore pressure diffusion modeling. Tectonophysics 424:209–22

Lowrie W., 1997. Fundamentals of geophysics. Cambridge: Cambridge University Press, ISBN 0-521-46728-4.

Mallika K., Gupta H., Shashidar D., Purnachandra Rao N., Yadav A., Rohilla S., Satyanarayana H. V. S., Srinagesh D., 2012. Temporal variation of b value associated with the M 4 earthquakes in the reservoir-triggered seismic environment of the Koyna–Warna region, Western India. J Seismol. 17:1–4

Mcjunkin R. D., Shakal A. E., 1983. The Parkfield strong-motion array, California. Geology 36, 27-34

Mesimeri M., Papadimitriou E., Karakostas V., Tsaklidis G., 2013. Earthquake clusters in NW Peloponnese. Bull Geol. Soc. Greece,. XLVII/3, 1167-1176

Mignan A., Woessner J., 2012. Estimating the magnitude of completeness in earthquake catalogs. Community Online Resource for Statistical Seismicity Analysis

Mogi K., 1963. Some discussions on aftershocks, foreshocks and earthquake swarms - the fracture of a semi-infinite body caused by an inner stress origin and its relation to the earthquake phenomena. Bull. Earthq. Res. Inst. Univ. Tokyo, 40, 831–53

NCEDC, 2014. Northern California Earthquake Data Center. UC Berkeley Seismological Laboratory. Dataset. doi:10.7932/NCEDC

Omori F., 1894. On the after-shocks of earthquakes. J. Coll. Sci. Imp. Univ. Tokyo 7:111–200

Opršal I., Eisner L., 2014. Cross-correlation - an objective tool to indicate induced seismicity. Geophysical Journal International, ggt501

Papazachos B. C., 1975. Foreshocks and earthquake prediction, Tectonophysics, 28, 213–226

Parsons T., Dreger D. S., 2000. Static-stress impact of the 1992 Landers earthquake sequence on nucleation and slip at the site of the 1999 M7.1 Hector Mine earthquake, southern California, Geophys. Res. Lett. 27, 1949–1952

Passarelli L., Maccaferri F., Rivalta E., Dahm T., Boku E. A., 2012. A probabilistic approach for the classification of earthquakes as " triggered " or "not triggered ", Journal of seismology 17 (1), 165-187

Patanè D., Cocina O., Falsaperla S., Privitera E., Spampinato S., 2004. Mt Etna Volcano: a seismological framework. In: Bonaccorso, A., Calvari, S., Coltelli, M., Del Negro, C., Falsaperla, S. (Eds.), Geophysical Monograph, 143. Mt. Etna: volcano laboratory, American Geophysical Union, pp. 147–165

Plenkers K., Ritter J. R. R., Schindler M., 2012. Low signal-to-noise event detection based on waveform stacking and cross correlation: application to a stimulation experiment. J. Seismol.

Pollastro R. M., Jarvie D. M., Hill R. J., Adams C. W., 2007. Geologic framework of the Mississippian Barnett Shale, Barnett-Paleozoic total petroleum system, Bend arch Fort Worth Basin, Texas. AAPG Bull. 91, 405–436

Purcaru G., 1974. On the statistical interpretation of the Bath's law and some relations in aftershock statistics, Geol. Inst. Technic. and Ec. Study Geophys. Prosp., Bucharest 10, 35-84

Rabak I., Langston C., Bodin P., Horton S., Withers M., Powell C., 2010. The Enola, Arkansas, intraplate swarm of 2001Seismol.Res. Lett.81549–59

Rudziński L., Dębski W., 2012. Extending the double difference location technique for mining applications. J Seismol. 17, 1, p. 83–94

Rutqvist J., Rinald, A. P., Cappa F., Moridis G. J., 2015. Modeling of fault activation and seismicity by injection directly into a fault zone associated with hydraulic fracturing of shale-gas reservoirs. Journal of Petroleum Science and Engineering, 127, 377-386

Rymer M. J., Langenheim V. E., Hauksson E., 2002. The Hector Mine, California, earthquake of 16 October 1999: Introduction to thespecial issue,Bull. Seismol. Soc. Am.,92, 1147–1153

Serpelloni E., Vannucci G., Pondrelli S., Argnani A., Casula G., Anzidei M., Baldi P., Gasperini I., 2007. Kinematics of the Western Africa–Eurasia plate boundary from focal mechanisms and GPS data. Geophys. J. Int. 1–20

Shcherbakov R., Yakovlev G., Turcotte D. L., Rundle J. B., 2005. Model for the Distribution of Aftershock Interoccurrence Times, Phys. Rev. Lett., 95, 218501

Schweig E. S., VanArsdale R. B., Burroughs R. K., 1991. Subsurface structure in the vicinity of an interplate earthquake swarm, central Arkansas. Tectonophysics 186, 107–114

Scientists from the U.S. Geological Survey, Southern California Earthquake Center, and California Division of Mines and Geology, 2000. Preliminary report on the 16 October 1999 M 7.1 Hector Mine, California, earthquake. Seism. Res. Lett. 71, 11–23

Shakal A., Graizer V., Huang M., Borcherdt R., Haddadi H., Lin K.-W., Stephens C., Roffers P., 2005. Preliminary analysis of strong-motion recordings from the 28 September 2004 Parkfield, Californiaearthquake,Seismol. Res. Lett., 76(1), 27–39

Shearer P. M., 2009. Introduction to Seismology, 2nd, University of California, San Diego

Sicali S., Serafina Barbano M., D'Amico S., Azzaro R., 2014. Characterization of seismicity at Mt. Etna volcano (Italy) by inter-event time distribution, J. Volcanol. Geoth. Res., 270, 1-9

Skoumal R. J., Brudzinski M. R., Currie B. S., 2015. Distinguishing induced seismicity from natural seismicity in Ohio: Demonstrating the utility of waveform template matching, J. Geophys. Res. Solid Earth, 120

Smith R.B., Arabasz W.J., 1991. Seismicity of the intermountain seismic belt. In: Slemmons, D.B., Engdahl, E.R., Zoback, M.D., Blackwell, D.D. (Eds.), Neo-tectonics of North America. Geological Society of America, Boulder, Colorado, pp. 185–228

Southern California Earthquake Center. Caltech.Dataset (SCEDC), 2013. doi:10.7909/C3WD3xH1

Suckale J., 2009. Induced seismicity in hydrocarbon fields, Advances in Geophysics, 51, ch. 2, 55- 106

Sykes L.R., 1970. Earthquake swarms and sea-floor spreading. J. Geophys. Res. 75, 6598–6611

Tosi P., De Rubeis V., Sbarra P., 2009, GeoPlanet: Earth and Planetary Sciences, 1:323-337

Turuntaev S. B., Eremeeva E. I., Zenchenko E. V. 2012. Laboratory study of microseismicity spreading due to pore pressure change. J Seismol. 17, 1, p. 137–145

Utsu T., 1961. A statistical study on the occurrence of aftershocks, Geophys. Mag. Tokyo 30, 521-603

VanArsdale R. B., Schweig E. S., 1990. Subsurface structure of the eastern Arkoma Basin. American Association of Petroleum Geologists Bulletin 74, 1,030–1,037

Vecchio A., Carbone V., Sorriso-Valvo L., De Rose C., Guerra I., Harabaglia P., 2008. Statistical properties of earthquakes clustering, Nonlin. Processes Geophys., 15, 333-338

Vidale J. E., Shearer P. M., 2006. A survey of 71 earthquake bursts across southern California: Exploring the role of pore fluid pressure fluctuations and aseismic slip as drivers, J. Geophys. Res., 111, B05312

Waite G. P., Smith R. B., 2004. Seismotectonics and stress field of the Yellowstone volcanic plateau from earthquake first-motions and other indicators, J. Geophys. Res., 109, B02301

Waite G. P., Smith R. B., 2002. Seismic evidence for fluid migration accompanying subsidence of the Yellowstone caldera, J. Geophys. Res., 107(B9), 2177

Wiemer S., Wyss M., 2000. Minimum magnitude of complete reporting in earthquake catalogs: examples from alaska, the western united states, and japan, Bull. Seismol. Soc. Am., 90, 859{869. 6, 7, 14, 15, 16, 17, 24, 28, 29, 30, 32

Wyss M., Hasegawa A., Wiemer S., Umino N., 1999. Quantitative mapping of precursory seismic quiescence before the 1989, m7.1 o -sanriku earthquake, japan, Annali Di Geo sica, 42, 851{869. 6, 14, 29

Zaliapin I., Ben-Zion Y., 2016. A global classification and characterization of earthquake clusters. Geophysical Journal International, 207, 608–634

Zoback M. D., 2007. Reservoir Geomechanics. Cambridge University Press,Cambridge, UK

Zobin V. M., Nishimura Y., Miyamura J., 2005. The nature of volcanicearthquake swarm preceding the 2000 flank eruption at Usu volcano,Hokkaido, Japan,Geophys. J. Int.163,265–275

WEBPAGE REFERENCES

[1] Cooperative institute for Research in Environmental Sciences at the University of Colorado at Boulder (2017)
(http://cires.colorado.edu/~bilham/Honshu2011/Honshu2011.html)

[2] Earth Sciences Division - Lawrence Berkeley National Laboratory (2017)
(http://esd1.lbl.gov/research/projects/induced_seismicity/primer.html)

[3] USGS Earthquake Hazards Program (2017)
https://earthquake.usgs.gov/earthquakes/search/

[4] USGS Earthquake Hazards Program (2017)
(https://earthquake.usgs.gov/research/parkfield/2004.php)

[5] Southern California Earthquake Data Center at Caltech (2017)
(http://www.scsn.org/index.php/earthquakes/speqrep/20050416-m5-2-wheeler-ridge/)